

# MPSE 2014

MARS – CONNECTING PLANETARY SCIENTISTS IN EUROPE



## WORKSHOP PROGRAMME AND ABSTRACTS

WARSAW, 3-5 JUNE 2014







### Scientific committee

Daniel Mège – Chairman (daniel.mege@twarda.pan.pl)  
ING PAN, Wrocław (WROONA Research Group)

Agustin Chicarro - Associate Chairman (achicarr@rssd.esa.int)  
European Space Agency/ESTEC, Noordwijk

Jurek Grygorczuk – Associate Chairman (jurekgry@cbk.waw.pl)  
CBK PAN, Warsaw

Joanna Gurgurewicz – Associate Chairman (jgur@cbk.waw.pl)  
ING PAN, Wrocław (WROONA Research Group) and CBK PAN, Warsaw

Hans Rickman – Associate Chairman (Hans.Rickman@physics.uu.se)  
CBK PAN, Warsaw

Olivier Witasse - Associate Chairman (owitasse@rssd.esa.int)  
European Space Agency/ESTEC, Noordwijk

### Local organization committee

Agata Białek (aprzepiorka@cbk.waw.pl)  
CBK PAN, Warsaw

Anna Łosiak (anna.losiak@twarda.pan.pl)  
ING PAN, Wrocław

Karol Seweryn (kseweryn@cbk.waw.pl)  
CBK PAN, Warsaw

### Excursions

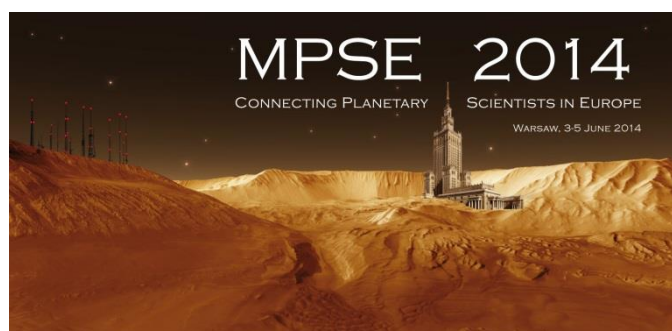
Morasko Meteorite Reserve: Andrzej Muszyński (anmu@2wp.pl), Adam Mickiewicz University, Poznań

Discovery of Warsaw: Anna Łosiak (anna.losiak@twarda.pan.pl), ING PAN, Wrocław

# Mars – Connecting Planetary Scientists in Europe MPSE 2014

Warsaw, 3-5 June 2014

Polish Academy of Sciences, Space Research Centre  
ul. Bartycka 18A, 00-716 Warsaw



Programme	page 4
Abstracts	page 12
Review lectures	page 12
Contributed presentations	page 23
Author index	page 78
Affiliations and e-mail addresses of registered participants	page 82



# PROGRAMME

## TUESDAY, 3 JUNE

---

8:15 9:00 Welcome coffee and on-site registration

9:00 9:10 Welcome address

### Morning session - Invited review lectures

9:10 9:40 **ESA and its science missions**

*Agustin Chicarro*

9:40 10:10 **Mars exploration in ESA**

*Agustin Chicarro*

10:10 10:30 Coffee break

10:30 11:30 **The atmosphere and climate of Mars**

*Franck Montmessin*

11:30 12:30 **Habitability of Mars, Enceladus, Europa and Titan – challenges in astrobiology and planetary research**

*Jean-Pierre de Vera*

12:30 – 14:00 Lunch break

Martian rover demonstration: Magma White (ABM Space Education)

### Afternoon sessions - Contributed talks

#### Space policy and industry

14:00 14:20 Poland in ESA – International cooperation in Mars exploration

*Beata Mikołajek-Zielińska*

14:20 14:40 Astri Polska

*Marie-Catherine Palau*

#### Planetary mapping

14:40 15:00 Detailed CTX-based geomorphologic mapping in Western Valles Marineris

*Krzysztof Dębniak, Daniel Mège and Marion Massé*

15:00 15:20 Creation of the Phobos Atlas based on Mars Express mission data

*Alexander Kokhanov, Irina Karachevtseva, Anatoliy Konopikhin, Anatoliy Zubarev, Irina Nadezhkina, Ljudmila Mitrokhina, Natalia Kozlova, V. Patraty and Jürgen Oberst*

#### The current Martian atmosphere and associated surface processes

15:20 15:40 Mars Climate Sounder observations of wave structure in the north polar middle atmosphere of Mars during the summer season

*Paulina Wolkenberg and John Wilson*

- 15:40 16:00 SHARAD data mapping for surface ice detection  
*Luigi Castaldo, Daniel Mège, Roberto Orosei, Giovanni Alberti and Joanna Gurgurewicz*
- 16:00 16:30 Coffee break and poster/exhibition session
- 16:30 16:50 Ice melting by radiantly heated dust grains on the Martian Northern Pole  
*Anna Łosiak and Leszek Czechowski*
- 16:50 17:10 Conditions for the appearance of interfacial liquid water at the northern hemisphere of Mars  
*Ákos Kereszturi and Thomas Appéré*
- 17:10 17:30 Seasonal flows on dark martian slopes, thermal condition for liquescence of salts  
*Konrad Kossacki and Wojciech Markiewicz*

**Asteroids and comets**

- 17:30 17:50 Comet 9P/Tempel 1: evolution of the surface  
*Konrad Kossacki*
- 17:50 18:10 Thermal conductivity determination from active measurements – Influence of boundary conditions  
*Agata Białek, Marek Banaszkiewicz, Roman Wawrzaszek, Jerzy Grygorczuk and Karol Seweryn*
- 18:10 18:30 Dynamical evolution of H chondrite parent asteroid – Record in the Pułtusk meteorite  
*Agata Krzesińska*

18:30 – 21:00 ESA-sponsored drink,  
**Poster session and MExLab Phobos exhibition**

**WEDNESDAY, 4 JUNE**

---

- 8:00 8:30 Coffee and tea

**Morning session - Invited review lectures**

- 8:30 9:30 **The early Martian environment: an astronomical view**  
*Hans Rickman and Uffe Jorgensen*
- 9:30 10:30 **Early crust formation on Mars, the meteorite evidence: impact breccia with 4.4 Ga zircons**  
*Roger Hewins*
- 10:30 11:00 Coffee break
- 11:00 12:00 **Planetary seismology: From the Moon with Apollo to Mars with InSight**  
*Taichi Kawamura, Philippe Lognonné and the SEIS/InSight Team*

12:00 – 13:30 Lunch break  
Martian rover demonstration: Scorpio III (Wrocław University of Technology)

## Afternoon sessions - Contributed talks

### Ancient dynamics of Mars

- 13:30 13:50 Potential of magnetic measurements for detection of horizontal movements of the Martian crustal blocks  
*Marek Lewandowski, Waldemar Jóźwiak and Krzysztof Mizerski*
- 13:50 14:10 Clast classification in Martian meteorite NWA7034/NWA8114  
*Jane MacArthur and John Bridges*
- 14:10 14:30 Evidence for post-Noachian highly viscous lavas in southern highlands of Mars  
*Petr Brož, Ernst Hauber, Thomas Platz and Matt Balme*

### Mission concepts, instruments and sensors

- 14:30 14:50 Polish Analogue Mars Rover Program  
*Mateusz Józefowicz and Sebastien Meszyński*
- 14:50 15:10 The importance of adequate activity planning strategies for successful human Mars missions  
*Sebastian Hettrich, Aline Dinkelaker, Efstratia Salteri, Leila Ghasemzadeh, Ali Alizade, Elena Lupu, Isabella Pfeil, Carmen Felix, Tilo Kauerhoff and Nina Sejkora*
- 15:10 15:30 Highlights from the MARS2013 Mars Analog Expedition  
*Gernot Groemer and Anna Łosiak*
- 15:30 16:00 Coffee break
- 16:00 16:20 Technological features and concept of planetary highland terrain hopper  
*Łukasz Wiśniewski, Jerzy Grygorczuk, Daniel Mège, Joanna Gurgurewicz, Tomasz Kuciński, Tomasz Barciński, Hans Rickman and Agata Nicolau-Kuklińska*
- 16:20 16:40 Optical sensors designed in frame of the AEROFASST project in Space Research Centre PAS  
*Piotr Wawer, Mirosław Rataj, Paweł Grudziński, Łukasz Płatos and Maciej Kalarus*
- 16:40 17:00 Investigation of the Martian lightning activity and the subsurface of Mars  
*Joanna Kozakiewicz, Andrzej Kułak and Janusz Młynarczyk*
- 17:00 17:20 Penetrators for planetary subsurface exploration  
*Jerzy Grygorczuk, Łukasz Wiśniewski, Bartosz Kędziora, Marcin Dobrowolski, Marta Tokarz, Jacek Krasowski, Marek Banaszekiewicz, Karol Seweryn and Roman Wawrzaszek*
- 17:20 17:40 Measurements of physical parameters of the regolith during operation of ultralight mobile drilling system  
*Karol Seweryn*
- 17:40 18:00 Numerical simulations of the quadrupole mass analyser in context of its potential application on the Low Velocity Penetrator  
*Agata Nicolau-Kuklińska and Karol Seweryn*

18:15 – 19:15

**Visit of Space Research Centre PAS technological laboratories**

## THURSDAY, 5 JUNE

---

8:00 8:30 Coffee and tea

### Morning session - Invited review lectures

8:30 9:30 **Comparison of terrestrial planets**

*Angelo Pio Rossi*

9:30 10:30 **Volcanism and tectonism on Mars**

*Ernst Hauber*

10:30 11:00 Coffee break

11:00 12:00 **Why study Phobos and Deimos?**

*Jürgen Oberst*

12:00-13:30 Lunch break

Martian rover demonstration: HUSAR-5 (Széchenyi István Gimnázium, Sopron)

### Afternoon sessions - Contributed talks

#### Glaciations and tectonism on Mars

13:30 13:50 The motion of Martian glaciers and geothermic heat flow

*Leszek Czechowski*

13:50 14:10 Early Hesperian Warm-Based Glaciation in Isidis Planitia, Mars

*Thomas Guidat, Stéphane Pochat, Olivier Bourgeois and Ondřej Souček*

14:10 14:30 Origin of the observed deformation in Valles Marineris: an equatorial fossilised glacier system and no regional tectonics

*Daniel Mège, Olivier Bourgeois, Marine Gourronc, Frédéric Gueydan, Olga Kromuszczyńska, Magdalena Makowska, Stéphane Pochat, Krzysztof Dębniak and Joanna Gurgurewicz*

14:30 14:50 Ornak (Tatra Mountains) as a terrestrial analogue for Martian deep-seated gravitational spreading (sackung)

*Olga Kromuszczyńska, Daniel Mège and Antoine Lucas*

14:50 15:10 Mechanical modelling of deep-seated gravitational spreading in Valles Marineris, Mars

*Magdalena Makowska, Frédéric Gueydan and Daniel Mège*

15:10 15:40 Coffee break

### **Rocks, grains and minerals**

- 15:40 16:00 Alteration on Mars: study of near-infrared spectra of terrestrial basalts altered in contrasted climate conditions  
*Joanna Gurgurewicz, Daniel Mège, Véronique Carrère, Anne Gaudin, Joanna Kostylew, Yann Morizet and Marta Skiścim*
- 16:00 16:20 Alteration features in basalts identified by atomic force microscopy and implications for Mars  
*Marta Skiścim, Joanna Gurgurewicz and Daniel Mège*
- 16:20 16:40 Variable fluorescence imaging for life detection – promising tool or not?  
*Jana Kvíderová*
- 16:40 17:00 Martian beaches sands – The characteristics of olivine weathering in a beach environment  
*Anna Losiak, Barbara Woronko and Robert Craddock*
- 17:00 17:20 Determining the size and shape of Martian grains  
*Joanna Kozakiewicz*

### **General discussion**

- 17:20 18:20 *Discussion moderated by Agustin Chicarro, Ákos Kereszturi and Daniel Mège*
- 19:30 Conference dinner at Dawne Smaki

## **FRIDAY, 6 JUNE**

---

### **Post-conference excursions**

#### **Excursion 1 - Morasko Meteorite reserve**

08:00 Departure from Warsaw (bus)

20:30 Return to Warsaw

#### **Excursion 2 - Discovery of Warsaw**

9:00 Departure from Zamkowy Square

End of excursion depending on participants

## PHOBOS EXHIBITION

Original thematic maps from the new Atlas of Phobos prepared by the MIIGAiK Extraterrestrial Laboratory, Moscow (presentation by Kokhanov et al. on Monday) will be displayed in the poster area throughout the workshop.

## POSTER SESSION

### **Asteroids, comets and impacts**

Thermophysical properties of NWA 6255 (L4) chondrites – preliminary results. *Katarzyna Łuszczek and Radosław A. Wach*

A new model of physical decay of Jupiter family comets. *Hans Rickman, Sławomira Szutowicz and Kamil Wójcikowski*

The methods of Impact probability calculations. *Hans Rickman, Tomasz Wiśniowski, Paweł Wajer, Ryszard Gabryszewski, Giovanni Valsecchi*

### **Planetary atmospheres**

Temperature profiles obtained using two retrieval methods on Venus. *Paulina Wolkenberg and Marek Banaszkiewicz*

### **Education**

Planetary science and Mars related education in Hungary. *Ferenc Horvai*

Morphotectonics of Mars at the University of Warsaw. *Wojciech Ozimkowski*

### **Martian hydrology and volatiles**

Interaction of volatiles and the surface of Mars. *Maria Błęcka*

The model of Martian rivers. *Leszek Czechowski, Piotr Witek and Katarzyna Misiura*

Interfacial water on Mars and its possible role on hydrogen peroxide decomposition. *Ákos Kereszturi and Sándor Gobi*

Dynamical modeling of fluvial deposition processes on Mars. *Piotr Witek and Leszek Czechowski*

Evidence of water from LHB on the largest Martian crater Hellas in comparison to other craters. *Natalia Zalewska*

### **Mass wasting processes**

Landslide propagation: simulations of granular gravitational collapse using molecular dynamics. *Timur Borykov, Anne Mangeney, Daniel Mège and Patrick Richard*

### **Mission concepts, instruments and sensors**

Remote Science Support Team during MARS2013: testing a map based system of data processing and utilization for the future long-duration planetary missions. *Anna Łosiak, Izabela Gołębiowska, Csilla Orgel, Linda Moser, Jane MacArthur, Andrea Boyd, Sebastian Hettrich, Natalie Jones and Gernot Groemer*

Exploration of Mars and Phobos with Galago, the Highland Terrain Hopper. *Daniel Mège, Joanna Gurgurewicz, Jerzy Grygorczuk, Łukasz Wiśniewski, Hans Rickman, Marek Banaszkiewicz, Tomasz Kuciński and Krzysztof Skocki*

Data fusion of soil measurements for traversability assessment of Martian surface: assumptions and concepts for new missions. *Piotr Węclewski and Krzysztof Skocki*

### **MPSE 2014 Rover demonstrations**

Scorpio 4 as an example of student approach to human-operated mobile robot construction. *Szymon Dzwonczyk*

Planetary rover robotics experiment in education: carbonate rock collecting experiment of the HUSAR-5 rover of the Széchenyi István High School, Sopron, Hungary. *Ágota Lang, Kristóf Szalay, Ábel Kocsis, Péter Prajczner and Szaniszló Bérczi*

Autonomic laboratory module for the SCORPIO 4 rover. *Agnieszka Rumińska*

### **Planetary Mapping**

SHARAD data mapping for surface composition detection. *Luigi Castaldo, Daniel Mège, Roberto Orosei, Giovanni Alberti and Joanna Gurgurewicz*

Thermal data processing for high-resolution mapping of Valles Marineris, Mars. *Marta Kubiak, Daniel Mège, Joanna Gurgurewicz, Jakub Ciqzela and Krzysztof Dębniak*

A Phobos atlas derived from images of the high resolution stereo camera (HRSC) on Mars Express. *Marita Wählisch, Konrad Willner and Jürgen Oberst*

The new topography of outer satellites - Io, Ganymede and Eneladus - derived from Voyager, Galileo and Cassini images. *Anatoliy Zubarev, Irina Nadezhdina, Evgeniy Lazarev, V. Patraty, Irina Karachevtseva, Alexander Kokhanov, Natalia Kozlova and Jürgen Oberst*

# ABSTRACTS

## Review Lectures

ESA's Science Programme addresses the fields of Solar System exploration as well as Astronomy and Astrophysics (including Fundamental Physics). The Sun is being studied by the Ulysses and SOHO missions, while Solar-Terrestrial interactions are addressed by the Cluster mission. Planets and minor bodies are the focus of the Giotto, Cassini-Huygens, Mars Express, Smart-1, Rosetta, Venus Express and Bepi-Colombo missions. The Universe is being studied by Cos-B, IUE, Exosat, Hipparcos, Hubble, ISO, XMM-Newton, Integral, Herschel, Planck, Lisa Pathfinder, JWST and Gaia. In addition, ESA is participating in a number of collaborative missions from other agencies such as Hinode and Double-Star for Solar-Terrestrial interactions, Kaguya, Chang' E-1 and Chandrayaan-1 for planetary studies, and Akari, Corot and Microscope for astronomy. Future science missions, which are currently being developed in ESA for the 'Cosmic Vision' science programme, include Solar Orbiter and Juice (Jupiter and Europa) in the Solar System area, and Euclid (dark matter), Cheops and Plato (exoplanets) in Astronomy. In addition, candidate missions for the Exploration programme, such as the Mars science network mission called Inspire and the Phobos sample return mission called Phootprint will also be presented.

ESA's Mars Express mission was launched in 2003 and has been orbiting Mars for over ten years, providing data with an unprecedented spatial and spectral resolution on the surface, subsurface, atmosphere and ionosphere of the red planet. The main theme of the mission is the search for water in its various states everywhere on the planet by all instruments using different techniques. A summary of scientific results of the mission will be given. Following Mars Express, European efforts in Mars Exploration are now taking place within the joint ESA-Roscosmos Mars Exploration Programme, starting in 2016 with the Trace Gases Orbiter (TGO) focusing on atmospheric trace gases. In 2018, an ExoMars rover will perform geochemical and exobiological measurements of the surface and the subsurface of the planet. A number of missions for 2020 and beyond are currently under study. Among those, one possibility is a Mars network science mission (named Inspire) of 3 surface stations, to investigate the interior of the planet, its rotational parameters, its atmospheric dynamics as well as the geology, mineralogy and astrobiological significance of each landing site. Inspire (without the need of an orbiter) represents a unique tool to perform new investigations of Mars, which could not be addressed by any other means. It will fill a longstanding gap in the scientific exploration of the Solar System by performing in-situ investigations of the interior of an Earth-like planet other than our own and provide unique and critical information about the fundamental processes of terrestrial planetary formation and evolution. Such mission has been considered a high priority by the planetary science community worldwide for the past 30 years, even though the long-term goal of Mars robotic exploration in Europe remains the return of rock and soil samples from the Martian surface before Humans eventually go to Mars. This mission will represent a step beyond NASA's Insight mission.

**Introduction:** One of the main challenges in astrobiology and planetary research in the near future is to realize space missions to study the habitability of Mars and the icy moons of the Jovian and Saturnian system. Mars is an interesting object to search for fossilized life because of its much more water driven wet history of its past. River beds, sedimentary deposits indicating the presence of lakes [1] as well as a supposed but highly debated presence of a former ocean on the north hemisphere [2] are clearly showing that the atmosphere must have been much denser and the conditions much more habitable than nowadays. Even today still water activity is present in specific niches on the surface of Mars [3]. This leads to the conclusion that the search for habitable environments on Mars and the presence of bio-traces of extinct or extant life is a reasonable enterprise to be conducted in the next space missions. But Mars is not the only promising candidate to find life in our solar system. The icy moons, like the Jovian moon Europa where water driven resurfacing activity must regularly happen because of the low amount of impact craters on the icy crusts as well as the clear observations of cryo-volcans and fissures and cracks with colored deposits coming from the inner side of a global ocean are clearly showing, that the ocean can be a habitable environment [4]. The Saturnian moon Eneladus seems also be a promising candidate to search for life. On this moon high water plumes come out of an ocean covered by its ice crust [5]. Some observations by the probe of Cassini also have shown, that besides the presence of water and salts a high number of simple and complex organics was observed within these plumes. Also for the Saturnian moon Titan an ocean is supposed beneath the icy crust and this moon has not to be neglected in future astrobiology-driven exploration missions. Because of these very important observations of the last decades international and interdisciplinary scientific teams are working on new types of space missions with the main task to search for life including work performed in planetary analog field sites, work in the lab and analysis performed in planetary simulation facilities combined with research done in space on specific exposure facilities as there are satellites and the International Space Station (ISS). The technology developments and scientific approaches try to solve problems which might occur if we would like to detect life. For that technology is used and tested in planetary analog environments like in the deep sea as well as in dry and cold deserts and different life detectors are developed and used during these field campaigns before testing them in space and using further in the next space exploration missions to Mars and the icy moons. Taken into account the international planetary protection guidelines which clearly formulate to first prevent contamination of a planets and moons and their special regions which might be habitable before sending probes on the surface, important work for cleaning and sterilizing the complex technology is necessary and sometimes a big challenge for engineers to fulfill these guidelines.



**Figure:** Promising habitable objects in our solar system: Mars, Europa and Enceladus. Are there niches which are colonized at least by microorganisms?

**References:**

- [1] Goldspiel J.M. and Squyres S.W. (1991), Ancient aqueous sedimentation on Mars, *Icarus*, 89 (2), 392-410.
- [2] Di Achille G. and Hynes B.M. (2010), Ancient ocean on Mars supported by global distribution of deltas and valleys, *Nature Geoscience*, 3, 459 – 463.
- [3] McEwen A.S. et al. (2011), Seasonal Flows on Warm Martian Slopes. *Science* 333 (6043), 740-743.
- [4] Crawford G.D. (1988). Gas-driven water volcanism and the resurfacing of Europa. *Icarus*, 73 (1), 66–79.
- [5] Hunter Waite J. et al. (2006), Cassini Ion and Neutral Mass Spectrometer: Enceladus Plume Composition and Structure, *Science*, 311 (5766), 1419-1422.

**Introduction:** Mars lacks plate tectonics and crustal recycling, and the long-term evolution of the crust-mantle system of Mars is driven by mantle convection, partial melting, and silicate differentiation [1]. A morphologically diverse inventory of volcanic landforms populates the Martian surface, most of which have close terrestrial analogs such as lava flows, shield volcanoes, volcanic cones, pyroclastic deposits, and dikes. However, environmental conditions (gravity, atmospheric pressure) play an important role on eruption processes [2], hence the morphology of eruption products is not identical on Earth and Mars. While magmatic activity was intense and spatially widespread during the Noachian and Hesperian, it became focused on the Tharsis and Elysium provinces in the Amazonian period [3,4]. Martian igneous rocks, as known today, are predominantly basaltic in composition, and remote sensing data, in-situ data, and analysis of the SNC meteorites indicate that their source regions were located at depths between 80 and 150 km, with degrees of partial melting ranging from 5 to 15 % [1]. Furthermore, magma storage at depth appears to be of limited importance, and secular cooling rates of 30 to 40 K<sub>Gyr</sub><sup>-1</sup> were derived from surface chemistry for the Hesperian and Amazonian periods. These estimates are in general agreement with numerical models of the thermo-chemical evolution of Mars, which predict source region depths of 100 to 200 km, degrees of partial melting between 5 and 20 %, and secular cooling rates of 40 to 50 K<sub>Gyr</sub><sup>-1</sup> [1]. In addition, these model predictions largely agree with elastic lithosphere thickness estimates derived from gravity and topography data. Major unknowns related to the evolution of the crust-mantle system are the age of the shergottites, the planet's initial bulk mantle water content, and its average crustal thickness.

The tectonic history of Mars corresponds roughly to the magmatic one, except for the global dichotomy, the largest and oldest tectonic feature, the origin of which is still unknown. As is expected for a one-plate planet [5] without evidence for past or present plate tectonics, Mars does not exhibit structural evidence for large-scale lateral crustal mobility

(e.g., strike-slip faulting). Instead, tectonism on Mars appears to be dominated by “vertical tectonics”, i.e. deformation related to the emplacement of large magmatic loads (e.g., “plume tectonics” [6,7]). Extension is mainly accommodated by large sets of long and narrow “simple” grabens which typically radiate outwards from centers of magmatic activity. Large systems of contractional features (wrinkle ridges, interpreted as thrust-propagation folds) form spatial patterns that are concentric around Tharsis or regionally controlled by basins [8]. Both the sets of grabens and the concentric wrinkle ridges are consistent with deformation due to magmatic loading at Tharsis. Other structural features are not obviously associated with global-scale centers of magmatic activity. A few large and complex extensional features resemble terrestrial continental rifts [9]. Lobate scarps are interpreted as surface-breaking thrust faults [e.g., 10] and are not associated with other large-scale features.

**References:** [1] Grott M. et al. (2013) Long-Term Evolution of the Martian Crust-Mantle System, *Space Sci. Rev.*, 174, 49-111. [2] Wilson L. and Head J. W. (1994) Review and analysis of volcanic eruption theory and relationships to observed landforms, *Rev. Geophys.*, 32, 221-263. [3] Werner S.C. (2009) The global Martian volcanic evolutionary history, *Icarus*, 201, 44-68. [4] Hauber E. et al. (2011) Very recent and wide-spread basaltic volcanism on Mars, *Geophys. Res. Lett.* 38, L10201. [5] Solomon S.C. (1978) On volcanism and thermal tectonics on one-plate planets, *Geophys. Res. Lett.*, 5, 461-464. [6] Maruyama S. (1994) Plume tectonics, *J. Geol. Soc. Japan*, 100, 24-49. [7] Mège D. and Masson P. (1996) A plume tectonics model for the Tharsis province, Mars, *Planet. Space Sci.*, 44, 1499-1546. [8] Chicarro A. et al. (1985) Global and regional ridge patterns on Mars, *Icarus*, 63, 153-174. [9] Hauber E. et al. (2010) Martian rifts: Structural geology and geophysics, *Earth Planet. Sci. Lett.*, 294, 393-410. [10] Watters T.R. et al. (2000) Displacement-length relations of thrust faults associated with lobate scarps on Mercury and Mars: Comparison with terrestrial faults, *Geophys. Res. Lett.*, 27, 3659-3662.

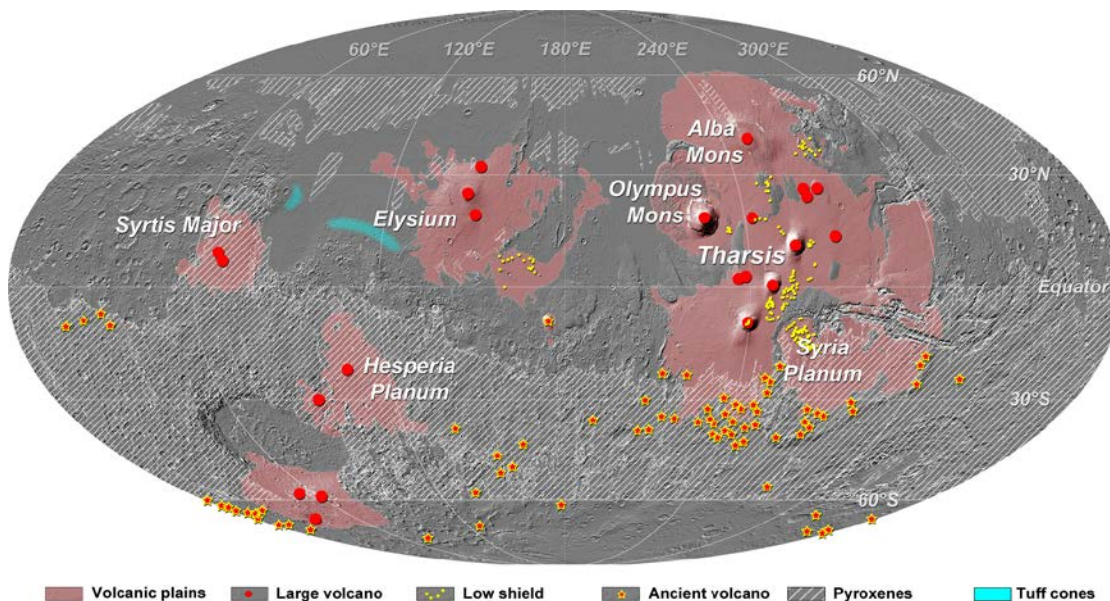


Figure 1 | Global distribution of known volcanic surface features (modified from [1]).

**Introduction:** Current models of Mars geology are based on orbital observations, surface rover work, and the study of Martian meteorites. However, it is clear that the common Mars meteorites, the SNCs, are unlike most of the observed surface materials of Mars in age and composition. The newly discovered paired meteorite breccias NWA 7034, NWA 7533, etc. [1-3], give us access to ancient crustal material.

**Petrology:** NWA 7533 contains crystal and rock clasts in both the grey matrix and dark grey lumps in the matrix (Fig. 1). Two black melt spherules and numerous highly feldspathic (white) clasts are conspicuous in Fig. 1. The dark lumps are clast-laden melt rocks with very fine-grained mesostases, characteristic of impact cratering. Slightly coarser grained microbasalts are clast-free melt rocks. The compact crystalline breccia matrix consists of submicron-sized pyroxene and plagioclase, plus crystal clasts down to about 5µm in size [2-4].

The medium grained clasts are monzonitic, noritic and pyroxenitic [2]. Magnetite-ilmenite assemblages indicate a very high degree of oxidation (QFM +2 to +3). There is extensive fractionation to an augite, chlorapatite, Na-rich plagioclase, orthoclase, zircon assemblage in the monzonitic clasts, and clasts and xenocrysts of these phases are observed in the fine-grained components.

The breccias contain magnetite, maghemite, ferrihydrite and nanophase Fe oxide [1,3,11,12]. Ferrihydrite is formed by low temperature hydrous alteration (<200°C). (Ni-rich) pyrite veins in NWA 7533 cut matrix and all clast types. It grew at higher temperature and later than alteration [13].

**Geochemistry:** The fine-grained facies of NWA 7533 are enriched in siderophile elements relative to SNC meteorites, at levels similar to those in lunar breccias [3]. The enrichment is equivalent to 5% CI chondrite. The noritic-monzonitic rocks are also enriched in siderophiles and hence must be formed by impact melting of regolith [3], though there are also Ni-poor pristine orthopyroxenites [13]. The breccias are depleted in S [3] and clasts lack magmatic sulfides.

Oxygen isotope data show interaction of fractions of NWA 7034 with H<sub>2</sub>O yielding high Δ<sup>17</sup>O [5]. However, several levels of Δ<sup>17</sup>O occur in zircons in NWA 7533, implying the different regions of impact melt saw different amounts of interaction with H<sub>2</sub>O during crystallization [6]

**Geochronology:** We reported a 4.43±0.03 Ga crystallization age for zircons in noritic and monzonitic rocks in NWA 7533 [3], confirmed by crystallization ages of 4.4-4.5 Ga for plagioclase [7]. There is evidence of resetting of zircon and K feldspar at ~1.7 Ga [3,7].

Dates for NWA 7034 include zircon crystallization at ~4.4 Ga and resetting of zircon and phosphate at 1.4-1.5 Ga. [8,9]. An Sm-Nd isochron giving 4.39±0.08 Ga “primarily dates pyroxene” crystallization in NWA 7034 [10].

**Comparison with Mars:** NWA 7533 fine-grained material has a similar composition to Gusev soils [2]. The most Mg-rich pyroxenes are similar to those in ALH 84001. The rover Curiosity has analyzed a wide variety of rocks including some similar to the monzonitic clasts in NWA 7533. We show our data for one such clast along with ChemCam data [14] for a Gale crater sample (Fig. 2).

NWA 7034 has nine times higher magnetism (IRM) than the highest SNC value due to fine Fe oxide [11]. Only a few km of breccia could explain the magnetic fields observed in the southern hemisphere of Mars [11]. Infrared spectra show a 3-µm band in the surface of Mars and in NWA 7533 [12]. This feature originates from an -OH bearing phase, and ferrihydrite best reproduces the band shape [12].

**Summary:** At 4.43 Ga, Mars crust contained highly fractionated (K-feldspar-rich) rocks. It had experienced degassing of its mantle and atmosphere-hydrosphere-surface interaction [2]. Early cratering produced regoliths and thick impact melts. There was redistribution of leached elements, e.g. S, and regolith dust across the planetary surface. Compaction of the breccia matrix [3,4] may have been at the time of resetting of ages (1.4-1.7 Ga) and was followed by hydrothermal alteration depositing pyrite.

**References:** [1] Agee C. B. et al. (2013) *Science* 339, 780–785. [2] Hewins R. H. et al. (2013) *LPS XLIV*, Abstract #2385. [3] Humayun M. et al., (2013) *Nature* 503, 513-516. [4] Muttik N. et al. (2014) *LPS XLV*, Abstract #2763. [5] Ziegler K. et al. (2013) *LPS XLIV*, Abstract #2639. [6] Nemchin A. et al. (2014) *LPS XLIV*, Abstract #1740. [7] Bellucci et al. (2014) *LPS XLV*, Abstract #1327. [8] Yin Q.-Z. (2014) *LPS XLV*, Abstract #1320 [9] Tartèse R. et al. (2014) *LPS XLV*, Abstract #2020. [10] Nyquist L. et al. (2013) *LPS XLV*, Abstract #5318. [11] Rochette, P. et al. (2013) *LPS XLIV*, Abstract #1343. [12] Beck P. et al. (2014) *LPS XLV*, Abstract #2097. [13] Hewins R. H. et al. (2014) *LPS XLV*, Abstract #1416. [14] Sautter V. et al. (2014) *J. Geophys. Res. Planets* 119,1-17.

**Acknowledgements:** Thanks to the numerous authors of the cited papers on NWA 7533, and especially to B. Zanda who organized the consortium.



Fig. 1. Sawed surface of NWA 7533, ~2 cm wide.

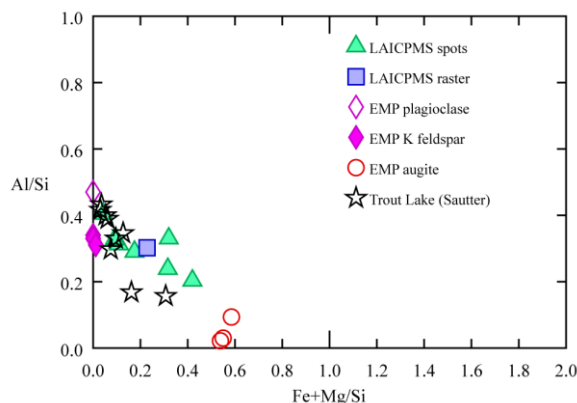


Fig. 2. Comparison of NWA7533-3 monzonitic Clast II with ChemCam data for Trout Lake from Gale Crater [14].

**Introduction:** Origin and evolution of planets and satellites is one of the most interesting and important subjects in planetary science. To investigate them, internal structure of these solid bodies provides essential pieces of information. For the Earth, seismology has been one of the most successful methods carried out to provide quantitative estimation of its internal structure. There is a great interest and need for seismic investigation for other satellites and planets and understand their seismic activity and internal structure in comparative way. Here, we will introduce the past and the future of planetary seismology. First, we will discuss what we learned from lunar seismology. Then we will introduce our future mission of InSight, which will aim for first seismic detection on Mars.

**Lunar Seismology-Apollo Seismic Experiment:** First, we will discuss the achievements made in Apollo Seismic Experiment, which is the only successful extraterrestrial seismic observation so far. During Apollo mission, 5 seismic stations were deployed on the lunar surface; Apollo 11, 12, 14, 15 and 16 (e.g. [1]). While the seismometer at Apollo 11 site was operated only for couple of weeks, other seismometers observed lunar seismic events until the termination of Apollo missions. The experiment provided us with 5 and half years of network observation data and more than 13000 seismic events were reported [2]. The data showed that there are three types of seismic events on the Moon. First, deep moonquakes occurs at about 900 km depth and occurs repeatedly at distinctive source regions. This is the most frequently observed seismic event on the Moon. The second is shallow moonquakes, which occur at about 200km depth. These are events with relatively large magnitudes but they are rare seismic events. Last is meteorite impact. Since the Moon has no or very thin atmosphere, meteorites impacts hit the lunar surface without being burned out. While they are not a major seismic source for the Earth, they are important seismic source for the Moon. Using such events various investigations have been done for lunar seismology and the data is still an important source of information for lunar seismology today.

One of the important achievements of lunar seismology was that they provided inner structure model of the Moon. Investigations show that the Moon has distinctive layered structure, which we refer as crust, mantle and core. The estimation of crust thickness has been done since 80s and they were revisited in early 2000s. While studies on 80s used seismic events with various epicentral distance and estimated crustal thickness of ~60km[3], recent studies used Monte-Carlo sampling methods or systematic exploration and obtained thinner crust of ~40 km [4,5]. Recent results from GRAIL gravimetric observation estimated global crust thickness that is consistent with seismic observation [6]. For mantle structure, there are still uncertainties in its estimations. This is mainly due to the sparse ray densities and a small number of seismic rays that probed into the deep region of the Moon. Finally, recent studies succeeded in detecting the first core phase. They estimated the core size to be ~330 km radius with partial melt region of ~480 km radius[7]. The seismic

investigation with Apollo data had great contribution in uncovering in the inner structure of the Moon. At the same time, as we see in the example of mantle structure, there is still many uncertainties and problems to be solved.

**Mars Seismology- InSight:** The INSIGHT NASA Discovery mission will deploy in September 2016 a 3 axis Very Broad band seismometer and a 3 axis SP seismometer, as well as other instruments enabling the installation of a complete geophysical observatory recording seismic, heat flow, magnetic and geodetic signals, in addition to atmospheric wind, pressure and temperature.

We first present the science goals status of the SEIS experiment and its development status. The SEIS sensor assembly, which contains both the VBB and SP seismometer, will be deployed on the Martian ground by a robotic arm from a Phoenix-type lander platform and protected by a wind and thermal shield. The wind and thermal shield, a vacuum sphere for VBBs and a passive compensation system will achieve a very high protection of the seismometers against temperature and pressure variations, allowing the sensor to operate in the rough Martian thermal environment while reaching a detection threshold below  $10^{(-9)}$  m/s/s  $\text{Hz}^{(-1/2)}$  in the VBB bandwidth and  $10^{(-8)}$  m/s/s  $\text{Hz}^{(-1/2)}$  for the SP. A leveling system will allow the VBB to operate, while providing to both seismometer the best possible mechanical coupling with the ground motion. The SEIS instrument will be provided by CNES, which will coordinate a wide set of international contributors from the Institut de Physique du Globe de Paris, the Imperial College from London and the Open University, the Max-Planck Institute of Lindau, the École polytechnique fédérale de Zurich (ETHZ), the Jet Propulsion Laboratory and the Institut de l'Aéronautique et de l'Espace from Toulouse.

We then illustrate the science goals by a focus on the capability of INSIGHT to detect either quakes or Impacts. For impacts, this can be done with both the seismometers and the pressure sensor. We conclude with the perspective of the mission in term of quake detection.



Figure 1: Integration of the SEIS sensor heads. The sphere includes the 3 long period seismic sensors, while the 3 short period are located on 3 boxes around the leveling ring

**References:** [1] Lammlin et al., 1974, *Rev. Geophys. Space Phys.*, 12, 1-2 [2] Nakamura et al., 1981, *University of Texas Institute for Geophysics Tech Rept* 18, Galveston, 1981 revised 2004 [3] Nakamura, Y., 1983, *JGR*, 88, 677-686 [4] Khan et al., 2000, *GRL*, 27, 1591-1594 [5] Lognonné et al., 2003, *EPSL*, 6637, 1-18 [6] Wiczorek et al., 2013, *Science*, 339, 671-675, [7] Weber et al., 2011, *Science*, 331 309-312.

**Introduction:** Mars possesses a tenuous atmosphere composed essentially of CO<sub>2</sub>, with a surface pressure of only 7 mbar. After 40 years of a nearly continuous space exploration of the Red planet, Mars's system has become the second best known planetary body of the solar system after the Earth. This review presentation will aim at providing a general overview of the knowledge assembled to date on the Martian atmosphere and climate inferred both from observations and from the ever growing body of theoretical works.

**Mars atmosphere structure and dynamics:** Its structure has been characterized thanks to decades of exploration, using remote sensing instruments as well as in situ measurements performed by several probes during their descent through the Martian atmosphere before landing. This tenuous atmosphere is as transparent to solar radiation as Earth's is, such that most of the energy is deposited at the base of the atmosphere. This creates in return a region of active convection in the first kilometers above the surface, akin to Earth's planetary boundary layer. In parallel, Mars's atmosphere sustains additional warming thanks to the mineral particles stripped from the Martian regolith that absorb in the blue portion of the solar spectrum. The thermal structure exhibits a tight control by the amount of suspended mineral dust, which is in turn controlled by the strength of the winds at the surface, thereby creating a strong dynamical feedback. The atmosphere of Mars is too cold and too dry to allow liquid water formation, yet shows prominent icy cloud formation that also exerts significant impact on the radiative budget. With no ozone layer to give rise to a stratosphere, the Martian troposphere appears far more developed vertically than Earth's is, allowing transport by winds over large depths (>60 km) of the atmospheric column. The average pattern of Mars atmosphere dynamics shows resemblance with that of the Earth with global circulation cells redistributing the excess of heat across the planet. The talk will be illustrated by several examples of observations recently made from the Martian orbit by Mars Express and by other missions currently in operations. It will also make use of the theoretical predictions made by Mars Climate Models, which have gained significant maturity in the recent years.

**Composition and Chemistry:** Measurements made thirty years ago by the Viking landers established the exact composition of the atmosphere on Mars as 95.3% carbon dioxide, 2.7% nitrogen and 1.6% argon, with smaller amounts of oxygen (0.15%) and water vapour (0.03%). The Martian atmosphere is submitted to an intense photochemical activity, led by photolysis of water vapor with subsequent creation of the main oxidizing species, the hydroxyl radicals. The study of the catalytic cycles controlled by hydroxyls has been the focus of numerous photochemical modeling works, as they may eventually supply the needed mechanism to allow CO<sub>2</sub> recombination, balancing loss through photodisso-

ciation, and permitting the long-term sustainment of the current CO<sub>2</sub> atmosphere. Recent observations made from the orbit have also shed a new light on Martian oxygen species, in particular molecular oxygen and ozone whose formation in the polar regions of Mars is a direct indicator of how strong and variables are the exchanges of airmasses between the sunlit equatorial regions and the polar nights. The current status of our understanding of the main cycles controlling Martian photochemistry and their observational evidences will be presented.

**Martian Trace Gases, the case of water and methane:** The study of water on Mars has been a central and permanent quest of Mars exploration, as illustrated by the long-standing "Follow the water" theme of NASA, shared by other leading space exploration programs. Water, which in the liquid phase is considered to be an essential ingredient for the emergence of life as we know it, is however present in very low abundances on Mars. Identification of its major reservoirs ---the atmosphere, surface ice, and permafrost--- has allowed scientists to quantify Mars water global inventory to a value far inferior to Earth water inventory: most estimations suggest that a liquid layer of water of only a few meters depth would form if all reservoirs were condensing or melting to cover the Martian surface globally. There has been an accumulation of evidences that Martian water behaves in a cyclic manner, thereby establishing the paradigm of a water cycle on Mars. The first multi-annual monitoring of water vapor performed in the 70's revealed that the same seasonal and spatial pattern qualitatively repeated itself for nearly two consecutive years. Several missions have confirmed this preliminary conclusion: water seasonal variation appears to be controlled by exchanges between various reservoirs, achieving, on an annual basis a stationary state with minor inter-annual differences. An overview of our current perspective on Martian water cycle will be presented. Water is a trace gas in the Martian atmosphere, and could be the main one, if not the only one. However, the detection of CH<sub>4</sub> could point to the possibility that, either a subsurface hydrothermal activity has been at work relatively recently, or some biogenic sources could still be active or have been active in the past. The hunt for trace gases of either origin is a major goal of Mars exploration, considering the potential implications for Mars's present and past activity.

In 1877, Asaph Hall, an astronomer at the United States Naval Observatory, discovered the two Martian satellites Phobos and Deimos. The origins of the two moons have been uncertain to the present day. They may have co-accreted with the parent planet, or formed from Martian basin ejecta. Alternatively, they may represent captured primitive asteroids or comets.

Phobos is moving deep in the gravity field of Mars, hence, its orbit is a powerful sensor for various dynamic parameters in the Martian satellite system, which include the Martian gravity field, its temporal variations, as well as shape-, interior structure-, and rotation parameters of Phobos itself. Ultimately, Deimos is expected to escape from its orbit, while Phobos will disrupt from tidal stresses and disintegrate in the Martian atmosphere within time scales of tens of millions years.

The mass of Phobos has been determined from radio science data obtained during spacecraft flybys, as well as by modeling of its secular motion. More information on the body's interior may be derived from tracking of its rotation and forced librations. Current interior structure modeling suggests that Phobos may be highly porous and to a large extent homogeneous. However, small inhomogeneities, perhaps involving a low-density regolith layer, or mass anomalies associated with the large crater Stickney, cannot be ruled out.

Phobos and Deimos are subjected to an intense meteoroid bombardment. Indeed, the surfaces of the satellites are covered by numerous impact craters, which represent indicators for the source of the meteoroid population and the ages of the satellites' surfaces. It is most puzzling that Phobos appears rather old, in contrast to its short remaining lifetime. The meteoroid impacts are known to produce escaping dust, which is predicted to form dust rings within the orbits of Phobos and Deimos. However, no such rings have been detected to the present day.

The heavily cratered terrain of Phobos is a unique geologic laboratory. It is cut by systems of grooves, the origins of which are still uncertain more than three decades after their discovery. They may represent chains of secondary craters from Stickney, faulting introduced by tidal stresses and non-synchronous rotation, or impact ejecta from Mars.

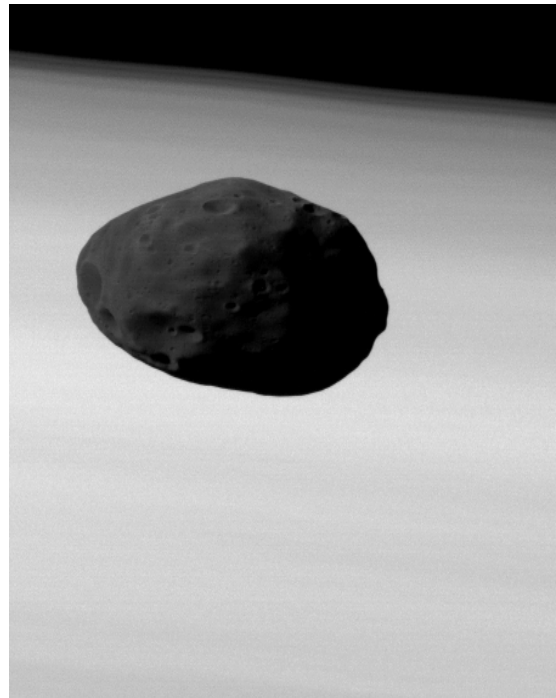


Fig. 1: Phobos and Mars in the background (image credit: Mars Express / ESA / DLR / FU Berlin)

With Mars Express currently being the only Mars spacecraft to carry out Phobos flybys on a regular basis, a wealth of geoscientific data is accumulating. Geodetic control point networks, shape models, and maps for Phobos are continuously improving, which are essential planning tools for remote sensing and landing site selection of future Phobos missions.

Any progress in our knowledge on the origin, evolution, and characteristics of Phobos and Deimos requires the joint analysis and discussion of all available data. Ultimately, however, new missions to Phobos and Deimos, including sample returns may be needed. Space mission planners have identified Phobos and Deimos as targets, from where the recovery of extraterrestrial samples may be comparably straightforward. Also, Phobos has been suggested as a “water-stop” for manned missions to Mars. Hence, it is likely that we see exploration missions to Phobos and Deimos in the near future.

We review the circumstances around the formation of planet Mars according to recent dynamical models and theories for terrestrial planet formation, and taking into account the recent progress in isotopic dating of the planet's origin. All this may be consistent with Mars being essentially an embryo rather than a full-grown planet. In this context we will discuss the applicability of the Grand Tack scenario versus the classical planetary accretion model

We will also focus on the likely composition of the primordial Martian mantle and crust in terms of volatiles -- in particular H<sub>2</sub>O -- and platinum group elements (PGE). One of the main issues is whether the infant planet Mars had a substantial volatile inventory or was essentially dry. We will discuss the role of the Late Heavy Bombardment (LHB) in bringing water to Mars based on recent modeling efforts concerning the extent, nature and consequences of this bombardment. The question of whether the LHB was dominated by cometary or asteroidal impactors will be penetrated.

The geochemical evidence about the amount and nature of the post core formation influx of chondritic material coming from the PGE abundances in Martian meteorites will be discussed as a possible indicator of the nature of the LHB impactors. Finally, we will judge the implications of several isotope ratios (like D/H) as observed in different solar system objects for choosing between the different scenarios of planetary evolution that we present.

**Introduction:** Terrestrial planets (Figure 1) provide key information to understand our Solar System (Table 1). They constitute the most accessible record of geological histories, which strongly complement each other [e.g. 1].

Our approach in decoding their history is necessarily Earth-centric, because the only other body with samples of known geologic context is the Moon. Nevertheless, during the last few decades the knowledge of other rocky bodies greatly increased.

Mars possibly hosts the most complex and diverse non-terrestrial geological history [e.g. 2, 3], sharing several aspects with Earth, from basic processes to large-scale dynamics, especially in its earliest history. Mars and Earth have striking similarities of present surface processes as well (eolian, periglacial and alike), but also substantial, and not well-understood, differences.

The complex past of Venus is valuable but inaccessible to a large extent [e.g. 4,5]. Still, its evolution, despite similar size and mass so different from that of Earth, is of importance to understand possible pathways of our own planet's future [e.g. 6]: The geological and atmospheric history of Earth's twin poses many questions on their diverging evolution.

Mercury, for a long time less known and very challenging to explore, has recently revealed a surprising complexity [e.g. 7], including compositional and volcanic diversity and even the possible presence of volatiles on its surface, in addition to the record of early turbulent phases of its surface evolution, [8,9].

Even the Moon, possibly the best-known Solar System body besides Earth, still holds many open questions [e.g. 10], such as details of its formation and early evolution of the Earth-Moon system, the extent and exact timing of large impact basin formation, the possible late-stage volcanism and the refinement and validation of overall Lunar chronology, key to the Inner Solar System as a whole.

A brief review of current understanding of the surface geology of Inner Solar System planets and moons will be provided, with a few inferences to the interior evolution, similarities and differences between them and Earth, our reference Terrestrial Planet.

**References:** [1] Fishbaugh, K. E., et al. (2007). *Geology and Habitability of Terrestrial Planets* (Vol. 24). Springer. [2] Carr, M. H., & Head III, J. W. (2010). Geologic history of Mars. *Earth and Planetary Science Letters*, 294(3), 185-203. [3] Rossi, A. P., & van Gasselt, S. (2010). Geology of Mars after the first 40 years of exploration. *Research in Astronomy and Astrophysics*, 10(7), 621. [4] Strom, R. G., Schaber, G. G., & Dawson, D. D. (1994). The global resurfacing of Venus. *Journal of Geophysical Research: Planets* (1991–2012), 99(E5), 10899-10926 [5] Hansen, V. L., & López, I. (2010).

Venus records a rich early history. *Geology*, 38(4), 311-314. [6] Bengtsson, L., Bonnet, R. M., Grinspoon, D., Koumoutsaris, S., Lebonnois, S., & Titov, D. (2013). Towards Understanding the Climate of Venus. *Towards Understanding the Climate of Venus*, ISSI Scientific Report Series, Vol. 11, ISBN 978-1-4614-5063-4 [7] Solomon, et al. (2008) Return to Mercury: a global perspective on MESSENGER's first Mercury flyby. *Science*, 321(5885), 59-62. [8] Marchi, et al. (2013). Global resurfacing of Mercury 4.0-4.1 billion years ago by heavy bombardment and volcanism. *Nature*, 499(7456), 59-61. [9] Neumann, G., et al. (2013). Bright and dark polar deposits on Mercury: Evidence for surface volatiles. *Science*, 339(6117), 296-300. [10] Geiss, J., & Rossi, A. P. (2013). On the chronology of lunar origin and evolution. *The Astronomy and Astrophysics Review*, 21(1), 1-54.



**Figure 1:** Terrestrial Planets (and the Moon) disks compared, to scale, clockwise Earth, Moon, Mars, Venus, Mercury. Atmospheres mask partially the surface of Earth and Mars and totally that of Venus.

Body	Radius (km)	Mass (kg)	$\rho_{unc}$ (g.cm <sup>3</sup> )
Mercury	2440	$3.3 \times 10^{23}$	5.3
Venus	6052	$4.87 \times 10^{24}$	4.0
Earth	6371	$5.97 \times 10^{24}$	4.1
Moon	1737	$7.35 \times 10^{22}$	3.3
Mars	3,390	$6.42 \times 10^{23}$	3.7

**Table 1:** Basic parameters of Terrestrial planets

# Contributed presentations

**Introduction:** Thermal measurements on surface and subsurface layers of planets, satellites, comets and asteroids play important role in determination of its physical and chemical properties as well as qualifying and quantifying of processes i.e. heat and gas transfer, attenuation wave etc. In particular heat conduction is connected with structural properties of porous media such as volatile content, sublimation temperature of volatile components, cohesion, and the size of grains forming the regolith constitute. But the determination of the thermodynamic parameters with appropriate accuracy is not trivial. The regolith is a fine-grained and loose material with very low thermal conductivity coefficient, i.e. lunar regolith thermal conductivity is estimated at  $1.72 - 2.95 \times 10^{-2}$  W/m/K [1], which is considered as an extremely low value. The modelling of thermodynamic processes occurring in different mediums, has been a field of interest for group of scientists and engineers from Space Research Centre PAS for a couple of years. That resulted in participation in missions like Rosetta or Phobos-Grunt, for which the penetrators for geotechnical purposes including thermal conductivity determination has been developed [2], [3], [4] and [5].

**Problem definition:** The thermal conductivity sensors mounted on MUPUS and CHOMIK have a shape of cylinder with finite length. For this case the heat transfer equation in cylindrical coordinate system has a form shown below (1).

$$\frac{\partial T_i}{\partial t} = \frac{k_i}{\rho_i C_{pi}} \frac{\partial}{\partial r} \left( \frac{1}{r} \frac{\partial T_i}{\partial r} \right) + \frac{k_i}{\rho_i C_{pi}} \frac{\partial^2 T_i}{\partial z^2} \quad (1)$$

where  $k_i$  is the thermal conductivity,  $\rho_i$  is density,  $C_{pi}$  is specific heat,  $T_i$  is the temperature. The axial symmetry is assumed, thus the  $\theta$  variable is not here considered. Solution for such equation with different initial and boundary conditions for two composite solid regions are widely presented in [6] and [7]. Since the surface and subsurface layers of planets, comets or asteroids are composed of granular material, the contact between sensor and the tested medium shall not be considered as an ideal. Due to that fact authors introduce here the thermal contact conductance  $H$  in one of the boundary conditions (2), which was not considered in [6] and [7] but discussed in [8].

$$k_i \frac{\partial T_i}{\partial r} + H(T_i - T_j) = 0 \quad (2)$$

The contact conductance influence on medium temperature is presented on Figure 1. The higher contact conductance is the more heat is being transferred from the heated sensor into the medium.

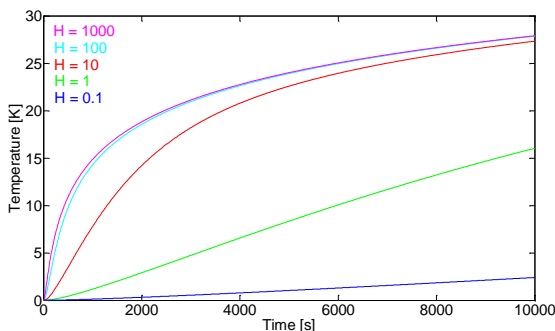


**Figure 1** The contact conductance influence on medium temperature measured profile.

The problem has been solved semi-analytically (in Fortran and Matlab) and numerically (in Comsol) for different types of boundary condition, which include different initial temperatures for sensor and the medium or the power applied to the sensor. In addition couple of tests in materials of known thermal conductivity coefficient in vacuum conditions has been performed. Results from the theoretical model will be compared with the measurement data to validate the model.

**Conclusions:** Temperature is a very important parameter characterizing the surface and subsurface layers of the planetary bodies. The heat transfer from the interior of the body to the exterior is driving factor in determining and predicting the evolution of the planet. It is known that the effective thermal conductivity coefficient is closely related with physical properties of the material e.g. porosity chemical composition, density, cohesion or grain size. The mechanisms of the heat transport like radiation, convection and conduction are well known from the physical and mathematical point of view. But while the regolith has very low thermal conductivity coefficient the determination of this value from the experiment is very difficult. Therefore calculations performed for set of different boundary conditions and validating theoretical models with tests will allow to properly analyse the data from missions like Rosetta. The determination of the thermal conductance is one of the most crucial elements. It depends on the contact conditions between the sensor and the medium and highly influence the temperature profiles. Therefore it is desired to estimate this value based on the test set up and prior measurement data analyses.

**References:** [1] Heiken, Grant, David Vaniman, and Bevan M. French. (1991), *The Lunar Sourcebook: a user's guide to the Moon*, New York: Cambridge University Press. [2] Spohn, T., Seiferlin, K., Hagermann, A., Knollenberg, J., Ball, A. J., Banaszekiewicz, M., Benkhoff, J., Gadowski, S., Gregorczuk, W., Grygorczuk, J., Hlond, M., Kargl, G., Kührt, E., Kömle, N., Krasowski, J., Marczewski, W., Zarnecki, J. C.. (2006), Mupus - a thermal and mechanical properties probe for the Rosetta Lander Philae. *Space Sci. Rev.*, Vol. 128, 339-362. [3] K. Seweryn, M. Banaszekiewicz, M. Grunwald, J. Grygorczuk, and T. Spohn. (2005), Thermal model of MUPUS penetrator. *Int. J. Heat Mass Trans.*, vol. 48, pp. 3713-3721. [4] Banaszekiewicz M., Seweryn K., Wawrzaszek R.. (2007), Thermal conductivity determination of cometary and asteroid materials. *Advances in Space Research*, vol 40(2) 226-237 [5] Rickman H, Słaby E, Gurgurewicz J, Śmigielski M, Banaszekiewicz M, Grygorczuk J, Królikowska M, Morsawski M, Seweryn K, Wawrzaszek R.. (2014) CHOMIK: A Multi-Method Approach for Studying Phobos, *Solar System Research*.. [6] J. V. Beck, K. D. Cole, A. Haji-Sheikh and B. Litkouhi. (1992), *Heat conduction usings Green's function*, Hampshire Publishing Corporation. [7] H. S. Jaeger and J. C. Carslaw. (1959), *Conduction of Heat in Solids*, second edition, London, Oxford University Press. [8] E. S. Hutter and N. I. Komle. (2012), Performance of thermal conductivity probes for planetary applications. *Geosci. Instrum. Method. Data Syst.* Vol 1, pp. 53-75.

**Introduction**

Although Mars today is a dry, cold planet, it may once have been much warmer and wetter [1][6]. Understanding geochemical and degassing history of various volatiles is most important in examination the history of Martian climate and the surface of Mars [4]. How much of the atmospheric volatiles have been incorporated into the rocs of Martian crust for example through the action of water in the past is fundamental and still not solved question [3] [5].

**The role of volatiles in evolution of Martian surface**

The volatiles (e.g. water and carbon dioxide) are molecules that readily evaporate, converting to their gaseous form. Such substances can be released from the crust and planetary interior into the atmosphere and then influence climate. In favorable atmospheric condition these substances can be also retransformed to their previous form. For example on Mars, significant amounts of carbon dioxide go back and forth between polar ice caps and the atmosphere depending on the season (this gas freezes into the polar ice caps during the cold time). The examples of geochemical cycle models of the interaction between the atmosphere, hydrosphere, and regolith of Mars, current understanding the sources of volatiles, the evidences for different climates in the past and various agents of surface modification of Martian surface will be shortly reviewed.

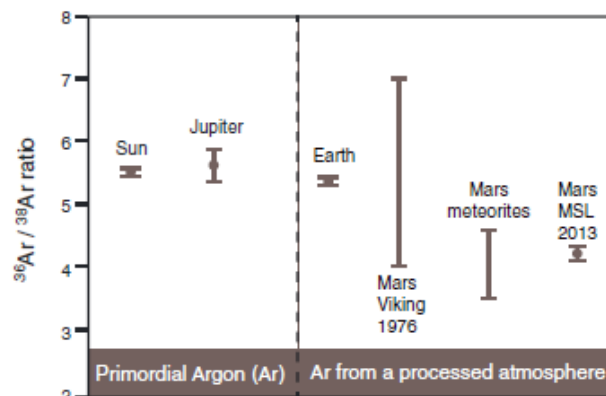


Fig.2 Comparison of the  $^{36}\text{Ar}/^{38}\text{Ar}$  ratio measured in the atmosphere of Mars by Curiosity's SAM-QMS in 2013 with the Viking results in 1976, Mars meteorites, Earth, Jupiter and the Sun. [2]

*Acknowledgements:* The work was supported by the grant: 2011/01/B/ST9/05442

**References:**

[1] Schaefer M.W. and H. Leidecker (1993) Geochemical cycle model for Mars, *Geochim. Cosmochim. Acta*, 57, 4619.  
 [2] Atreya S. K. et al. (2013) Primordial argon isotope fractionation in the atmosphere of Mars measured by the SAM instrument on *Curiosity* and implication for atmospheric loss. *Geophys. Res. Letters*, 40, 5605-5609. [3] Bridges, J.C. et al. (2001). Alteration assemblages in Martian meteorites: implications for near-surface processes. *Space Science Reviews*, 96(1-4), 365 -392. [4] Bethany L. et al. (2013) Geochemical Consequences of Widespread Clay Mineral Formation in Mars' Ancient Crust. *Space Sci Rev* 174, 329–364. [5] Kevin S. Hutchins and Bruce M. Jakosky, (1996) Evolution of Martian atmospheric argon: Implications for sources of volatiles *J. Geophys. Res.* 101, NO. E6, 14, 933-14,949. [6] Lewis J.S. (1997) *Physics and Chemistry of the Solar System., The Terrestrial Planets: Mars, Venus, and Earth*, and the references therein. Academic Press, US

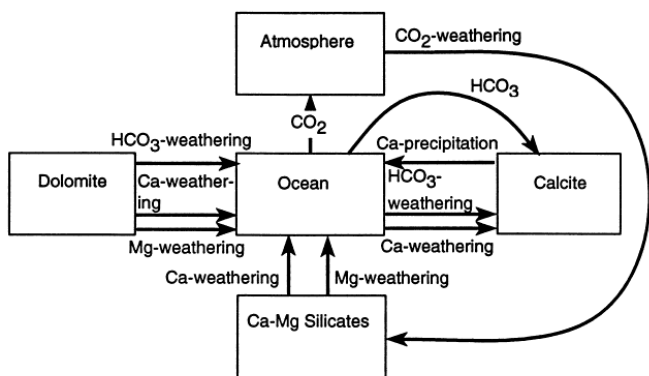


Fig. 1 The example of schematic diagram of geochemical cycle on early Mars. Arrow indicate fluxes of various species caused by different processes [1]

Noble gas species, such as argon and xenon, are particularly useful in establishing connections between the atmospheric and geochemical evolution of the planet. In our review the importance of processes affecting isotopes of argon ( $^{36}\text{Ar}$ ,  $^{38}\text{Ar}$ ,  $^{40}\text{Ar}$ ) will be shortly indicated and the new results from the quadrupole mass spectrometer of the Sample Analysis at Mars (SAM) instrument on Curiosity rover will be described. The  $^{36}\text{Ar}/^{38}\text{Ar}$  ratio of  $4.2 \pm 0.1$  determined by the SAM-QMS is the lowest value yet measured on any object in the solar system except SNCs. This measurement implies loss of atmosphere to space in the past 4 billion years. It also provides a definitive proof that SNCs come from Mars [2].

**LANDSLIDE PROPAGATION: SIMULATIONS OF GRANULAR GRAVITATIONAL COLLAPSE USING MOLECULAR DYNAMICS.** Timur Borykov<sup>1</sup>, Anne Mangeney<sup>2</sup>, Daniel Mège<sup>1,3</sup>, Patrick Richard<sup>4</sup>, <sup>1</sup>WROONA Group, Institute of Geological Sciences, Polish Academy of Sciences, Wrocław, Poland (timur.borikov@twarda.pan.pl), <sup>2</sup>Équipe de sismologie, Institut de physique du globe de Paris, UMR 7154 CNRS, France, <sup>3</sup>Laboratoire de planétologie et géodynamique, UMR CNRS 6112, University of Nantes, France, <sup>4</sup>LUNAM Université, IFSTTAR site de Nantes, France

**Introduction:** Landslides and debris flows sculpt the surface morphology on Earth as well as on other planets. They constitute one of the most efficient mass wasting processes on Mars. [1] Recent researches have studied the fundamental physics of the collapse of granular columns in experimental and numerical approaches [2, 3, 4]. Our work presents a 3D discrete element simulation (DEM) of the axisymmetric and planar (sidewalls) spreading of initially vertical granular columns, in which the runout of the grains and their dynamic motion are continuously monitored during the course of collapse, in order to understand better detailed processes of landslide propagation on Earth and Mars.

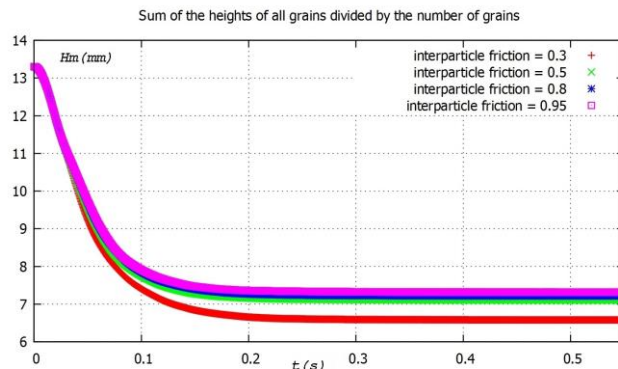
**Numerical model and results:** Simulation is performed using the numerical model and code MODY-GS [5]. This integrates Newton's equations of motion for each of a large number of colliding grains.

Here we systematically study the role of both the effects of the initial condition and input parameters related to the material properties in the spreading of the granular mass. The most important factors that can influence the granular flows properties are: particle-wall, inter-particle (Coulomb), and rolling friction, number of particles, size of grains, coefficient of restitution, aspect ratio and inclination angle. The collapse dynamics is shown to be dependent on the initial geometry of the planar or cylindrical column, and quite independent on the inter-particle (Figure 1) and particle-wall friction, as well as the number of grains for a grain number > 1000. We also observed that the coefficient of restitution  $e$  was extremely changing the behaviour of the systems for  $e \rightarrow 1$ ; in particular, this dramatic change is expected to become more important for increasing values of the aspect ratio.

The scaling for the runout distance showed both a linear and a power-law dependence on the aspect ratio of the initial column, in agreement with previous studies [2, 4]. In order to understand the dynamic behaviour better we analysed many velocity profiles (Figure 2) as a function of the run-out distance and height. The simulation results are in good agreement with previous experimental work (Figure 3) carried out in 3D and quasi-2D configurations [2, 4].

**Conclusions:** We reconfirm the dependence of final deposit shape on the column's initial aspect ratio, and that interparticle frictional effects play only a minor role in the dynamics of spreading. Several different patterns were observed, dependent on the initial aspect ratio, particle-wall and inter-particle friction. Our analysis of axisymmetric and planar granular flows reveal the subdivision into three regimes of flow behaviour dependent on the initial aspect ratio. Scaling laws for the runout and final deposit height as a function of the initial aspect ratio have been found.

**References:** [1] Lucas A., Mangeney A., Mège D.: *J. Geophys. Res. Planets*, 116, E10001 (2011) [2] Lube G., Huppert, H.E., Sparks R.S.J., Hallworth M.A.: *J. Fluid Mech.* 508, 175–199 (2004) [3] Staron L., Hinc: E.J.: *J. Fluid Mech.* 545, 1–27 (2005) [4] Lacaze, L., Phillips, J.C., Kersewell, R.R.: *Phys. Fluids* 82, 063302 (2008). [5] Richard, P., Valance, A., Metayer, J.-F., Sanchez, P., Crassous, J., Louge, M.Y. and Delannay R.: *Physical Review Letters*, 101, 248002 (2008)



Figures 1: Sum of the heights of all grains divided by the number of grains as a function of time (sidewalls case) for various values of interparticle friction.

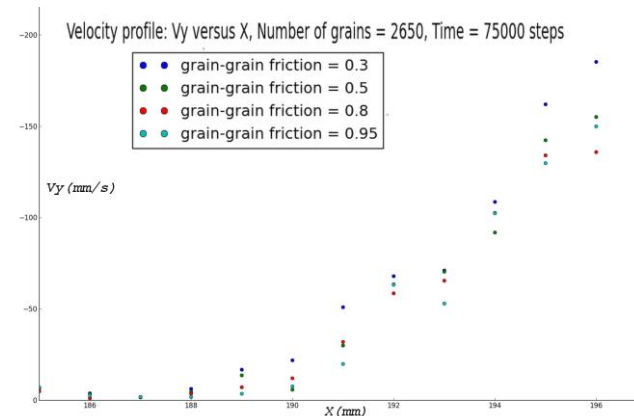


Figure 2: Vertical velocity profiles in the sidewalls case of granular columns. The simulations do not show significant changes in the velocity profiles when the inter-particle coefficient of friction increase.

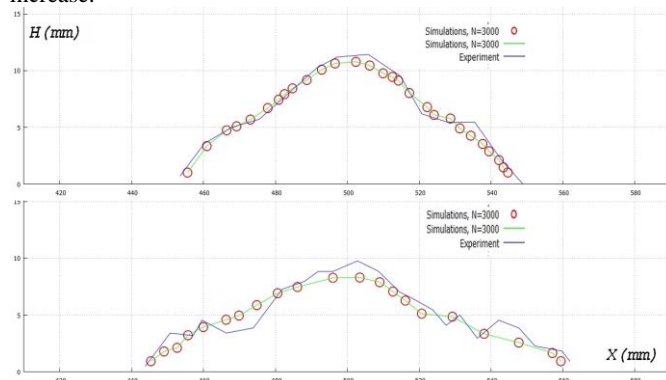


Figure 3: Numerical simulation of spreading of an initially cylindrical granular mass (grain-grain friction coefficient = 0.4, coefficient of rolling resistance = 0.133) at two different times for 3000 grains, compared to experimental results obtained in another work (Maxime Farin, IPGP).

**EVIDENCE FOR POST-NOACHIAN HIGHLY VISCOUS LAVAS IN SOUTHERN HIGHLANDS ON MARS.** Petr Brož<sup>1,2</sup>, Ernst Hauber<sup>3</sup>, Thomas Platz<sup>4</sup> and Matt Balme<sup>5</sup> <sup>1</sup>Institute of Geophysics ASCR, v.v.i., Boční II/1401, 141 31, Prague, Czech Republic, [Petr.broz@ig.cas.cz](mailto:Petr.broz@ig.cas.cz), <sup>2</sup>Institute of Petrology and Structural Geology, Charles University in Prague, Albertov 6, 128 00, Prague, Czech Republic <sup>3</sup>Institute of Planetary Research, DLR, Rutherfordstr. 2, 12489, Berlin, Germany, [Ernst.hauber@dlr.de](mailto:Ernst.hauber@dlr.de), <sup>4</sup>Institute of Geological Science, Freie Universität Berlin, Malteserstr. 74-100, Berlin, Germany, [Thom-as.Platz@fu-berlin.de](mailto:Thomas.Platz@fu-berlin.de) <sup>5</sup>CEPSAR, Open University, Milton Keynes MK7 6AA, UK, [Matt.Balme@open.ac.uk](mailto:Matt.Balme@open.ac.uk).

**Introduction:** Volcanism was globally widespread on Mars in the early history of the planet, but focused with ongoing evolution on two main magmatic provinces in Tharsis and Elysium [1]. On the other hand, evidence for post-Noachian (<3.7 Ga) volcanism in the Martian highlands is rare outside some isolated regions. It is generally thought that highland volcanism occurred early in Mars' history and stopped not later than ~1 Ga after planet formation [2,3]. Here we focus on two spectacular cones with outgoing flow-like features and three dome-like structures surrounded by flow-like units in Terra Sirenum, which may change this view.

**Data:** Images from CTX, HRSC, HiRISE and THEMIS-IR (day and night) were used for this study. Topographic information (e.g., heights and slope angles) was determined from single shots of the Mars Orbiter Laser Altimeter (MOLA) in a GIS environment, and from stereo images (HRSC) and derived gridded digital elevation models (DEM). Absolute model ages were determined from the crater size–frequency distributions, utilizing the software tool ‘cratertools’ and ‘craterstats’ applying the production function coefficients of [4] and the impact-cratering chronology model coefficients of [5].

**Geological setting:** The study area (184°E to 189°E/42°S to 41°S) is located in Terra Sirenum. The area was part of the large Eridania paleolake [6], where episodic liquid water may have persisted far into the Hesperian or even Amazonian period [7]. Hence, our area of interest was probably part of a former lake bottom and the observed surface may be relatively young.

**Morphology:** Several regions of relatively higher thermal inertia are visible in night-time THEMIS images of the study area (Fig. 1). They correspond to two well-developed cones that are associated with flow-like features, and three domical structures also associated with flow-like units. The edges of the flows seem to be relatively steep, reaching values between 4° and 20°. The flows originated from the centers of the cones. In the central part of the study area, three dome-like structures are associated with flows. HiRISE images reveal that the edifices together with their associated flows contain boulders up to several meters large. Two steep scarps are located at the edges of two domes and expose bright material is layered and shows signs of ongoing erosion. Preliminary age determinations based on crater counting suggest that the cones were formed at 0.5 to 1 Ga.

**Discussion:** Based on the similarities to terrestrial obsidian flows, we interpret these features as probably volcanic in origin and post-Noachian in age. They might represent Martian small-scale volcanic cones with associated lava flows, but they are different in morphology to previously observed Martian cinder cones or tuff rings/cones [8-10]. The flows associated with cones have steep edges; in strong contrast to basaltic flows in Tharsis that typically display a low relief and form very gentle slopes. The bright material exposed at the scarps may be pyroclastic material from explosive eruptions associated with the effusion of highly viscous lava (a

situation common on Earth). The observed domes seem to be unique to this region. However, they share some similarities with domical structures in Arcadia Planitia, interpreted as magmatic cryptodomes or extrusive lava domes formed by felsic lava [11,12].

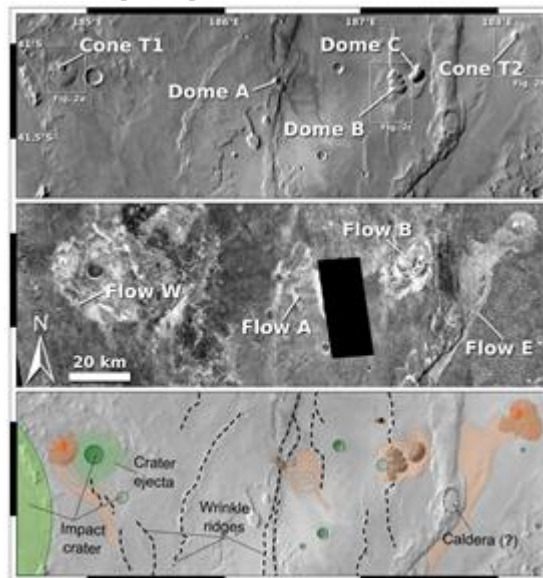


**Fig. 1:** Themis-IR day-time (upper image), night-time (middle), and interpretational map of the study area. The thermal contrast between the two upper images suggests the presence of flow-like structures associated with cones and domes.

**Conclusions:** The steep-sided morphology suggests that highly viscous lava formed them. If so, volcanic edifices composed of evolved magmas may be present in the ‘middle of nowhere’: in the southern highlands far away from any known volcanic centers. We currently have no explanation why and how evolved magmas might have been generated in that region. Our finding may expand our knowledge about evolved magmas on Mars [13-15], which seem to be more widespread than previously thought.

**References:** [1] Grott et al. (2013), *Space Sci. Rev.* 174, 49-111 [2] Williams et al. (2009), *Planet. Space Sci.*, 57, 895-916 [3] Xiao et al. (2012), *Earth Planet. Sci. Lett.*, 323-324, 9-18 [5] Ivanov (2001), *Space Sci. Rev.* 96, 87-104 [5] Hartmann and Neukum (2001), *Space Sci. Rev.* 96, 165-194 [6] Irwin et al. (2004), *J. Geophys. Res.* 109, E12 [7] Wendt et al. (2013), *Icarus* 225, 200-215 [8] Meresse et al. (2008), *Icarus* 194, 487-500 [9] Brož and Hauber (2012), *Icarus* 218, 88-99 [10] Brož and Hauber (2013), *JGR-Planets* 118, 1656-1675 [11] Rampey et al. (2007), *JGR-Planets* 112, E6 [12] Farrand et al. (2011), *Icarus*, 211(1), 139-156, [13] Wray et al. (2013), *Nature Geosci.* 6, 1013-1017 [14] Meslin et al. (2013), *Science* 341, 6153 [15] Sautter et al., *JGR-Planets* 119, 30-46.

**SHARAD DATA MAPPING FOR SURFACE COMPOSITION DETECTION.** Luigi Castaldo<sup>1</sup>, Daniel Mège<sup>1</sup>, Roberto Orosei<sup>2</sup>, Giovanni Alberti<sup>3</sup>, Joanna Gurgurewicz<sup>1,4</sup>, <sup>1</sup>Institute of Geological Sciences PAS, Wrocław, Poland, <sup>2</sup>Istituto di Radioastronomia, Istituto Nazionale di Astrofisica, Bologna, Italy, <sup>3</sup>CO.R.I.S.T.A., Napoli, Italy, <sup>4</sup>Space Research Centre PAS, Warsaw, Poland.

**Introduction:** Synthetic Aperture Sounding is an important advance over conventional sounding, and it can be used to directly resolve the stratigraphy of the subsurface and to determine the composition of the first meters of the surface. Radar echoes can be analyzed to retrieve the permittivity properties of the layers producing surface and subsurface reflections, to constraint or even identify their composition. The signal inversion of sub-surface sounding radar data is an inverse problem for which different approaches have been presented over the years [1], [2]. The Radar Shallow Subsurface Radar (SHARAD) was designed to study the interior of Martian sub-surface [3]. Data collection and processing should be transparent to the user. The first requirement, for the majority of users of SHARAD data, is that the data collection and processing techniques used to produce the images are not an issue so that their attention can focus on science. For the remote sensing scientist working on data processing, the goal is to model the relationship between geophysical parameters and sets of radar backscatter measurements. But to do this, some scientific input are needed in order to determine realistic parameter values that will be used for data calibration [4].

**Calibration model:** The classical method to calibrate the data, i.e. checks of the form of the impulse response, point targets such as trihedral corner reflectors with a large Radar Cross Section [5], cannot be employed on Mars surface, moreover the SHARAD reflectivity processing requires more than 2 TB of data volume. An automatic method for locating echoes has been developed to be applied to the set of global Mars data, dedicated to the extraction of the surface echo. Several parameters affect the surface echo power: the permittivity constant, roughness, and slope. Most backscattering models separate the effect of the permittivity constant from the remaining parameters [6]. In order to improve The S/N, a low-pass filter operates in azimuth, and a local regression is adopted using weighted linear least squares and a 2nd degree polynomial model on the radargrams for the benefit of keeping better uniformity of the horizontal continuity of the echoes. The wavelength of the signal is greater than the plasma frequency of the ionosphere, allowing it to pass there through. However, during the propagation of the wave, disturbances may occur, depending on the solar zenith angle between the satellite and the position of Mars. For this reason, only nocturnal data are used. A 3D electromagnetic model has been developed to estimate the backscattering from natural rough surface [7] in order to correct the variation of the echo power due to the observed geometry. A fractal geometry model has been adopted as it is scale invariant, and has high fidelity in surface backscattering estimate. The data adopted for the fractal backscattering estimate are the Precision Experiment Data Records of MOLA [8]. The model is based on the following main assumptions: (1) scattering takes place at the interface between two media, i.e. space and the Martian surface; (2) the first medium is supposed to have the permittivity of open space, the second medium is supposed to be homogeneous and non-dispersive. With these assumptions, the power backscattered by the surface is directly measurable from radargrams and can be evaluated by using the classical “radar equation” [9]. The calibration of the signal requires the de-

termination of a calibration area. The chosen calibration area is located inside the North Polar cap, between 82°N and 84°N, and between 180°E and 200°E. The area consists primarily of water ice with a few percent of dust [10].

**Surface composition:** The model reveals the contribution due to the permittivity properties of the surface material. This signal is highly dependent on physical parameters (permittivity and roughness) characterizing the near surface (0-10 m deep), we can therefore potentially learn about its composition. A calibration procedure has been assessed in order to derive a relationship between the geophysical parameters, the permittivity constant, and a set of radar backscatter measurements. The model to extract the permittivity constant of the surface of Mars from the echoes of the radar takes into account the signal distortion source. The relative strength of the surface echo is equated to the reflectivity, and the effects of surface roughness are modelled using the MOLA topographic dataset. The resulting information provides insight on the nature of the materials constituting the Martian surface. The results are the production of permittivity constant maps of the Martian surface.

**References:** [1] Smith, D.E., et al., (1999) The global topography of Mars and implications for surface evolution, *Science* 284, pp. 1495–1503. [2] Franceschetti, G., D. Riccio, (2007) *Scattering, Natural Surfaces, and Fractals*, BURLINGTON (MA) ACADEMIC PRESS. [3] Seu, R. J. Phillips, D. Biccari, R. Orosei, A. Masdea, G. Picardi, A. Safaeinili, B. A. Campbell, J. J. Plaut, L. Marinangeli, S. E. Smrekar, D. C. Nunes, (2007) SHARAD sounding radar on the Mars Reconnaissance Orbiter, *JOURNAL OF GEOPHYSICAL RESEARCH*, VOL. 112, E05S05, doi:10.1029/2006JE002745. [4] Currie, N. C., Ed., (1984) *Techniques of Radar Reflectivity Measurement*. Norwood, MA Artech House. [5] Gray, L., P. W. Vachon, C. E. Livingstone, and T. I. Lukowski, (1990) “Synthetic aperture radar calibration using reference reflectors,” *IEEE Trans. Geosci. Remote Sensing*, vol. 31, pp 374–383. [6] Ulaby, F., Moore, T.R., Fung, A., (1986) *Microwave Remote Sensing*. Artech House Publishers. [7] Castaldo L., et al., (2013) Scientific Calibration of SHARAD Data over Martian Surface, *SIGNAL PROCESSING SYMPOSIUM*, Jachranka Village, Poland, 978-1-4673-6319-8/13/S31.00 c IEEE /ISBN COPYRIGHT REG. NO. ISBN 978-1-4673-6318-1. [8] Smith, D.E., et al., (2001) Mars Orbiter Laser Altimeter (MOLA): Experiment Summary after the First Year of Global Mapping of Mars, *Journal of Geophysical Research* Volume 106, Issue E10, pages 23689–23722, 25 October 2001, doi: 10.1029/2000JE001364. [9] Albee, A.L., Arvidson, R.E., Palluconi, F. and Thorpe, T., (2001) Overview of the Mars Global Surveyor mission. *Journal of Geophysical Research* 106: doi: 10.1029/2000JE001306. issn: 0148-0227. [10] Grima, C., W. Kofman, J. Mouginot, R. J. Phillips, A. Hérique, D. Biccari, R. Seu, and M. Cutigni, (2009) North polar deposits of Mars: Extreme purity of the water ice, *Geophysical Research Letters*, 36(3), 2-5, doi:10.1029/2008GL036326.

**Introduction:** SHARAD is a synthetic aperture, orbital sounding radar, carried by NASA's Mars Reconnaissance Orbiter [1]. The echo from the surface itself is useful to study the first layer of the Mars surface. A proper mathematical model, in condition of favorable radar viewing geometry, interface scattering, surface and volume scattering, and material properties, may allow to realize a surface permittivity map. The study of the reflectivity of the surface echo is a means to obtain information on the composition and geometry of the ground. SHARAD data gathering and processing should be transparent to the user, the first requirement, for the majority of users of SHARAD data, is that the data collection and processing techniques used to produce the images should be irrelevant, and scientific properties should be the main interest. A mathematical method of calibration has been developed, adopting a models of surface scattering in place of "ground truth", to estimate the variation of geophysical parameter as geometry variations, slopes and material composition and possibility of ice presence, across the Martian surface.

**Scattering model:** Scattering from natural surfaces plays a fundamental role in wave propagation and remote sensing. Mathematical models of the natural surfaces on Mars or other ones too are not available because of surface complexity. Instead, the fractal geometry approach has been used, and proved useful because of the surface under investigation are originated by natural phenomenon and doesn't have artificial artefact [2, 3]. The reason is that forces that model natural surfaces (gravity and microgravity, tensions, frictions, vibrations, erosion, thermal and freezing gradients, chemical reaction, etc.; as well as periodic and aperiodic happenings: seasons and vegetation changes, sun, wind, rain, snow, slides, subsidence, etc.) generate surfaces whose topological dimension is larger than 2 [4]. The fractal geometry has been used to match a mathematical abstraction of fractal physics and electromagnetic field. Under those assumptions a model has been developed to use fractal geometry parameters from MOLA altimetry data [5, 6].

**Calibration modelling:** The signals extracted from the RDR need still several corrections in power in order to be comparable. These corrections show the influence of orbitographic phenomena (changes of altitude), technical issues (satellite orientation, acquisition mode) geometry of the acquisition signal. In order to handle the SHARAD data, some problems need to be solved:

- Tracking of the surface echo position in the recorded echoes in a simple and fast enough, but also robust way in order to minimize the number of errors in surface detection.
- Estimation of the power losses due to the shape of the geometry.

The calibration of the signal requires the determination of a constant that takes into account the backscattering gain due to the radar system and the surface in order to compensate the power losses due to the orbitographic phenomena [7]. The constant has been calculating starting from the power backscattered on a particular area on Mars where the permittivity constant is known, taking care to neglect all the terms depending on the geometry, ground and orbit.

**Results:** Signal calibration made possible the realization of mapping the real part of the permittivity constant for the

Martian surface (Figure 1). Such map provide a look into the nature of the materials constituting the Martian surface and to the statistical presence of ice. In particular, low values of surface permittivity indicate either a very loose, porous regolith or an ice-rich terrain, whereas high values are characteristic of solid rock. The permittivity constant maps can eventually be used to help identify the areas where ice can be found. The map shows the values of the real part of the permittivity constant of the Martian surface penetrating in the first layer till a maximum of 15 m. The value of the permittivity of water ice i.e.  $\epsilon_{ice}$ , can be selected in the map using Mätzler model [8] for pure ice as follows:

$$\epsilon_{ice} = \epsilon_M \pm std(\epsilon_{mod}) \quad (1)$$

Where respectively  $\epsilon_M$  is the value of the permittivity of pure water ice by the Mätzler model, while  $\epsilon_{mod}$  indicate the different values of the real part of permittivity for each resolution cell in the map.

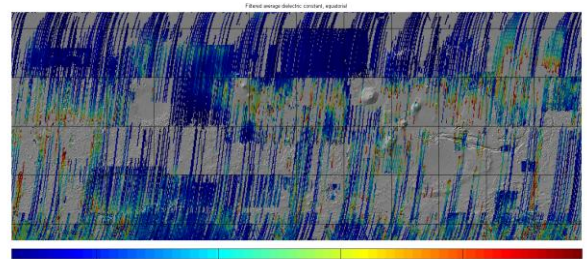


**Figure 1** Permittivity constant equatorial map of Mars [-70° 70°; 0° 360°]. The permittivity constant goes from the lowest value, assimilable to pure CO<sub>2</sub> ice or very porous regolith, to higher values, characteristic of solid rock. The water ice can be located in areas using (1).

**References:** [1] Seu, R., et al., (2007) SHARAD sounding radar on the Mars Reconnaissance Orbiter, *J. Geophys. Res.*, 112, E05S05, doi:10.1029/2006JE002745. [2] Mandelbrot, B. B., (1983), *The fractal geometry of nature*, Editor Freeman, San Francisco. [3] Brown, S.R., C.H. Scholz, (2012) Broad bandwidth study of the topography of natural rock surfaces, Article first published online: doi: 10.1029/JB090iB14p12575. [4] Franceschetti G., A. Iodice, M. Migliaccio, and D. Riccio, (1999) Scattering from natural rough surfaces modeled by fractional brownian motion two-dimensional processes, *IEEE Trans. Antennas Propag.*, vol. 47, no. 9, pp. 1405–1415. [5] Kreslavsky, M.A., Head, J.W. (1999), Kilometer scale slopes on Mars and their correlation with geologic units: initial results from Mars Orbiter Laser Altimeter (MOLA) data. *J. Geophys. Res.* 104, pp. 21911–21924. [6] Seu, R. et al., (2007) SHARAD sounding radar on the Mars Reconnaissance Orbiter, *J. Geophys. Res.*, VOL. 112, E05S05, doi:10.1029/2006JE002745. [7] Castaldo L., et al., (2013) Scientific Calibration of SHARAD Data over Martian Surface, Signal Processing Symposium, Jachranka Village, Poland, 978-1-4673-6319-8/13/S31.00 c IEEE / ISBN COPYRIGHT REG. NO. ISBN 978-1-4673. [8] Mätzler C., (1998), Microwave properties of ice and snow, in Schmitt, B., et al. (eds.) "Solar System Ices", *Astrophys. and Space Sci. Library*, Vol. 227, Kluwer Academic Publishers, Dordrecht, pp. 241-257.

**Introduction:** The rheology of glaciers is complicated. Generally it is solid but for very slow processes it behaves like a viscous fluid with the viscosity given by:

$$\eta(T) = \eta_0 \sigma^{(1-i)} \exp\left(\frac{E}{RT}\right)$$

where  $\eta_0$  is a constant,  $\sigma$  is the second invariant of deviatoric of stress tensor ( $\sigma$  is high for fast deformation),  $i$  is the power law index ( $i=1$  corresponds to a Newtonian fluid, but rather  $i>3$ ).  $E=E_0+pV_0$  is the activation energy of the dominant mechanism of deformation, where  $p$  is the pressure.  $R=8.314$  [J K<sup>-1</sup> mole<sup>-1</sup>] is the universal gas constant [1, 2].

Parameters  $\eta_0$ ,  $E_0$ ,  $V_0$  and  $i$  depend on many factors; e.g. size of ice crystal, content of gases, etc.. Note that  $E$  is proportional to the melting temperature.

Consider now the second factor: If  $i > 1$  then the term is low (i.e. viscosity is low) if the rate of deformation is high (i.e. for high velocity gradient).

**Numerical model:** We model considered processes of glacier's flow using the following equations [3]:

$$\rho_0 \frac{D\mathbf{v}}{Dt} = -\nabla p + \nabla \cdot (2\eta \mathbf{D}) + \rho \mathbf{g}$$

$$\frac{\partial T}{\partial t} + \mathbf{v} \cdot \nabla T = \kappa \nabla^2 T + q/c$$

where  $t$  is time [s],  $\mathbf{v}$  velocity vector [m s<sup>-1</sup>],  $\mathbf{D}$  tensor of rate of deformation [s<sup>-1</sup>],  $\rho$  density [kg m<sup>-3</sup>],  $\mathbf{g}$  gravity [m s<sup>-2</sup>],  $\rho_0$  density at  $T=0$ ,  $T$  temperature [K],  $\alpha$  coefficient of thermal expansion [K<sup>-1</sup>],  $\eta$  viscosity [Pa s],  $c$  specific heat [J kg<sup>-1</sup> K<sup>-1</sup>],  $\kappa$  coefficient of temperature diffusion [m<sup>2</sup> s] (note:  $\kappa = k/(\rho c)$  where  $k$  is thermal conductivity [W K<sup>-1</sup> m<sup>-1</sup>]).

We consider 1 dimensional (1 D) model. It could be used for regions in the middle part of glaciers – Fig. 1.

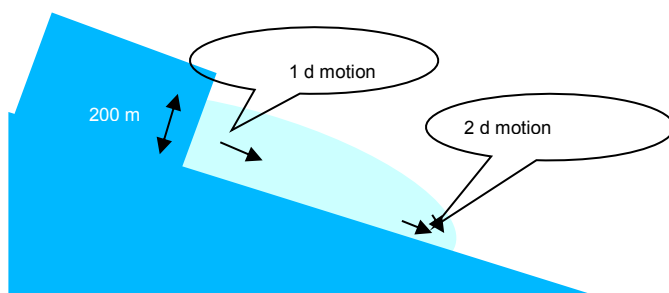


Fig.1. Sketch of flow regimes in a glacier.

**Earth-Mars comparison:** Gravity is the main driving force of glaciers. The gravity difference of these two planets leads to significant difference of glacier's motion – Fig. 2.

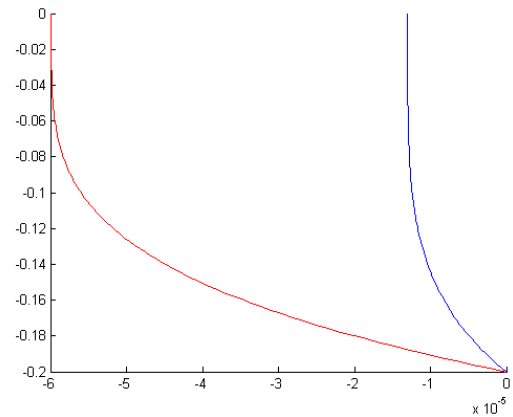


Fig. 2. Velocity profile (the vertical scale gives depth in m, the horizontal scale gives velocity in m s<sup>-1</sup>) for the Earth (red line) and for the Mars (blue line). The gravity is the only different parameter in these models.

**Role of geothermal heat flow:** We observe dramatic increase of the velocity for some critical value of heat flow density (similar to effect known as glacier surge but of different origin) for limited heat flow (~0.2 W m<sup>-2</sup>) – Fig. 3. Note that this value of heat flow is substantially less than for volcanic region (~20 W m<sup>-2</sup>).

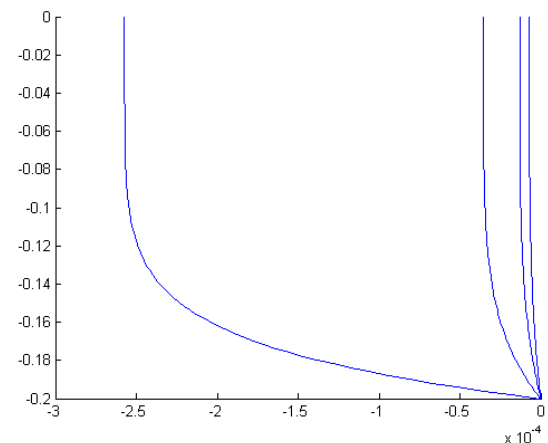
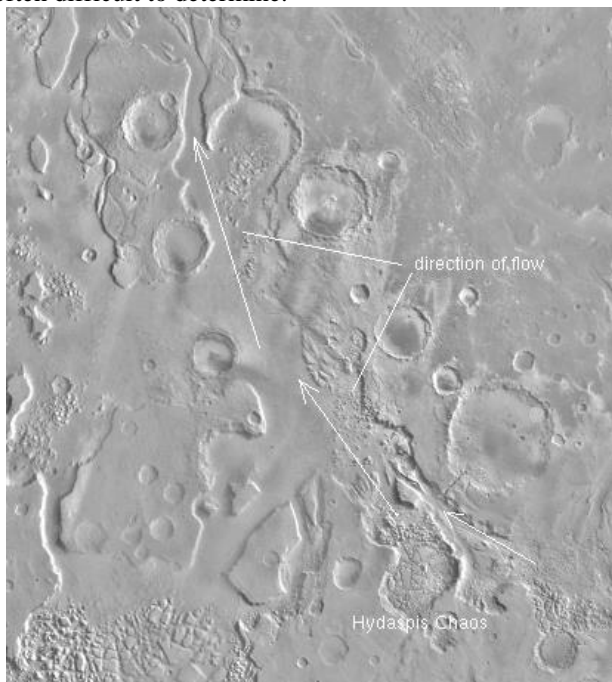


Fig.3. Effects of the heat flow variation for the Mars. The velocity profiles correspond to heat flow density of: 0.02, 0.05, 0.1, 0.2 W m<sup>-2</sup>, respectively (the leftmost line corresponds to the highest heat flow). The rest as in Fig. 2.

**Acknowledgements:** The research is partially supported by National Science Centre (grant 2011/ 01/ B/ ST10/06653). Computer resources of Interdisciplinary Centre for Mathematical and Computational Modeling of Warsaw University are also used in the research.

**References:** [1] Durham, W.B., Kirby, S.H., Stern, L.A., 1998, Rheology of planetary ices. In: Schmitt, B., de Bergh, C., Festou, M. (Eds.), Solar System Ices. Kluwer Academic Publishers, Dordrecht, 63-78. [2] Goldsby D. L., Kohlstedt D.L., 1997. Grain boundary sliding in fine-grained Ice-I, Scr. Mater. 37, 1399-1405. [3] Czechowski L., The motion of martian glaciers and geothermic heat flow. Martian Cryosphere Workshop, Wrocław, February 10th, 2014.

**Introduction:** There are a large number of traces of flowing liquid on the surface on Mars in the past. Two kinds of ancient 'rivers' are found: wide outflow channels and network systems of channels with tributaries similar to terrestrial river's systems. Those structures are often millions/bilions years old and they are considerably modified. So, many details are removed/destroyed and the origin of a given structure is often difficult to determine.



**Fig.1.** An example of the outflow channel

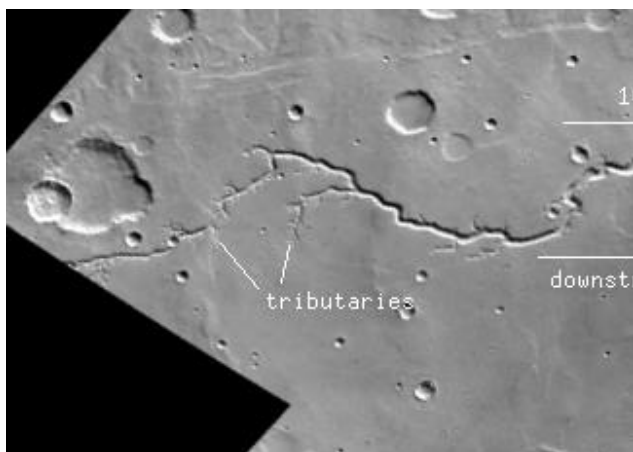


**Fig.2.** An example of the .network of channels with tributaries.

**Basic properties of possible flowing media:** a few different media should be considered for Mars:

- Fresh water: density
  - 1000 kg/m<sup>3</sup>, viscosity 0.00152 Pa s
- Brines:
  - 1200 kg/m<sup>3</sup>, viscosity 0.002 Pa s
- Silicate lava:
  - 2500-2900 kg/m<sup>3</sup>, viscosity 102-105 Pa s strongly temperature dependent
- Water ice and some silicates (glacier):

- 940-1100 kg/m<sup>3</sup>, nonlinear viscosity 105-107 Pa s depends on invariant of stress tensor.
- Mixture of water, sand and ice:
  - 950-1500 kg/m<sup>3</sup>, complicated rheology.

**Numerical model:** We started from modeling the fresh water river. We used model NCCHE based on the dynamical equations of the fluid and sediments transport [1, 2].

**Some results:** Fig. 3 presents two models where the gravity is the only different parameter. Note substantial differences between these models.

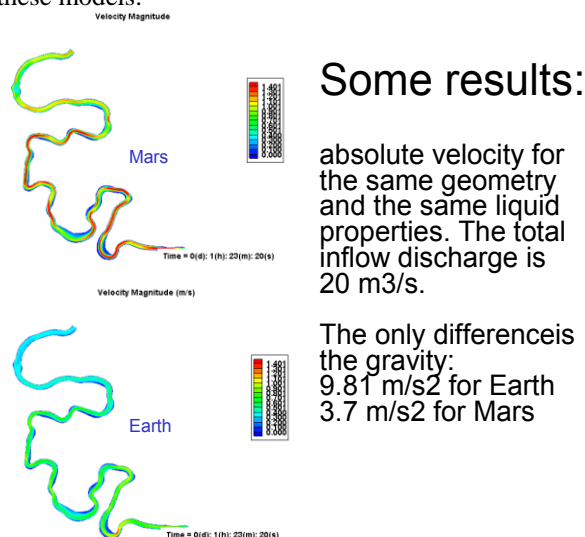


**Fig. 3.** Absolute velocity calculated for the same geometry and the same parameters of the flow. The gravity is the only different parameter in these models: for the upper model it is 3.7 m s<sup>-2</sup> and 9.81 m s<sup>-2</sup> for the lower model.

**Our plans:** We are going to determine basic differences between evolutions of flowing liquids on other celestial bodies comparing to Earth. It could be useful for interpretation of the data obtained from space missions. Note that the most of these data come from remote sensing. It is an important difference comparing to terrestrial sedimentology. The research will be continued in the frame of **Extraterrestrial River's Modeling Group**.

**Acknowledgements:** Programs developed by NCCHE are used in the research. The research is partially supported by National Science Centre (grant 2011/ 01/ B/ ST10/06653).

**References:** [1] Wu W., 2001. CCHE2D Sediment Transport Model (Version 2.1). Technical Report No. NCCHE-TR-2001-3. [2] Zhang Y., 2006. CCHE-GUI – Graphical Users Interface for NCCHE Model User's Manual – Version 3.0. Technical Report No. NCCHE-TR-2006-02.

**Introduction:** Images obtained by the Mars Reconnaissance Orbiter (MRO) Context Camera (CTX) covered ~85% of the Martian surface to February 2013 [1]. The images of resolution 6 m/pixel provide a good background for detailed landform mapping of Mars. We report on detailed geomorphologic mapping of western Valles Marineris based on USGS ISIS processing and ArcGIS mapping.

**Mosaicing procedure and datasets:** 607 CTX images were selected to cover the interior of 9 Valles Marineris chasmata (except Eos, Capri, and Ganges) and the adjacent plateaus. Each CTX image file was processed separately in sequence by 5 ISIS subprogrammes: *mroctx2isis*, *spiceinit*, *ctxcal*, *ctxevenodd*, and *cam2map*. The *cam2map* level was conducted by using a template file created previously in *maptemplate*. Image resolution was decreased to 12 m/pixel. The collection of processed images was then divided into 21 sets for mosaicing, for compliance with ISIS file size limitations. Tone matching was achieved in *equalizer* and mosaic creation in *automos*. Eventually, mosaic CUB files were converted to ArcGIS compatible PNG files using *isis2std*.

MRO HiRISE images and Mars Global Surveyor MOLA altimeter datasets were used for CTX image interpretation.

**Mapping:** Valles Marineris chasmata extend over 650 km x 2000 km in the equatorial part of Mars. Chasma walls, floors, and landforms inform on 4 Gy of Mars' history, recording a broad range of magmatic, tectonic, fluvial, lacustrine, glacial, eolian, and gravitational processes [2, 3]. The investigated areas include Ius, Tithonium and western Melas chasmata. The first mapping steps consist in mapping morphological features, i.e. trough contours, landslide scarps and main geomorphological bodies, ILDs, dune areas, sapping channels, spur and gullies, and wall types.

**New results:** This work has allowed new geomorphological observations to be made, as illustrated by the two examples below.

*Dune areas* are characterized by different sand source [5], dune type (barchans, transverse dunes, longitudinal dunes), exposure size (from ~100 m<sup>2</sup> to ~100 km<sup>2</sup>), and lithology (bright and dark dunes). The preliminary investigation based on 20 largest dune fields on the Ius Chasma

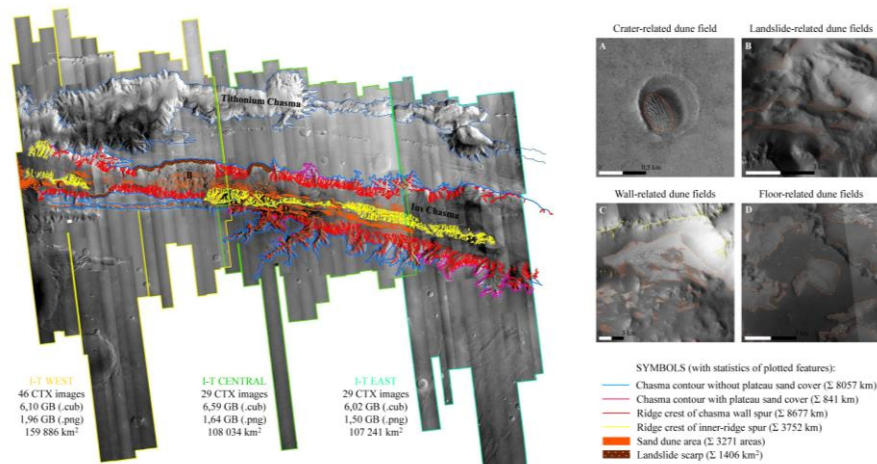
floor, shows that average dune spacing (measured between crests) is 50 m and the predominant facing direction of dune slopes is W-E. In vast, open floor areas a dune type (transverse, longitudinal) is dependent only on predominant wind direction inside chasma. Dune sands in western chasmata are delivered from intra-chasma main sources (landslides, walls) and secondary sources (interior layered deposits (ILDs), floors and craters) (Fig. 1A-D). Floor source is a stratigraphically homogeneous unit observed in the southern Ius trough, probably of detrital origin, in which dunes (Fig. 1D) occupy erosional hollows. They are thought to form *in situ*. Landslide-related dunes dominate in the northern trough. Dunes from wall sources are widespread.

*Spur and gully* morphology analysis has revealed three different types of gully morphology: active (with a visible evidence of modern sediment transport; common), inactive (with a lack of transport; rare) and grooved (displaying up to 100-meter wide shallow flat-floored linear grooves parallel or oblique to the local slope; common on the central Ius inner ridge). The grooves might result from a creeping process of viscous surface material.

**Summary:** Ongoing systematic high-resolution mapping in Valles Marineris is revealing geomorphologic features and processes that had not been recognized before. Full mapping will be completed in 2015.

**References:** [1] Harrison T. et al. (2009), Present-Day Gully Activity Observed by the Mars Reconnaissance Orbiter (MRO) Context Camera (CTX), *BAAS*, 41, 1113. [2] Mège D. and Bourgeois O. (2011), Equatorial glaciation on Mars revealed by gravitational collapse of Valles Marineris wallslopes, *Earth Planet. Sci. Let.*, 310. [3] Carr M. and Head J. (2010), Geologic history of Mars, *Earth Planet. Sci. Let.*, 294, 185-203. [4] Quantin C. and Allemand P. (2005), Fluvial and lacustrine activity on layered deposits in Melas Chasma, Valles Marineris, Mars, *J. Geophys. Res.*, 110 (E12S19). [5] Chojnacki M. et al. (2014), Valles Marineris dune field provenance and pathways, *Icarus*, 232.

**Fig. 1** Left: Current stage of development of the western Valles Marineris map. Right: Examples of different types of dune fields (right A-D).



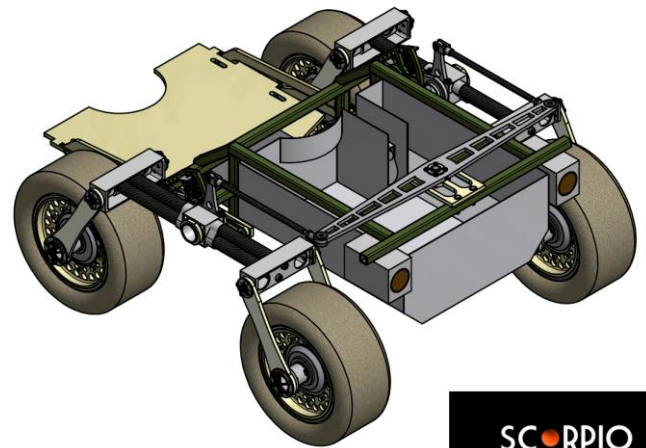
**SCORPIO 4 AS AN EXAMPLE OF STUDENT APPROACH TO HUMAN-OPERATED MOBILE ROBOT CONSTRUCTION.** Szymon Dzwonczyk, Project Scorpio, Wrocław University of Technology, [szymek@dzwonczyk.pl](mailto:szymek@dzwonczyk.pl), of-froad.pwr@gmail.com

Growing popularity of student teams involved in space engineering programs and competitions entails a great motivation for the university students to perform low-budget projects based on many simple yet effective ideas.

After a big success of the Scorpio 3 Mars Rover, which took second place in an international competition - University Rover Challenge, the Wrocław University of Technology student team started a more ambitious and innovative long-range project.

The Scorpio 4 project is a new approach to the subject of human-operated mobile scientific platforms, called rovers. As the Scorpio rover is planned to participate in future URC competitions and European Rover Challenge in 2014 as well, it's construction has to be universal and flexible. From the basis Scorpio 4 is planned to be a semi-autonomic human-operated vehicle, which means that the team had to verify most of the assumptions connected to professional constructions of Mars rovers. This point of view made the team think about building a robot, which could be more ergonomic and easily adaptable but still being able to perform some complicated science or human-assistance related tasks. This involved starting many research projects, such as for example: stereo-vision system with depth illusion, work on more intuitive operating of the rover and it's robotic arm, obstacle attention system and more human-focused approach to the rover off-road suspension.

Scorpio 4 Project statement is to build a simple and reliable mobile platform, which could support any professional scientific equipment, but could be operated by a non-professional user. It's main goal is to help scientists perform space related experiments still on Earth.



### The MARS2013 simulation

Based upon a series of precursor field missions, the OeWF – in partnership with the Ibn Battuta Center for Field Exploration and partners from 23 countries – organized a Mars analog mission in the Tafilalt-region near Erfoud in the Northern Sahara, Morocco, between 26th of January and 3rd of March 2013 (Fig 1).

Mars-analog simulations are regarded as the most comprehensive tool for optimizing the deployment and usage of expedition assets on Mars [1]. Scenarios and methods have been developed for surface mobility and field work, for in-situ exploration [2], regarding human factors [3] and on human-robotic cooperation [4] for various surface exploration strategies [5,6]. However, only few of these missions have fidelity levels, such as a) time-delayed communication between Earth and Mars, b) a realistic balancing of decision making autonomy between the space and the ground segment, or c) simultaneously managing multiple human and robotic assets.



**FIG.1.** Direct comparison of the Station Peyer test site of MARS2013 (after a sand storm causing the hazy atmospheric conditions, image take by K. Zanella-Kux) and Mount Sharp in the Gale crater, observed by Curiosity (image:NASA)

### Mission infrastructure

The MARS2013 field campaign comprised of: 1) a Mission Support Center (based in Innsbruck, Austria) divided into flight control, flight planning, remote science support and ground support teams; and 2) a field team (based near Erfoud, Morocco) including four analog astronauts wearing two analogue space suits. During the mission, data send from the field was analyzed by the Remote Science Support team during the following day and used by the Flight Plan team to prepare detailed plans for future actions of the Field Crew. Entire operation was coordinated by the Flight Control team.

Nineteen experiments in geoscience, (tele)robotics, human factors/biomedicine and astrobiology were conducted. Performed experiments included technical tests of two advanced spacesuit simulators, four robotic vehicles, a stationary sensor platform, a GPS-independent geolocation tool and a deployable shelter.

Ten minutes time-delay in communication between those Mission Support Center and field team was introduced in order to simulate the average time delay in communication between Earth and Mars ranging from 3 to 24 minutes. All of the tasks of remote science support team and field team were performed “blindly” (i.e. without any prior knowledge obtained from the field geological research of the landing site) to avoid unrealistically high situational awareness. Enforcing this concept facilitated a comparison between the

actual ground truth of this well-studied area and the hypothesis compiled solely by the simulated and field data.

### Selected Results

Complimentary to a series of robotic and spacesuit engineering tests, the following research highlights were obtained:

- Procedures describing interactions between large and diverse teams, working in condition of time-delay in communication on a planetary mission were defined.
- Despite the limitations of high fidelity analog-research and without prior knowledge of the test site, previous water activity was identified on a small scale.
- Measuring the work speed of an suited astronaut vs an unsuited test subject yielded a 1.3-fold increase.
- Using thermal inertia measurements as a field method for detecting cave entrances was demonstrated.
- Three robotic vehicles, two spacesuit simulators and a deployable shelter successfully tested (Fig. 2).
- A injury risk assessment of actual injuries yielded a ratio between the Mission Support Center vs field crew of 1:4, with an inversion of this ratio when it comes to non-traumatic incidents.
- Using a spatially referenced database was shown to be an efficient way of data processing and data utilization in a long-duration analog mission with large amount of data to be handled.



**Fig. 2:** The Aouda.X spacesuit simulator and the GLXP Puli rover demonstrating human-robotic interaction.

### References:

- [1] Osinski, G.R., Lee, P., Berinstain, A., et al. (2007) Science from a lunar or Martian base: lessons learned from the scientific exploration of the Haughton crater, Canadian High Arctic, *International Workshop-Exploring Mars and its Earth Analogs II*, Trento, Italy.
- [2] Cockellz C.S. (2001) Martian polar expeditions: problems and solutions, *Acta Astronautica* 49: 693-706.
- [3] Groemer, G., Gruber, V., Bishop, S., Peham, D., Wolf, L., Hoegl, B. (2010) Human performance data in a high workload environment during the simulated Mars expedition “AustroMars”, *Acta Astronautica* 66: 780–787.
- [4] Huntsberger, T., Rodriguez, G., Schenker, P.S. (2000) Robotics challenges for robotic and human Mars exploration, in: *Proceedings of the ROBOTICS2000, Albuquerque*, pp. 340-346.
- [5] Hoffman, J., Kaplan, D.I. (1997) Human exploration of Mars: the reference mission of the NASA Mars Exploration Study Team; *NASA Special Publication 6107*.
- [6] Kereszturi, A. (2011) Geologic field work on Mars: Distance and time issues during surface exploration *Acta Astronautica* 68: 1686-1701

**Summary:** The paper covers an overview of the penetrator devices which provide access to the underground layers of the planetary regolith. An important part of the article is devoted to the new driving concepts of drills and penetrators. The common feature of those mechanisms are their originality and application for planetary exploration. The demand for the use of those mechanisms is quite obvious in space exploration and in situ research. It can also be predicted that its role will expand in upcoming decades given the planned intensification of space exploration. Among reviewed instruments are several different kind of low speed penetrators, mainly self inserted by electromagnetically driven hammering. The first application domain of penetrators is to employ them as carriers of sampling devices and other various sensors for investigation of subsurface ground chemical and physical properties. Developed penetrators due to their high stroke energy and possible operation in microgravity conditions are very well adapted to that purpose. In 1997 CBK PAN proposed a unique solution that has not been applied before in space missions – a hammering insertion device [1] with an electromagnetic drive (Figure 1).



Fig.1. MUPUS - electromagnetically driven insertion device.

The main design challenge was focused on construction of possible simple but powerful drive. The principle of operation of the hammer-driven penetrator is well known and described in [1]. Here is only worth to remind that it bases on mechanical interaction between its three main masses components: mass of the hammer, mass of the inserted rod and the counter-mass (the inertial support of the system). Important is to optimize proportion between the masses components, however the hammer drive is one of the most crucial subsystem.

The requirements of simple but powerful drive fulfills an electromagnetic drive which can transform electric, accumulated in capacitor energy into direct linear motion of the hammer. The principle provides high acceleration of the hammer with relatively short (a few millimeters) stroke. In comparison, to parallel developed solutions where energy is accumulated in the helical spring [2] (Figure 2).



Fig.2. Mole penetrator KRET driven by the helical spring.

One of the electromagnetically driven penetrator's application is sampling of subsurface ground. For that reason a unique geological penetrator CHOMIK for the Phobos Sample Return mission has been developed [3] (Figure 3).

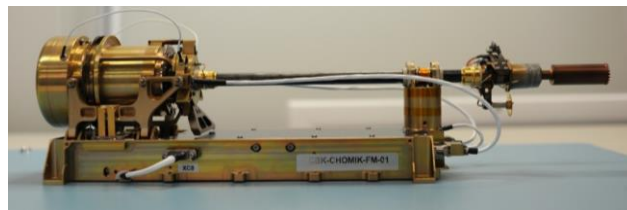


Fig. 3. CHOMIK – sampling geological penetrator

The electromagnetic direct drive has two intrinsic advantages: (1) mechanical simplicity of the drive which replaces motors, gears, screws, special latches or cams, necessary to realize energy transfer from the spring; (2) feasible for power settings (PS) while this feature is practically not achievable for the spring drive mechanisms. Power settings regulation allow to operate at optimal accommodation of the power to the adequate soil mechanical properties. Then destructive, higher than unavoidable overloads on sensors and electronics are not occurred. Possessing of many PS-es allows for selecting the most effective one for determined ground material properties. Figure 4 shows that insertion at PS3 requires 2-3 times less energy than on the other ones.

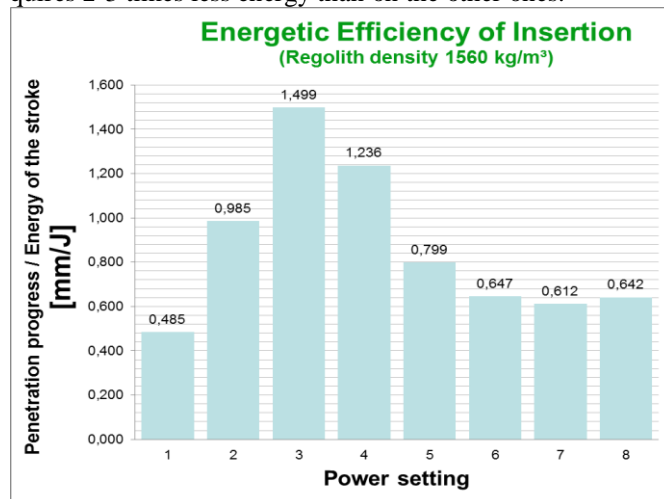


Fig. 4. Penetration progress depending on PS.

Recently a lot of development is focused on a new methods of penetration which are optimal for sampling acquisition. Below in Figure 5 is shown a system where the penetrator rod is divided into outer tube and inner rod and both elements are provided in separate drives.

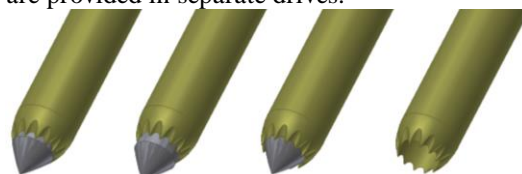


Fig. 5. Dual drive penetrator with sampling features.

**References:** [1] Grygorczuk, J., Banaszekiewicz, M., Seweryn, K., Spohn, T. (2007). MUPUS Insertion device for the Rosetta mission. *Journal of Telecommunications and Information Technology*. 1/2007, 50-53. [2] Grygorczuk, J. et al. (2009). Technological features in the new mole penetrator "KRET". In Proc. 13<sup>th</sup> ESMATS, Vienna, Austria. [3] Grygorczuk, J. et al. (2011). Advanced mechanisms and tribological tests of the hammering sampling device CHOMIK. In Proc. 14<sup>th</sup> ESMATS, Constance, Germany.

Isidis Planitia includes many landforms that result from paleo and contemporary climate regimes. These include the so-called Thumbprint Terrain [10], dating back from the Early Hesperian, but the origin of which is still under discussion [1,2,3,5,6,7,12,15]. A new geomorphic mapping initiative studying the basin of Isidis as a whole at high resolution has been completed for the first time. The data elucidates on landforms inter-relationship and spatial organization. Isidis Planitia is composed of several geological units according to Ivanov et al [9]. All the landforms described in this study are located on 3 of these units: (1) *HApC* unit, i.e. plain with Thumbprint Terrains located in the center of the basin, (2) *Hps* unit, i.e. smooth plain surrounding *HApC* unit and (3) *Hmk* unit composed of knobby material located discontinuously on *Hps* unit. Five categories landforms has been described: 1) a *Geological Contact* between *HApC* and *Hps* units; 2) cones organized in three different ways (*Aligned Cones*, *Isolated Cones* and *Cones in Fields*); 3) *Arcuate Ridges*; 4) *Simple Ridges* characterized by their sinuous shape; 5) *Linear Depressions*. We find relationships between all categories of landforms. The clearest one is the relationship between Aligned Cones (AC) and Arcuate Ridges (AR) that have similar morphometry (height, width, summit depression) and are located only on *HApC* unit. In addition, these landforms are arranged in a similar region-scale whorl-shape that suggests a pattern avoiding the center of the basin and end facing the geological contact between *HApC* and *Hps* units. AR are absent from the central area, which contains only cones organized in dense fields. Simple Ridges are perpendicular to the whorl-shape pattern. On *Hmk*

unit, they have the particularity to link Mounds between each other. Finally, Linear Depressions (LD) are sometimes filled with a SR on *HApC*. These landforms association are similar to wet-based glaciation environment on Earth. The pattern of periodic alternating arcuate shapes is similar in form and scale to ribbed moraines. Ribbed moraines are subglacially formed transverse ridges [4]. Movement of the ice sheet is a glacial process that reworks preexisting sediments into ridges and implies a warm-based ice sheet [4]. SR have characteristics similar to terrestrial eskers. They are associated to other glacial landforms such as mounds (potential kames) and moraines. Finally, Linear depressions share characteristics with terrestrial Tunnel Valleys.

The presence of these landforms assemblages in Isidis Planitia and especially their relationship to each other suggest a glacial origin, specifically a wet-based ice sheet. Indeed all these landforms require melt water for their formation. However, this interpreted ice sheet seems to have undergone different thermal regime considering the lack of interpreted landforms related to wet-based glaciation in the central area. We interpret the centre of Isidis Planitia to suggest the presence of a stagnant part of the former ice sheet. We suggest that this stagnating part results from a negative thermal anomaly of the lithosphere located below the centre of Isidis Planitia [8] that cooled the base of the ice sheet. This interpretation is consistent with climate models [13] that show snow accumulation for different obliquity of the planet in the NW area of Isidis, precisely where the whorl-shape pattern starts.

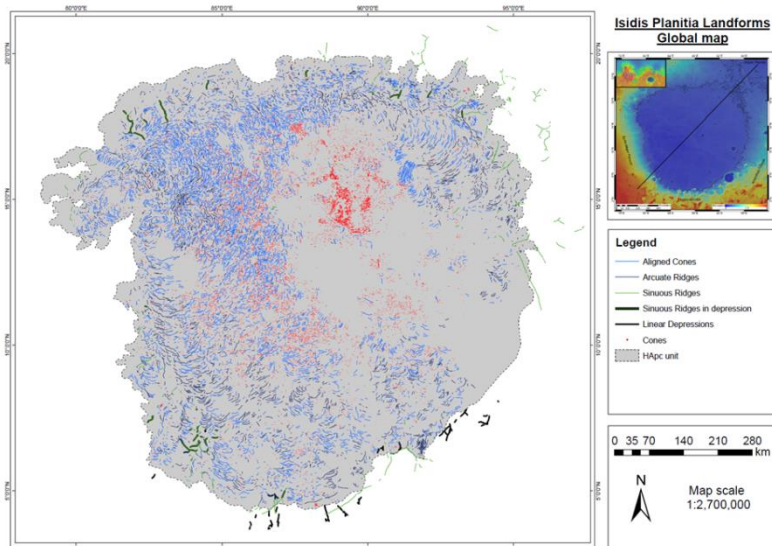


Figure 1: Global map of the different landforms in Isidis Planitia.

- References:** [1] Bridges et al (2003), *J. Geophys. Res.* 108, 1-17; [2] Bruno et al (2004), *J. Geophys. Res.* 109, 1-11; [3] Davis and Tanaka (1995), *Lunar Planet. Sci.* 26, 321-322; [4] Dunlop and Clark (2006), *Quaternary Sci. Rev.* 25, 1668-1691; [5] Fagents et al (2002), *Geol. Soc. Lond.* 202, 295-317; [6] Ghent et al (2012), *Icarus* 217, 169-183; [7] Griffazi and Schultz (1989), *Icarus* 77, 358-381; [8] Grott and Breuer (2010), *J. Geophys. Res.* 115, 1-16; [9] Ivanov et al (2012), *Icarus* 218, 24-46; [10] Kargel et al (1995), *J. Geophys. Res.* 100, 5351-5368; [11] Kehew et al (2012), *Earth Sci. Rev.* 113, 33-58; [12] Lockwood et al (1992), *Lunar Planet. Sci.* 23, 795-796; [13] Madeleine et al (2009), *Icarus* 203, 390-405; [14] Shreve (1985), *Geol. Soc. Am. Bull.* 96, 639-646; [15] Skinner and Mazzini (2009), *Mar. Petrol. Geol.* 26, 1866-1878.

**ALTERATION ON MARS: STUDY OF NEAR-INFRARED SPECTRA OF TERRESTRIAL BASALTS ALTERED IN CONTRASTED CLIMATE CONDITIONS.** Joanna Gurgurewicz<sup>1,2</sup>, Daniel Mège<sup>1,3</sup>, Véronique Carrère<sup>3</sup>, Anne Gaudin<sup>3</sup>, Joanna Kostylew<sup>4</sup>, Yann Morizet<sup>3</sup>, Marta Skiścim<sup>1</sup>, <sup>1</sup>Institute of Geological Sciences PAS, Wrocław, Poland, <sup>2</sup>Space Research Centre PAS, Warsaw, Poland (jgur@cbk.waw.pl), <sup>3</sup>Laboratoire de Planétologie et Géodynamique, UMR CNRS 6112, Université de Nantes, France, <sup>4</sup>Institute of Geological Sciences, University of Wrocław, Poland.

**Introduction:** Mafic rocks are widespread at the surface of Mars. Their existence has been inferred from the composition of Martian meteorites [1], from geomorphology, e.g. [2], and several orbital infrared data sets [3-6]. Evidence of basaltic surface composition comes from characteristic absorption bands of olivines and pyroxenes, and mineralogical abundance modelling [4-6], as well as *in situ* chemical analysis, e.g. [7].

Can information on the Martian environmental conditions prevailing during the alteration of its basaltic crust be inferred from near-infrared (NIR) spectra? In order to determine whether basalts altered in different environments have different spectral signatures, we analyzed the NIR spectra of basalts from arid cold and arid hot environments, as well as hot environments in which wet and arid climates occurred successively; any of these conditions may have been representative of the alteration conditions on Mars, present or past. The selected basalts are located in the Udokan area of Siberia, and in the Ogaden region of southeast Ethiopia. They are all alkali basalts, Ti-rich, and have the same mineralogical structure.

**Methods:** The mineral composition and structure of the Udokan and Ogaden basalts have been identified using polarizing microscope. The reflectance has been measured using the ASD FieldSpec® 3 spectrometer in the spectral range 0.35–2.5 μm, with 3 nm spectral resolution in the visible range and 10 nm in the infrared. Ninety-one spectra were acquired, both of the alteration rind surface and the internal part of the bulk samples, and of the whole-rock powders. Complementary information on composition of representative basalt samples have been retrieved from X-ray diffractometry and Micro-Raman spectroscopy.

**Results and discussion:** The NIR spectra of the alteration rind surface and the internal part of the bulk samples from cold and hot environment (Figure 1) are very similar, suggesting that the NIR spectra of Martian bulk rocks may be of limited help in identifying paleoenvironment conditions. Bulk rock spectra analysis reveals, however, that: (1) spectra of the least altered rocks display clear absorption bands of smectites, suggesting that a distinction between clays in weakly weathered basalts and clay-rich formations cannot be based solely on analysis of infrared spectra obtained from orbit; (2) the depth of the 1.9 μm water absorption band is not correlated with environmental humidity, possibly due to the weathering effect of groundwater, or to the hydration state of the secondary minerals. Therefore, the deep hydration bands, observed on many Martian spectra of mafic mineral-rich areas or in other geological contexts, e.g. [4], are not necessarily evidence of a past wet climate characterized by persistent water runoff during long-lasting wet seasons. They are also consistent with dry conditions, cold or hot, with only very limited or no precipitation.

Additional compositional information can be retrieved from rock powder spectra. Zeolites, which are identified in the Udokan basalt spectra, are indicators of ancient presence of groundwater or hydrothermal water. The restrictive pressure and temperature range of formation of some zeolites potentially helps in retrieving information on paleoclimate. The presence of calcite and iddingsite is ascertained by other

methods, but they are not apparent in bulk rock spectra and only weakly apparent in powder spectra, probably due to the nonlinear spectral response of intimately mixed minerals in basaltic rock.

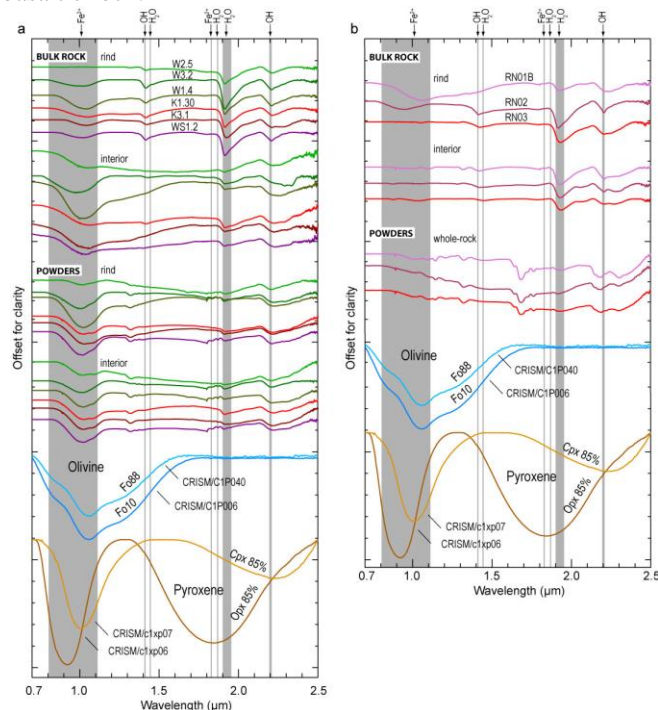


**Figure 1.** Representative reflectance spectra of the Ogaden basalts (a), Udokan basalts (b), and library spectra of the iron-rich primary minerals of basalt in the range 0.7-2.5 μm.

**Conclusion and perspectives:** Although the alteration conditions of the two series of terrestrial basalt samples are very contrasted, analysis of NIR spectra could not unequivocally discriminate between them. Other techniques are required for characterization of alteration features in basalts that can accurately infer paleoclimate. We are investigating whether atomic force microscopy can be used as a tool to identify diagnostic alteration features at the surface of basalts in the nanoscale [8].

**References:** [1] Nyquist L. E. et al. (2001), Ages and geologic histories of Martian meteorites, *Space Sci. Rev.*, 96, 105–164. [2] McEwen A. S. et al. (1999), Voluminous volcanism in early Mars revealed in Valles Marineris, *Nature*, 397, 584–586. [3] Christensen P. R. et al. (2000), Identification of a basaltic component on the Martian surface from Thermal Emission Spectrometer data, *JGR*, 105, 9609–9621. [4] Mustard J. F. et al. (2005), Olivine and pyroxene diversity in the crust of Mars, *Science*, 307, 1594–1597. [5] Salvatore M. R. et al. (2010), Definitive evidence of Hesperian basalt in Acidalia and Chryse planitiae, *JGR*, 115, E07005. [6] Poulet F. et al. (2009), Quantitative compositional analysis of martian mafic regions using the MEX/OMEGA reflectance data: 1. Methodology, uncertainties and examples of application, *Icarus*, 201, 69–83. [7] McSween H. Y. et al. (2004), Basaltic rocks analyzed by the Spirit rover in Gusev crater, *Science*, 305, 842–845. [8] Skiścim M. et al. (2014), Alteration features in basalts identified by atomic force microscopy and implications for Mars, abstract, this conference.

**THE IMPORTANCE OF ADEQUATE AIVITY PLANNING STRATEGIES FOR SUCCESSFUL HUMAN MARS MISSIONS.** Sebastian Hettrich<sup>1,2</sup>, Aline N. Dinkelaker<sup>3</sup>, Efstratia Salteri<sup>4</sup>, Leila Ghasemzadeh<sup>5</sup>, Ali Alizade<sup>5</sup>, Elena S. Lupu<sup>6</sup>, Isabella Pfeil<sup>7</sup>, Carmen V. Felix<sup>8,9</sup>, Tilo Kauerhoff<sup>5,10</sup>, Nina Sejkora<sup>11</sup> <sup>1</sup>German Federal Office for Radiation Protection, 85764 Oberschleissheim, Germany; <sup>2</sup>Ludwig Maximilian University of Munich, 80539 Munich, Germany; <sup>3</sup>Humboldt University of Berlin, 10099 Berlin, Germany; <sup>4</sup>Democritus University of Thrace, 67100 Xanthi, Greece; <sup>5</sup>Space Generation Advisory Council, 1030 Vienna, Austria; <sup>6</sup>Politehnica University of Bucharest, 060042 Bucharest, Romania; <sup>7</sup>Vienna University of Technology, 1040 Vienna, Austria; <sup>8</sup>International Association for the Advancement of Space Safety, 2201BB Noordwijk, The Netherlands; <sup>9</sup>Space Safety Magazine, 2200AC Noordwijk, The Netherlands; <sup>10</sup>Technische Universität München, 80333 Munich, Germany; <sup>11</sup>University of Innsbruck, 6020 Innsbruck, Austria.

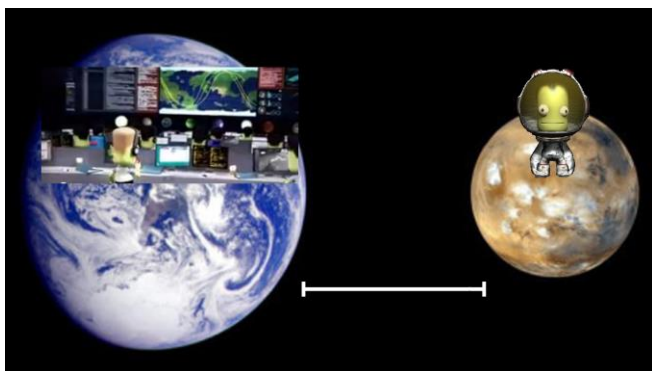


**Figure 1:** Minimal and maximal distances between Earth and Mars, causing delays in communication of 4.5 and 21 minutes respectively (Cartoon taken from Kerbal Space Program) [2].

**Introduction:** Sending human explorers to Mars will greatly expand our current knowledge of the Red Planet, due to their large advantage over robotic missions [1]. But going to Mars is cost intensive and bears great risks such as environmental hazards, technological failures or human factors [2]. Additionally, communication between Earth and Mars will be difficult; due to the long distances of 78 Mio. km at closest approach (opposition) and 377 Mio. km at farthest (conjunction), the signals will take between 4.5 and 21 minutes one way (see figure 1), thus disabling the possibility of real-time communication and real-time support [2].

**Activity Planning Strategy:** A crewed Mars mission therefore requires not only a good preparation of the crew and the best hardware available, but also adequate strategies for the planning and execution of activities during the mission [2]. An optimal planning strategy enables the maximal amount of time and resources to be spent on scientific research on Mars, while leaving enough margins to account for the safety of the astronauts. Figure 2 shows a flow chart that provides an overview of the different parameters that influence the set-up of a proper scheduling for a human Mars mission [2]. Additionally, a planning strategy has to address the communication difficulty and has to be well balanced between stability and flexibility to provide the optimal support for the astronauts on Mars to maximise the scientific value of the mission while minimising the risks [2][3].

Here we present the different aspects that need to be taken into account to provide a well thought-through activity schedule and explain possible solutions shown in figure 3. These are namely the 3-days-in-advance planning strategy and the 1-day-in-advance planning strategy, developed to meet the requirements of such a long-distance human planetary exploration mission to Mars [3][4].

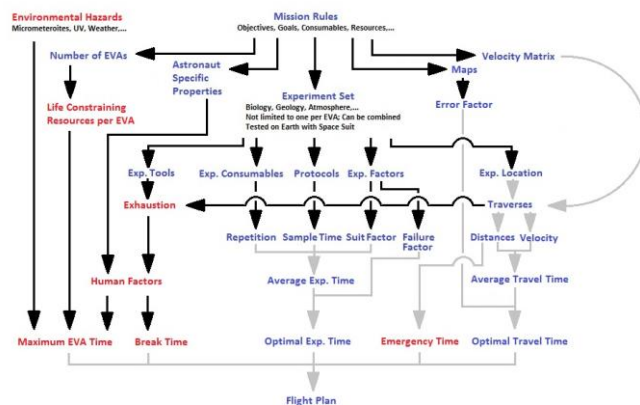


**Figure 2:** Inputs and dependencies for the development of planning strategy and the activity planning for a human Mars mission [2] (larger figure provided in presentation).

### 1-day-in-advance planning strategy

	Morning			Evening		
Day 1	MCC	Deadline for change requests	Activity Plan for Day 2	FD Authorisation	Upload to field	
	Field	Field Activity Day 1	Field Activity Day 1	Field Activity Day 1	Field Reports Day 1	
Day 2	MCC	Mission Analysis for Day 1	Deadline for change requests	Activity Plan for Day 3	FD Authorisation	Upload to field
	Field	Field Activity Day 2	Field Activity Day 2	Field Activity Day 2	Field Reports Day 2	
Day 3	MCC	Mission Analysis for Day 2	Deadline for change requests	Activity Plan for Day 4	FD Authorisation	Upload to field
	Field	Field Activity Day 3	Field Activity Day 3	Field Activity Day 3	Field Reports Day 3	
Day 4	MCC	Mission Analysis for Day 3	Deadline for change requests	Activity Plan for Day 5	FD Authorisation	Upload to field
	Field	Field Activity Day 4	Field Activity Day 4	Field Activity Day 4	Field Reports Day 4	

### 3-days-in-advance planning strategy

	Morning			Evening		
Day 1	MSC	Deadline for change requests	Activity Plan for Day 4			
	Field	Field Activity Day 1	Field Activity Day 1	Field Activity Day 1	Field Reports Day 1	
Day 2	MSC	Deadline for change requests	Mission Analysis for Day 1	Activity Plan for Day 5	FD Authorisation	
	Field	Field Activity Day 2	Field Activity Day 2	Field Activity Day 2	Field Reports Day 2	
Day 3	MSC	Deadline for change requests	Mission Analysis for Day 2	Activity Plan for Day 6	FD Authorisation	Upload to field
	Field	Field Activity Day 3	Field Activity Day 3	Field Activity Day 3	Field Reports Day 3	
Day 4	MSC	Deadline for change requests	Mission Analysis for Day 3	Activity Plan for Day 7	FD Authorisation	Upload to field
	Field	Field Activity Day 4	Field Activity Day 4	Field Activity Day 4	Field Reports Day 4	

**Figure 3:** Schematics of the 1-day-in-advance planning and the 3-days-in-advance planning strategies [3] (larger figure provided in presentation).

**References:** [1] Turner, M.J.L. (2004), *Expedition Mars*, Springer Praxis Publishing Ltd, London Berlin Heidelberg New York Hong Kong Milan Paris Tokyo. [2] Hettrich, S. (2012), Human-robotic Mars science operations: itinerary optimisation for surface operations, Master thesis, Institute for Astro-and Particle Physics, University of Innsbruck, Austria. [3] Hettrich, S. et al. (2014), Planning strategies for Mars (analog) missions: real-time, 3-days-in-advance and 1-day-in-advance planning, AIAA-Space Operations Conference 2014 Technical Paper, (in review). [4] Hettrich S. et al. (2014), Efficiency Analysis of the MARS2013 Planning Strategy, *Astrobiology*, (in print).



In a country with no space program an analogue space program is a good, cost-effective and advantageous solution. Planetary analogue research is becoming a significant area of activities. This young discipline, being widely used within a framework of practically every space exploration program still calls for proper recognition as an independent specialization and for codification of methodologies. Since space exploration activities are expanding from the hermetical community of state agencies and institutes to a wider community of numerous groups of small science teams, organizations, private entrepreneurs and even SMEs, planetary analogue research is often their only way to get involved and to contribute with their technological concepts and scientific methods. These concepts and methods are by definition cost effective and allow further popularization of space exploration.

Recently an attempt to organize the discipline of analogue research has been made in a form of preparation of the “Vienna Statement of Analogue Research”. It was undertaken by several organizations including Mars Society national chapters and the Austrian Space Forum. Specific activities follow, such as international analogue missions, competitions, and even programs, carried out by these organizations. The European Commission has recognized the need to support analogue research by having a dedicated funding scheme within the FP7 and H2020 programs.

Poland has much achievement in this field. This paper will focus on analogue rovers only. Between 2009-2013 student analogue Mars rovers from Poland have participated in the University Rover Challenge in Utah, USA, winning this competition twice. All together 9 Polish teams from 5 Polish universities have participated, and a few more teams have been established at other universities. For 2014 the European Rover Challenge is planned in Poland.

Polish rover teams were not short-term projects, but in several cases they have been established as development lines. These include: Magma > Magma White (commercial) > M4K (commercial) > Magma2 rover family developed at Nicolaus Copernicus Toruń, Białystok University of Technology and commercialized by ABM Space Education, and Scorpio > Scorpio2 > Scorpio3 from Wrocław University of Technology. Copernicus and Hyperion rover projects from Toruń and Białystok are also two-year projects.

All these rovers share common characteristics, resulting from the challenge rules. [1] These characteristics and functions constitute a good basis for non-challenge R’n’D activities related to robotized research but also to astronaut support activities. Development of the rovers is accompanied by involvement of scientists, especially geologists and planetologists. Development is funded by universities, private sponsors and by the Ministry of Science and Higher Education.

After the challenges a commercial version of a rover: Magma White, was built at ABM Space Education and it has been used for R’n’D projects funded from private and state funds. The spin-off has also its investor. The analogue missions and projects include:

- Dachstein 2012 Mars simulation, an international project in Alpine ice caves. WISDOM ground penetrating radar for Exomars mission was tested on-board Magma White. [2]
- Morocco 2013 Mars simulation in Sahara, with international teams and L.I.F.E. laser chlorophyll detector on-board. [3]

- Magma-Laser project, funded by Austrian and Polish institutions, involving a robotic arm for L.I.F.E. detector.
- Permafrost electrical resistivity module development, with Geology Institute of Polish Academy of Sciences.
- Further ground penetrating radar research is pending.
- Virtual Magma Rover – a simple online simulator of Polish rovers, by a specialized private studio (WroVision).
- Outreach and education action.

The activities include engineering of the rovers, software, but also finding, visiting and studying of existing and new planetary analogue sites, as well as development of laboratory analogues. All this calls for coordination of efforts and definition of goals of joint activities. Proper compatibility should be maintained. Advantages of such a program are obvious. It allows synergy of ideas and academic resources, and concentration/retaining of the human resources. Furthermore there are entities in Poland that develop specialized instruments that can be used and could be tested on-board analogue rovers. These include ground penetrators (such as Space Research Center PAS devices), drills, specialized cameras and sensors, both for space and non-space use. Other entities, such as TME, Archimedes and GM System are interested in supporting the program. There is a need for steady financing and this can be easier to achieve in case of a coordinated action. This program would constitute a pool to be used/purchased or developed within higher TRL projects, such as Faster or competitive European rover projects, European robotic clusters and eventually in MREP-2 projects. It might also allow proposing projects within PRODEX, as national contributions. It would constitute an interesting testing offer for international developers of MREP-2 instrumentation.

Summarizing: the program will be an international R’n’D market offer [4], as well as a national tool for development and specialization, allowing efficient utilization of allocated funding, with future benefits in a form of full participation of Poland in space exploration. The program should be open for international partners.

- [1] Józefowicz M, Meszyński S, et al. (2010) Problematyka zawodów University Rover Challenge. Wybrane wytyczne dla robota operującego w warunkach pustynnych, PIAP [2] Ciarletti V, et al (2012) WISDOM a GPR for the ExoMars Rover Mission. *LPI Contributions* 1683: 1126 [3] Groemer G, et al (2014 in printing), Field Trial of a Dual Wavelength Fluorescent Emission (L.I.F.E.) Instrument and the Magma White Rover During the Mars2013 Mars-Analog Mission, *Astrobiology* [4] Meszyński S, Józefowicz M, Analog Mars Rover Service as a Robotic Hardware and Team Building Platform, *GSTF Journal of Engineering Technology (JET)*, Vol. 2 No. 3, Dec 2013



Fig. 1. Magma White in Sahara with L.I.F.E. and analogue suit

# CONDITIONS FOR THE APPEARANCE OF INTERFACIAL LIQUID WATER AT THE NORTHERN HEMISPHERE OF MARS.

Kereszturi A.<sup>1,2</sup> Appéré T.<sup>3</sup> <sup>1</sup>Research Centre for Astronomy and Earth Sciences, H-1121 Budapest, Konkoly Thege M. 15-17, Hungary (e-mail: [kereszturi.akos@csfk.mta.hu](mailto:kereszturi.akos@csfk.mta.hu)); <sup>2</sup>New Europe School for Theoretical Biology and Ecology; <sup>3</sup>Institut de Planétologie et d'Astrophysique de Grenoble, Université Joseph Fourier, CNRS/INSU, Grenoble, France.

**Introduction:** We analyzed the possibility of microscopic scale interfacial liquid water formation at the seasonal water ice annulus of the northern hemisphere of Mars, such interfacial liquid water in the southern hemisphere at Richardson crater [1] was earlier found. Here we searched for evidence of similar features in the northern hemisphere using OMEGA, TES [2] and THEMIS [3] data. A ring-like water ice annulus without CO<sub>2</sub> ice surrounds the shrinking seasonal CO<sub>2</sub> ice cap at northern and was analyzed with OMEGA in details [4]. The surface temperature there is close to the threshold limit for interfacial water formation, what is ~190 K for typically 10 pr- $\mu$ m atmospheric column water content [5]. Here we use the term liquid interfacial water for the thin, undercooled layer between solid water ice and minerals, beside this on mineral surfaces without ice cover atmospheric may also exist [6].

**Methods:** OMEGA hyperspectral images were used to identify the location of CO<sub>2</sub> ice and H<sub>2</sub>O ice covered terrains as well as ice free, barren surface that might still be hydrated. We used the results from [7] without any new processing; the detailed methodological description of the processing is described in that paper. The outputs of the C (0.92-2.7  $\mu$ m) spectral channel of OMEGA were spectrally and radiometrically calibrated into reflectance factor values, and standard spectral parameters were calculated for the continuum reflectance, CO<sub>2</sub> ice band depth and H<sub>2</sub>O ice band. The boundaries of the seasonal deposits in term of albedo, CO<sub>2</sub> ice and H<sub>2</sub>O ice were then retrieved from the OMEGA dataset. Temperature data was obtained by the TES instrument aboard MGS [8] daytime surface temperatures az 12-14 LMST. The spatial resolution of TES data is 3-8 km, while for THEMIS instrument is 100m used with methodology of [9].

**Results:** Figure 1 shows the zonally averaged results obtained at low spatial resolution (TES and OMEGA). It shows that at latitude above 45°N there is a certain period of time when the temperature of the water ice annulus is above 190 K. This duration is nearly constant above 58°N, ranging between 6-10° of L<sub>s</sub> (respectively 10 and 17 days or sols).

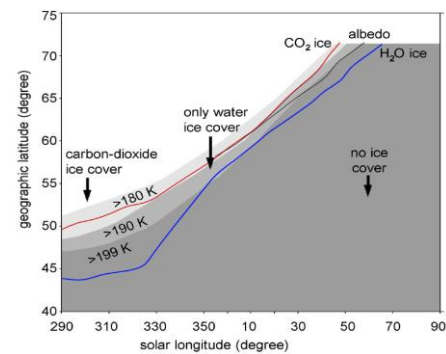


Figure 1. Recession curves according to latitude and solar longitude. The outer edge of the CO<sub>2</sub> ice cap is marked by a red line. The outer edge of the cap in term of albedo is marked by a black, in term of H<sub>2</sub>O ice is marked by a blue line. The gray shadowed area marks the locations where the zonal average maximal daytime temperature is above 180 K.

The duration of the water ice cover is between 15°-50° of L<sub>s</sub> (24-80 days or sols), e.g. more than two Earthly months there is a period of time every day with possibly liquid interfacial water. The presence of an only water ice covered terrain is in agreement with the results of [10]. Figure 2. shows that surface temperature is close to 150 K on terrains covered by CO<sub>2</sub> ice. At the water ice annulus patchy distribution of surface temperature exists: patches at 150 K can be attributed to remnants of CO<sub>2</sub> ice while terrains at 171 K are covered by

water ice. This spatial segregation between CO<sub>2</sub> ice and H<sub>2</sub>O ice is likely due to preservation of CO<sub>2</sub> ice on north facing slopes. Southward the surface is homogeneously covered by water ice which temperature increases towards the south, particularly at L<sub>s</sub>=44° when it increases from 171 K at 70.5°N to 186 K at 68.5°N. It may be due to the increase of the partial pressure of water vapor above the surface towards the south, as reported by [11]. On the southern part of the annulus patchy distribution of H<sub>2</sub>O ice can be observed. At L<sub>s</sub>=44° and 68°N, patchy terrains at 186 K are covered by water ice while patchy terrains at 197 K are defrosted.

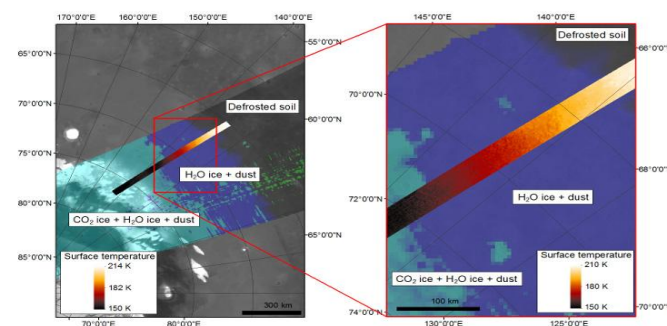


Figure 2. Pairs of overlapping OMEGA observation 2946\_1 and THEMIS observation 119329009, both acquired at L<sub>s</sub> ~44° during MY 28. OMEGA image correspond to the large image with light blue, medium blue and gray units. These units mark out terrains covered by CO<sub>2</sub> ice contaminated by H<sub>2</sub>O ice and dust (in light blue), terrains covered by H<sub>2</sub>O ice contaminated by dust (in medium blue) and defrosted terrains (in transparent gray). THEMIS image is the thin stripe with color ranging from dark brown to light yellow. The background is MOC albedo data acquired in summer [12].

**Discussion:** Part of the area of the water ice annulus satisfies conditions for the presence of interfacial water, at least around local noon. THEMIS observation at L<sub>s</sub>=44° shows patches of water ice at 186 K. The above-mentioned 180-190 K is relevant for the average atmospheric vapor content on Mars of 10 pr- $\mu$ m. During northern spring, the atmospheric water vapor concentration can reach 40 pr- $\mu$ m at L<sub>s</sub>=70-75° at the area of the water ice annulus (~75°N) [13]. The number of days with temperature above the threshold limit for the best longitudinal region (300°-330°E) at 55°-70°N is 10-30 days or sols. Between about 45°-55°N the duration peaks between 80 and 110 days. Moreover, water ice is likely present on the surface for a twice longer period if one includes autumn to this analysis, probably around 200 days of presence at 50°N.

**Acknowledgments:** This work was supported by ESA ECS Co 4000105405 (No. 98076.), the OTKA PD 105970; and the financial supports from CNES through its “Système Solaire” program. This work used data from the OMEGA instrument (CNES/IAS) aboard the MEX mission and acknowledged for the ESA.

**References:** [1] Kereszturi et al. 2011. *PSS* 59, 26-42., [2] Kieffer, Titus 2001. *Icarus* 154, 162-180., [3] Wagstaff et. al 2008. *PSS* 56, 256-265., [4] Appéré et al. 2011. *JGR* 116 (E15), E05001. [5] Möhlmann 2008. *Icarus* 195, 131-139., [6] Bryson et al. 2008. 34th LPSC #2123., Möhlmann 2008, [7] Appéré et al. 2011. *JGR* 116 (E15), E05001., [8] Christensen et al. 1992. *JGR* 97(E5), 7719-7734., [9] Wagstaff et. al 2008. *PSS* 56, 256-265., [10] Wagstaff et. al 2008. *PSS* 56, 256-265., [11] Pankine et al. 2010. *Icarus* 210, 58-71, [12] Caplinger, M. A., Malin, M. C., 2001. *JGR* 106, 23595-23606., [13] Pankine et al. 2010. *Icarus* 210, 58-71.

# INTERFACIAL WATER ON MARS AND ITS POSSIBLE ROLE ON HYDROGEN PEROXIDE DECOMPOSITION.

Kereszturi A<sup>1,2</sup> and Gobi S<sup>1</sup>, <sup>1</sup>Research Center for Astronomy and Earth Sciences, H-1121 Budapest, Konkoly Thege Miklós út 15-17., <sup>2</sup>New Europe School for Theoretical Biology and Ecology, (email: [kereszturi.akos@csfk.mta.hu](mailto:kereszturi.akos@csfk.mta.hu)).

**Introduction:** During local spring, thin (nm thick) liquid, undercooled interfacial water could be present between the surface covering water ice and the minerals below, mainly by Van der Waals forces [1] in Richardson crater at the southern circumpolar region [2] at the outer ring-shaped area of Dark Dune Spots. Here the daytime max. temperature surpass the threshold limit of interfacial water formation around 180 K where H<sub>2</sub>O<sub>2</sub> might decompose

**Methods:** To estimate the speed of possible reactions, lab. data [3,4,5,6,7] and thermodynamical kinetic calculations were used. Here the half life term means the duration while the half of the original quantity/mass of is decomposed. H<sub>2</sub>O<sub>2</sub> might decomposes: H<sub>2</sub>O<sub>2</sub> → H<sub>2</sub>O + ½ O<sub>2</sub>. The reaction rate is influenced by pH and temperature. H<sub>2</sub>O<sub>2</sub> solution is stable under pH 4.5, with increasing pH decomposes rapidly. As a rule of thumb if the reaction temperature increases by 10 K the rate of reaction doubles. The presence of transition metal ions in solution can catalyse the decomposition (homogeneous catalysis). Heterogeneous catalysis happens by metals and metal oxides [7,8] that speed up the process. The pH of the Martian regolith by Vikings' LR tests is pH=7.2±0.1 [9], by Phoenix lander is pH=7.7±0.5 [10]. Current conditions disfavour the solving of Fe suggested by the WCL of Phoenix lander [12]. But the immobility of Fe does not mean that Fe can not be active chemically now, and in the past it was mobile producing iron bearing phyllosilicates [13].

**Iron supported decomposition:** Fe<sup>2+</sup> and Fe<sup>3+</sup> catalyse the decomposition of H<sub>2</sub>O<sub>2</sub> into H<sub>2</sub>O and O<sub>2</sub>. If the concentration of Fe<sup>2+</sup> is high relative to H<sub>2</sub>O<sub>2</sub>, oxidation takes place in acidic conditions (pH below 4.5). At higher pH values, the formation of iron-hydroxo complexes and precipitation slows the reaction. The activation energy and the rate constant were found to be 35.6 kJmol<sup>-1</sup> and 5.5 × 10<sup>-3</sup> s<sup>-1</sup> at 300 K [3], the half life is ~2 minutes at 300 K, at 200 K is roughly 44 hours.

The catalytic effect of Fe<sup>3+</sup> ion is similar to that of Fe<sup>2+</sup>. The rate constant was determined to be 1.0 × 10<sup>-4</sup> sec<sup>-1</sup>, i.e. its half-life is around 2 hours at 300 K, at 200 K the half-life of H<sub>2</sub>O<sub>2</sub> is 80 days. Although mobile Fe was not accessible, but immobile Fe (e.g. in the form of Fe-oxides) at the mineral surface might still accelerate the decomposition. In Table 1. the effectivity of possible reaction pathways can be compared.

Table 1. Comparison of possible H<sub>2</sub>O<sub>2</sub> decomposition pathways on Mars in thin interfacial water film around 200 K

reaction type / agent	half life around 200 K	required condition	information regarding the possibility of the reactions on Mars
thermal decomposition	> 1000 years	no extra cond. is required	might take place, only temperature matters, probably produces very slow decomposition alone
Fe <sup>2+</sup>	44 hours	pH < 4.5	Fe is present and mobile at acidic pH, got oxidized into Fe <sup>3+</sup> by dissolution or UV-weathering
Fe <sup>3+</sup>	80 days	pH < 4.5	Fe is present, in the bright regions as amorphous gels and sulphates, mobile at acidic pH
SiO <sub>2</sub> , Al <sub>2</sub> O <sub>3</sub> , TiO <sub>2</sub>	120 year, 300 and 25 days	no extra cond. is required	probably present in the regolith
Fe(III)-oxides	20 days	no bulk acidity is required	abundant in the regolith, bulk pH is in the current range

Among the solvents Fe<sup>2+</sup> and Fe<sup>3+</sup> ions could decrease the half life to days if pH>4.5. Fe<sup>2+</sup> is got oxidized to Fe<sup>3+</sup>, the decomposition rate depends on Fe<sup>2+</sup> stability and is influenced by Fe/H<sub>2</sub>O<sub>2</sub> ratio. Mobile Fe ions supported decomposition probably does not happen today – but Fe on mineral surfaces supports the decomposition by heterogeneous catalysis. The thickness of the interfacial water layer influenced by temperature, hygroscopicity of the mineral surface, and solved non H<sub>2</sub>O components [22]. Laboratory results show [24] solved salts increases this thickness, and solved impurities at 235 K produce thickness in liquid films up to 0.5 nm [25],

what is more than one monolayer, while around 200 K up to 3 monolayers [26]. More than one monolayer could be present today, and even thicker liquid layer might exist in the past.

The H<sub>2</sub>O<sub>2</sub> molecules probably deposit by airfall together with aerosols in summertime onto the defrosted surface, exactly where the thin liquid layer forms. Here H<sub>2</sub>O<sub>2</sub> molecules could be close to mineral Fe centers, and decomposition might take place without substantial transport. Beside the effect of possible decomposition, the surface concentration of H<sub>2</sub>O<sub>2</sub> also depends on the ratio of production (by UV and electrostatic forces [27] plus accumulation (by dust settling) and the decomposing reactions together.

**Discussion:** Currently thermal driven decomposition is slow, the chemical ingredients in the liquid might play stronger role than temperature expected in the Amazonian. Fe<sup>2+</sup> ions in solution are the most important, which produce half life of H<sub>2</sub>O<sub>2</sub> around 1-2 days at low temperature. Even if the conditions today are unfavourable for such reaction, H<sub>2</sub>O<sub>2</sub> decomposition might still happen without mobile Fe and bulk acidity in liquid films by heterogeneous catalysis. This pathway could decompose H<sub>2</sub>O<sub>2</sub> with half life of ~20 days. In the 1. and 2. monolayers the chemical processes differ from that of in the bulk volume, but in thicker layer conditions became similar to bulk environment.

**Conclusion:** Currently at 200 K and Phoenix lander's wet chemistry laboratory results, the pH is not favourable for Fe mobility that supports decomposition. But at volcanically active periods decomposition might take place at the current temperature range if solved sulphur produces pH<4.5. Interfacial water probably appeared regularly in the Amazonian and during volcanic activity might produce better sites for any possible biogen activity with less H<sub>2</sub>O<sub>2</sub> there than other terrains without this liquid interfacial water. During more favourable period by rotational axis change driven climatic changes, the duration of water ice cover might be longer and salts could increase the thickness of the liquid layer.

By heterogeneous catalysis, decomposition without acidic pH and mobile Fe can happen at mineral surfaces containing Fe with half life of 20 days in bulk water, and longer timescale in thin interfacial liquid today. This might be important in the Amazonian when low temperature was present occasionally with elevated acidic conditions by volcanism. Under volcanically influenced acid weathering conditions [28], mobile Fe ions could decompose much H<sub>2</sub>O<sub>2</sub>, generating less aggressive environment in the top regolith. Our knowledge is limited on chemical processes in thin liquid film although such process might work not only at the seasonal but also at the permanent cap around the embedded dust grains there [29].

**Acknowledgment:** This work was supported by the ESA ECS Co 4000105405 (No. 98076.) and the OTKA PD 105970.

**References:** [1] Möhlmann 2008. *Icarus* 195, 131–139. [2] Kereszturi, Rivera-Valentin 2012. *Icarus* 221, 289–295. [3] Haber, Weiss 1934. *Proc. Roy. Soc.* 147, 332–351. [4] Beers, Sizer 1952. *J. Biol. Chem.* 195, 133–140. [5] Frankenburg et al. 1952. Acad. Press Inc., New York, 367–428. [6] Takagi, Ishigure 1985. *Nucl. Sci. Eng.* 89, 177–186. [7] Hiroki, LaVerne 2005. *J. Phys. Chem. B.* 109, 3364–3370. [8] Lousada, Jonsson 2010. *J. Phys. Chem. C.* 114, 11202–11208. [9] Plumb et al. 1993. *LPI Results from the MSATT Program*, Part 1, 40–41. [10] Hecht et al. 2009. *Science* 325, 64–67. [12] Kounaves 2012. *Intern. Works. on Instrum. Planet. Missions*, #1005. [13] Bibring et al. 2007. *Science* 317, 1206. [24] Bian et al. 2009. *J. Chem. Phys.* 130, 134709. [25] Boxe et al. 2012. *IJA* 11(3), 169–175. [26] Kossacki, Markiewicz 2010. 41th *LPSC* #1702. [27] Atreya S. et al. 2006. *Astrobiology* 6, 439–450. [28] Chevrier, Mathé 2007. *PSS* 55, 289–314. [29] Losiak 2014 Contemporary sulfate formation at the Martian Northern Polar Cap. 2<sup>nd</sup> *Martian Cryosphere Workshop*, Wrocław.

**CREATION OF THE PHOBOS ATLAS BASED ON MARS EXPRESS MISSION DATA.** A. Kokhanov<sup>1</sup>, I. Karachevtseva<sup>1</sup>, A. Konopikhin<sup>1</sup>, A. Zubarev<sup>1</sup>, I. Nadezhkina<sup>1</sup>, L. Mitrokhina<sup>1</sup>, N. Kozlova<sup>1</sup>, V. Patratiy<sup>1</sup>, and J. Oberst<sup>1,2</sup>, <sup>1</sup>Moscow State University of Geodesy and Cartography (MIIGAiK), MIIGAiK Extraterrestrial Laboratory (MExLab), Gorokhovskiy per., 4, 105064, Moscow, Russia, e-mail: i\_karachevtseva@miigaik.ru, <sup>2</sup>German Aerospace Center (DLR), Institute of Planetary Research, Rutherfordstrasse 2, 12489 Berlin, Germany.

**Introduction:** Phobos surface cartography is a challenging task due to small size and irregular shape of the body. Early maps of Phobos were based on airbrush techniques and show the surface of the small body only schematically. Russia has a long traditions in study and mapping of the Martian satellites. Recently, despite the failure of the launch of the Phobos-Grunt mission, it was decided to continue the exploration of Phobos. New spacecraft called "Boomerang" will be created with the same basic science program as Phobos-Grunt project, start of the mission is planned for 2022. Atlas of Phobos is the result of collaborative work based on modern Mars Express data. Atlas which summarizes available image processing data, surface measurements and results of geoanalyses will help us in planning of the future mission.

**New Phobos Mapping:** Methods of image processing and modern GIS technologies provide the opportunity for high quality planetary mapping. The new Phobos DTM and global orthomosaic have been used for developing a Phobos GIS [1] based on ArcGIS tools (<http://www.arcgis.com>). Phobos geodatabase provides data for various surface spatial analyses: statistics of crater density, as well as studies of gravity field, geomorphology, and photometry. The new Phobos Atlas will include: control points network and fundamental body parameters as a reference basis for Phobos research as well as GIS analyses of surface objects and geomorphologic studies. According to the structure of the atlas we used different coordinate system and various projections. Most projections are based on the sphere with radius 11.1 km according to IAU recommendations [2]. To maintain continuity and heritage of early maps we have prepared the layout for wall map using the modified Bugaevsky projection (1: 150 000). The projection is based on the three-axial ellipsoid with axis  $a=13.24$  km,  $b=11.49$  km,  $c=9.48$  km, which were calculated during photogrammetry processing of SRC images [3].

All global topographic and thematic maps of Phobos are presented in scale 1: 250 000. These maps depending on the content are made in one part in equidistance cylindrical projection or in three parts: the central area between  $\pm 60^\circ$  parallels is projected in Mercator projection, polar areas from ( $\pm$ )  $50^\circ$  to ( $\pm$ )  $90^\circ$  are projected in azimuthal conformal (stereographic) projection. The grid is applied in  $20^\circ$  and signed in planetocentric coordinates with east-positive longitude from  $0^\circ$  to  $360^\circ$ . One of the global maps shows dynamic heights, obtained from gravity field modelling [3], which are useful to study mass wasting effects and regolith mobility.

Besides global maps we compiled a large-scale Phobos topographic map (1: 75 000). This map is divided into 8 sheets according to proposals suggested for planetary cartography [4]. Each of sheets represents an area between  $\pm 60^\circ$  parallels and projected in Mercator projection with the main parallel and main meridian in the center of each sheet. For the polar areas we used the same stereographic projection as described for global maps. Based on geometric heights, contours were generated and plotted. For the designation of landforms and areas, we refer to the Gazetteer of Planetary Nomenclature (<http://planetarynames.wr.usgs.gov/>) which contains 20 named Phobos objects. All names also have been presented in Russian. The another multi-sheeted map (1:120 0000 -

1: 150 000) represents the crater distribution on the Phobos surface by sub/anti-Mars sides, leading/trailing sides and polar areas.

**Conclusions:** The new Phobos Atlas will contain about 30 Phobos thematic original maps that illustrate the surface of the small body based on Mars Express data. Some large-scale maps (1: 60 000 – 1:30 000) in oblique azimuthal projection describe several Phobos regions with more detail as these are based on images with higher resolution. Besides maps, the atlas also includes description of the results of various studies of Phobos: calculations of gravity field [3], geomorphology parameters of craters [5], calculations of surface roughness [6], morphometry studies [7], statistics of crater size-frequency distributions based on multi-fractal approach [8], and surface compositional studies based on HRSC color-channel data [9]. The Phobos spatial data products which used for mapping are available at the MIIGAiK Geoportal (<http://carsrv.mexlab.ru/geoportal/>), developed for planetary data storage [1].

**Acknowledgments:** The Phobos study was supported by RBRF under grant for "Geodesy, cartography and research satellites Phobos and Deimos" (Helmholtz-Russia Joint Research Group), grant agreement № 11-05-91323, partly supported by a grants from the Ministry of Education and Science of the Russian Federation (Agreement № 11.G34.31.0021 dd. 30/11/2010) and for "Development of a Planetary Data Geoportal to provide access to results of research on planets and satellites of Solar system", grant agreement 14.B37.21.1303.

**References:** [1] Karachevtseva I.P. et al. (2014) The Phobos information system. *PSS, Phobos Book*, <http://dx.doi.org/10.1016/j.pss.2013.12.015>. [2] Archinal, B. A. et al. (2009) Report of the IAU working group on cartographic coordinates and rotational elements. *Cel. Mechanics & Dyn. Astronomy* 109, 101–135. [3] Zubarev, A. E. et al. (2012). Problems of processing of remote sensing data for modeling shapes of small bodies in the Solar system, *Mod. Probl. of remote sensing of the Earth from Space*. 9, 277-285 (in Russian). [3] Uchaev et al. (2013). Multiscale representation of gravitational fields of small celestial bodies. *Izv. Vyssh. Uchevn. Zaved., Geod. Aerofotos'emka* 4, 3-8 (in Russian). [4] Greeley R., Batson G., (1990). Planetary Mapping. *Cambridge University Press*. [5] Basilevsky A.T. et al. (2014) Surface Geology and Geomorphology of Phobos, *Phobos Book. PSS*, in press. [6] Karachevtseva I. P. et al (2012). GIS mapping of Phobos on the results of data processing of remote sensing satellite Mars Express, *Mod. Probl. of remote sensing of the Earth from Space*. V. 9, № 4. 304-311 (in Russian). [7] Kokhanov A.A. et al. (2013) Depth/Diameter Ratio and Inner Walls Steepness of Large Phobos Craters. *LPSC 44 Abstracts # 2289*. [8] Uchaev, Dm. et al. (2012). Multifractal approach to crater distribution modelling according to their diameters. *Izv. Vyssh. Uchevn. Zaved., Geod. Aerofotos'emka* # 6, 3-8 (in Russian). [9] Patsyn V.S, et al. Research of spectrometric characteristics of the surface of Phobos on the HRSC data from the Mars Express spacecraft. *Mod. Probl. of remote sensing of the Earth from Space*, V. 9, № 4, 312-318 (in Russian).

**Introduction:** Comet 9P/Tempel 1 was imaged during two consecutive perihelion passages (Deep Impact in 2005 and Stardust-Next in 2011). The Deep Impact mission imaged approximately one third of the nucleus [5], while the SN mission extended the coverage about two times. Hence, evolution of a one third of the surface can be investigated. However, viewing conditions are different. Comparison of high resolution images gives unique opportunity to investigate changes of the surface of a comet nucleus between two consecutive perihelion passages. According to [7] the only significant change in morphology occurred along one long scarp located at  $\sim 40^\circ\text{S}$ . [6] reported that "at least two crudely triangular salients evident in 2005 have disappeared by 2011". These structures had sizes about 50 m, and their lack in newer images suggests significant retreat of the scarp, locally up to 50 m. At the time of imaging in 2005 the scarp was generally facing the solar direction and looked bright. However, due to almost half-circular shape of the scarp some parts were oriented nearly perpendicularly to the solar direction. The scarp was also the source region for most of the jets observed during SN mission [7].

I attempted to derive material properties of the nucleus beneath the selected scarp located at  $40^\circ\text{S}$  from the observed recession rate. For this purpose I simulated recession of the model scarp due to sub-dust sublimation of ice.

**Model:** I investigated local recession of the inclined scarp, long and high when compare to the thermal skin depth. The latter allows calculation of the heat and vapor diffusion in 1D in the direction locally perpendicular to the surface. Simulations were performed for different locations: at the inclined slope and at the horizontal surface above, or below the scarp. According to [7] in the region imaged by DI and SN there are no albedo patches, like those determined to be exposures of dirty ice. Thus, in this work the whole surface is covered some dust. The recession rate of the sloped surface may significantly depend on the local geometry. I use model previously used to simulate emission of water from comet 9P/Tempel 1 due to sublimation beneath the dust mantle. More recent versions of the model were described in [3], [4]. In all cases I considered comet nuclei without topographic features. Now, I consider local evolution of the nucleus in the vicinity of a scarp.

My model includes:

- evolution of the nucleus cohesion due to sintering of ice grains (so called Kelvin effect which modifies grain-to-grain contact areas, but does not affect degree of compaction);
- changes of porosity, due to sublimation/condensation in the medium;
- crystallization of amorphous water ice;
- sublimation of the CO ice (also explosive);
- sublimation of H<sub>2</sub>O ice covered by the dust mantle, taking into account the temperature dependent sublimation coefficient ([1], [2], [4]);
- diffusion of the vapor through the dust and the resulting recession of the surface;
- illumination dependent on the local orientation of the surface.

**Results:** The calculated horizontal recession rate of the slope is up to 30 m per orbital period, while the observed scarp receded locally up to 50 m. This difference indicates,

that the recession of the observed scarp is enhanced by rejection of ice grains, or even larger chunks of material due to fast outflow of vapor. This could explain also the observed high brightness of the scarp. The required rejection of material is reproduced when the depth to amorphous H<sub>2</sub>O ice and CO ice is about ten meters, or less. It is unknown, what could be the reason for locally small depth to amorphous H<sub>2</sub>O ice and CO ice.

**References:** [1] Gundlach B., Skorov Y.V., and Blum J. (2011). Outgassing of icy bodies in the Solar System - I. The sublimation of hexagonal water ice through dust layers. *Icarus*, 213, 710-719. [2] Kossacki K.J., Markiewicz W.J., Skorov Y., and Koemle N.I. (1999). Sublimation coefficient of water ice under simulated cometary-like conditions. *Planet. Space Sc.* 47, 1521-1530. [3] Kossacki, K.J., and Szu-towicz, S. (2012). Main Belt Comet P/2008 R1 Garradd: Duration of activity. *Icarus*, 217, 66-76. [4] Kossacki, K.J., and Markiewicz, W.J. (2013). Comet 67P/CG: Influence of the sublimation coefficient on the temperature and outgassing. *Icarus* 224, 172-177 [5] Thomas et al. (2007). The shape, topography, and geology of Tempel 1 from Deep Impact observations. *Icarus* 187, 4-15. [46] Thomas et al. (2013). The Nucleus of Comet 9P/Tempel 1: Shape and Geology from Two Flybys. *Icarus* 222, 453-466. [7] Veverka J. et al. (2013). Return to Comet Tempel 1: Overview of Stardust-NExT results. *Icarus* 222, 424-435.

## SEASONAL FLOWS ON DARK MARTIAN SLOPES, THERMAL CONDITION FOR LIQUESCENCE OF SALTS.

K.J. Kossacki<sup>1</sup>, W.J. Markiewicz<sup>2</sup>. <sup>1</sup>University of Warsaw, Inst. of Geophys., Pasteura 7, 02-093 Warsaw, kjkos-sac@igf.fuw.edu.pl. <sup>2</sup>Max-Planck-Inst. für Sonnensystemforschung, Justus-von-Liebig-Weg 3, 37077 Göttingen, Germany

**Introduction:** Recurring slope lineae (RSL) are seasonally growing long, dark features on Mars surface. They are found mostly on equatorward inclined steep dark slopes, in the south hemisphere and in mid-latitudes. The RSLs are typically 0.5-5 m wide and up to 40% darker than the average local surface. They are observed year after year in the same locations, on the slopes inclined by more than 25. RSLs start growing at  $L_s \sim 240^\circ$  and disappear at  $L_s \sim 20^\circ$ . RSL are observed only on areas of steep slopes needs further explanation. See [2], [3], [4]. It is important, that RSL are observed not just on any steep slope, but on dunes of east-west orientation. This implies, that close to the very warm slopes inclined toward equator are very cold slopes facing poles. Several scenarios have been proposed for the formation of RSL. One of the potential processes is the surface flow of brines. This assumes salt deposits in a near surface layer throughout the slope in question or at least near the top. Indeed RSLs usually extend downslope from bedrock outcrops. Serious problem is the need of sufficiently high humidity. Surface temperature of the slopes, where RSLs were so far identified is very high. Thus, presence of pure water ice at small depth is unlikely. The necessary humidity may only diffuse from a ground ice reservoir beneath the cold slope.

**Model:** We assume the regolith has layered structure. This is because: (i) the low thermal inertia [3] indicates low thermal conductivity of the material, at least in the diurnal thermal skin layer, while (ii) some ice reservoir is needed to keep humidity in the pores sufficiently high to allow formation of brines. It is not known, at what depth salt is present, if it is present at all. Thus, we considered few possibilities. The depth to the potential reservoir of the ground ice is also unknown. However, if it is larger than few meters, it is unlikely to maintain high humidity in the pores at a depth of tens of centimeters.

**Results:** We simulated evolution of the temperature and humidity in the regolith in the region, where the RSLs have been observed. We considered layered regolith with an upper layer of low thermal inertia  $I_{dry}$ , free of salt overlying layers composed of non-volatile grains and salt. We have found, that the increase of the regolith temperature above  $T_{eutectic}$  exactly in the period when RSLs were observed is possible only in specific situations.

The condition  $RH > DRH$  (relative humidity higher than the deliquescence relative humidity) can be also met, but only when the uppermost layer of the regolith is very fine grained and some ice is present in the regolith at a depth of few meters. For the details see [1].

Our conclusion that deliquescence is possible only in a narrow range of environmental conditions indicates, that other mechanisms for the formation of RSLs may be more common.

**References:** [1] J. Kossacki and W.J. Markiewicz (2014). Seasonal flows on dark martian slopes, thermal condition for liquecence of salts, *Icarus* 233 (2014) 126–130. [2] McEwen et al. (2010) The High Resolution Imaging Science Experiment (HiRISE) during MRO's Primary Science Phase (PSP). *Icarus*, 205, 2-37. [3] McEwen et al. (2011). Seasonal Flows on Warm Martian Slopes. *Science* 333, 740-741. [4] D.E. Stillmann et al. (2014), New observations of martian southern mid-latitude recurring slope lineae (RSL) imply formation by freshwater subsurface flows, *Icarus* in press.

**Introduction:** The size and shape of grains in aeolian deposits provide important information about aeolian transport and wind conditions. For instance, the size of grains is a crucial factor for establishing threshold wind velocities required to initiate grain motion.

Terrestrial sediments are studied using sieve analysis, but on Mars, such a method still cannot be applied. There is however, another possibility as various Martian deposits are clearly visible in images acquired during *in situ* missions. From such images the size, and shape of grains can be estimated, and it has been done manually in several publications [1, 2, 3]. Manual methods, however, are time-consuming and tedious, and the number of images is increasing. In this work, the automated method is presented as well as the results of statistical analysis of an exemplary Martian grain samples.

**Methodology:** The presented fully automated method is based on the algorithm, which enables to detect individual grains and measure their size and shape. The algorithm uses a set of image processing operations associated with filtering, extraction and segmentation, and is implemented in Wolfram *Mathematica*. Using the algorithm, it takes few minutes to derived data from an image.

The algorithm was tested on various terrestrial samples. The results were compared with results from sieve analysis. The histograms for an exemplary sample obtained by those two methods are shown in Figure 1.

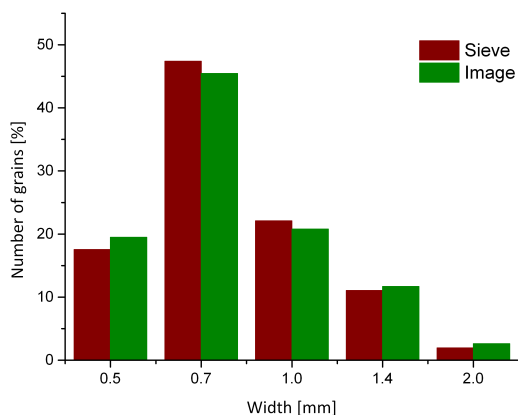


**Figure 1.** Histograms for a studied sand sample obtained by sieve analysis (sieve) and the automated method (image).

**Results:** The Microscopic Imagers (MI) on the Mars Exploration Rover (MER) mission took thousand of images along the traverse of the rover Spirit in Gusev Crater and the rover Opportunity in Meridiani Planum.

Using the developed method, it is possible to detect individual particles in the MI images, and knowing the physical size of the area covered in the MI images, it is simple to determine their size.

An example of such detection can be seen in Figure 2. Particles truncated by the image or partially buried were automatically omitted as their size and shape cannot be estimated. The size-distribution curves were obtained and grain properties such as diameter, length, width, circularity or elongation were measured. The grain diameter was defined as the diameter of the equivalent disk. In Table 1 are presented some re-

sults of the statistical analysis of the grains visible in the image shown in Figure 2.

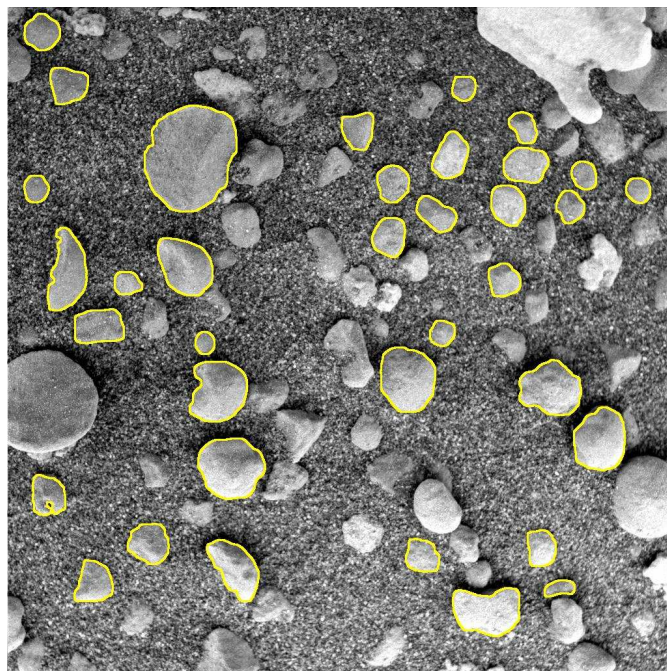


**Figure 2.** Detection of grains in the image of the Meridiani Planum deposit (taken on sol 15). Truncated or partly buried grains were automatically omitted. The image is 32 mm across.

	Value
Number of grains	36
Median diameter	1.73 mm
Mean diameter	1.90 mm
Standard deviation	0.72 mm
Mean circularity	0.84
Mean elongation	0.20

**Table 1.** Statistical analysis of the grains shown in Figure 2.

**Conclusions:** The developed automatic method allows fast granulometric analysis of various deposits. It provides similar results to sieve analysis or those obtained by manual methods. Furthermore, it allows studying the shape of grains, does not have any limitation on the size of grains, and permits to separate adjacent particles. The presented method can be used to study Martian as well as terrestrial materials.

**References:** [1] Yingst R. A. *et al.* (2008), Morphology and texture of particles along the Spirit rover traverse from sol 450 to sol 745, *JGR*, 113, E12S41. [2] Weitz C. M. *et al.* (2006), Soil grain analyses at Meridiani Planum, Mars *JGR*, 111, E12S04. [3] Jerolmack D. J. *et al.* (2006), Spatial grain size sorting in eolian ripples and estimation of wind conditions on planetary surfaces: application to Meridiani Planum, Mars, *JGR*, 111, E12S04.

**Introduction:** Successful future exploration of Mars requires a profound knowledge of the Martian environment. It is therefore necessary to investigate some major environmental aspects as lightning activity or the structure of the planetary subsurface.

Such an investigation may be performed using ELF electromagnetic waves (3-3000 Hz). An ELF electromagnetic wave generated by lightning activity propagates around the globe in a waveguide made of two electrically conductive spheres: the surface and the ionosphere. By studying ELF waves propagation in the ground-ionosphere waveguide, it is possible to examine the properties of the subsurface, the lower layers of the ionosphere, and to identify ELF waves sources. For instance, the Schumann resonance phenomenon, generated by ELF waves, can be used as a tool for groundwater detection.

As ELF propagation is of a global nature, one measuring station is enough to perform some basic research.

Using an analytical method, we are able to obtain relationships between the measured parameters and various properties of the environment.

**Instruments:** The lightweight measuring equipment consists of a low-power ELF receiver, two magnetic antennas and one electric antenna. In this work, we present the parameters of some exemplary antennas and intensity of discharges they enable to detect on Mars.



**Figure.1** Visualization of electric and magnetic antennas at the Martian surfaces.

**Methodology:** When an ELF wave is propagating from its source to a receiver the environmental properties, such as: electrical conductivity or permittivity of the surface, influence its propagation parameters. Using an analytical method based on a solution of Maxwell's equations, we can estimate the structure and composition of the Martian subsurface measuring the propagation parameters.

To present the possibilities of the method, we studied a direct scenario with the hypothetical models of the planetary subsurface and ELF sources. For these models, we present the ELF pulses propagation and the Schumann resonance spectra.

**Results:** In this theoretical approach, we assume double-layered models of the Martian subsurface. In these models, the upper layer has a very low conductivity ( $\sigma = 10^{-7}$  S/m), as there is no liquid water present at the planetary surface. For the lower layer we propose three models: two with water reservoirs and one without them. The conductivity profiles for the subsurface with water aquifers were based on the work of Clifford *et al.* [1]. In these models, the thickness of the upper layer is only 10 km, and the conductivity of the lower layer is  $10^{-2}$  S/m (a case with brines) or  $10^{-4}$  S/m (a case with low-salinity aquifers). In the model without water reservoirs (a dry

case), the low conductive layer is 40 km deep, and the conductivity of the lower layer is  $\sigma = 10^{-2}$  S/m. To illustrate the influence of the ground on ELF propagation, we also consider the model with a perfectly conducting ground.

To calculate the propagation of ELF pulses, we assume that the source of an ELF wave has the form of the delta function and an amplitude of  $1 \text{ C} \cdot \text{km}$  [2].

The Schumann resonance spectra and the waveforms of the ELF pulses for the models are shown in Fig.2 and Fig.3.

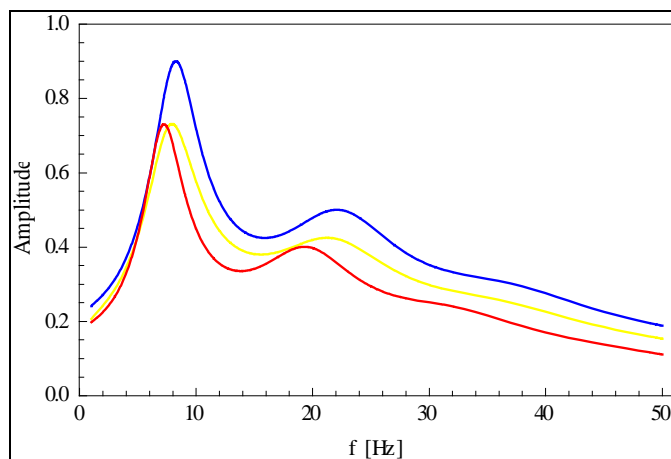


**Figure.2** The Schumann resonance spectra for the different models of the Martian subsurface: with brines (blue line), with low salinity aquifers (yellow line), dry (red line). All spectra were normalized to the amplitude of the model with the perfectly conducting ground.

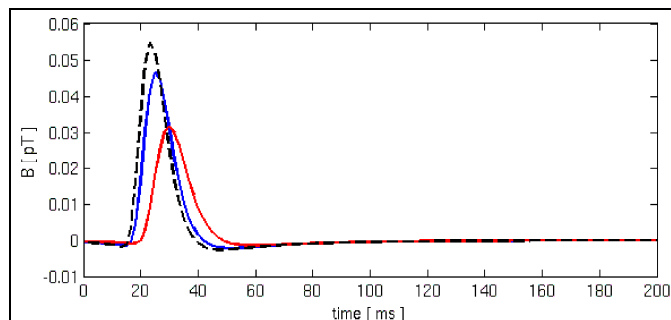


**Figure.3** The waveforms of the ELF pulses at a propagation distance of 5 Mm in the Martian waveguide with the perfectly conducting ground (dashed line), with brines (blue line), and without aquifers (red line) [2].

**Conclusions:** The results demonstrate that the developed methodology and receiving system may be used to measured global electromagnetic parameters of the subsurface, atmosphere and intensity of electrical discharges.

**References:** [1] Clifford, S.M. *et al.* (2010), The Depth of the Martian Cryosphere: Revised Estimates and Implications for the Existence and Detection of Subpermafrost Groundwater, *JGR*. vol. 115, E07001. [2] Kułak, A. *et al.* (2013), An Analytical Model of ELF Radiowave Propagation in Ground-Ionosphere Waveguides With a Multilayered Ground, *IEEE Transactions on Antennas and Propagations*, Vol. 61, No. 9, 10.1109/TAP.2013.2268244.

# ORNAK (TATRA MOUNTAINS) AS A TERRESTRIAL ANALOGUE FOR MARTIAN DEEP-SEATED GRAVITATIONAL SPREADING (SACKUNG).

Olga Kromuszczyńska<sup>1</sup>, Daniel Mège<sup>1,2</sup> and Antoine Lucas<sup>3</sup>, <sup>1</sup>WROONA Group, Institute of Geological Sciences, Polish Academy of Sciences, Research Centre in Wrocław, Podwale St. 75, PL-50449 Wrocław, Poland (okromuszczyńska@twarda.pan.pl; daniel.mege@twarda.pan.pl), <sup>2</sup>Laboratoire de planétologie et géodynamique, UMR CNRS 6112, University of Nantes, France, <sup>3</sup>AIM Laboratory, Paris-Diderot University, Paris, France.

**Introduction:** Uphill-facing normal faults scarps and crestal grabens, which are characteristic of deep-seated gravitational spreading (DSGS) of topographic ridges, or sackung [1,2], are described in Coprates Chasma in Valles Marineris, Mars [3], and at the Ornak ridge, in the Polish Tatras (Figure 1a), and displacements are compared.

**Data and methods:** The vertical offset of the normal faults are estimated from topography data and corrected from scarp erosion by assuming the fault dip angles to be 60-70°, typical of normal faults in extensional settings on Earth [eg. 4]. Fault displacement in Coprates Chasma has been obtained along 11 profiles located on the northern slope of the sagging ridge, using stereo-derived CTX digital elevation models having a grid spacing of 30 meters and vertical accuracy of 15 meters [5]. Displacement data at Ornak have been calculated from field measurements. Thirteen topographic profiles across the Ornak ridge top (Figure 1.c) were obtained using GPS device Garmin GPSmap 62s. Vertical accuracy of GPS has been qualitatively and quantitatively evaluated.

### Results:

**Mars - Coprates Chasma.** The vertical offset of DSGS normal faults is between 40 and 1000 metres, with an average value of about 300 metres [5].

**Earth - Ornak.** The results of profile analysis shows that the vertical displacement of faults related to DSGS are from a few tens of centimeters to 34 metres (Figure 1.d).

**Conclusions:** DSGS vertical displacements on Mars and Earth differ by one order of magnitude at least. This difference corresponds to one order of magnitude of difference in ridge height and width: 5500 m and 22000 m for Coprates Chasma, respectively, versus 450 m and 1250 m for Ornak. Cumulated vertical displacement scaled to ridge height is almost similar, 0.04 at Coprates Chasma and 0.02 at Ornak. The vertical offsets of DSGS fault scarps are therefore homothetic.

**References:** [1] Zischinsky U. (1966) On the deformation of high slopes, *Proc. 1st Congr. Int. Soc. Rock Mechanics*, 2, 179–185. [2] Varnes D.J. et al. (1989) Topographic and structural conditions in areas of gravitational spreading of ridges in the western United States, *U.S. Geol. Surv. Prof. Pap.*, 1496. [3] Mège D. and Bourgeois O. (2011) Equatorial glaciations on Mars revealed by gravitational collapse of Valles Marineris wallslopes, *Earth Planet. Sci. Lett.*, 310, 182–191 [4] Gudmundsson, A. (1992) Formation and growth of normal faults at the divergent plate boundary in Iceland, *Terra Nova*, 4, 464-471. [5] Kromuszczyńska O. et al. (2012) Giant Sackung Scarps in Valles Marineris, *Lunar Planet. Sci.* 43 (Abstract 1161).

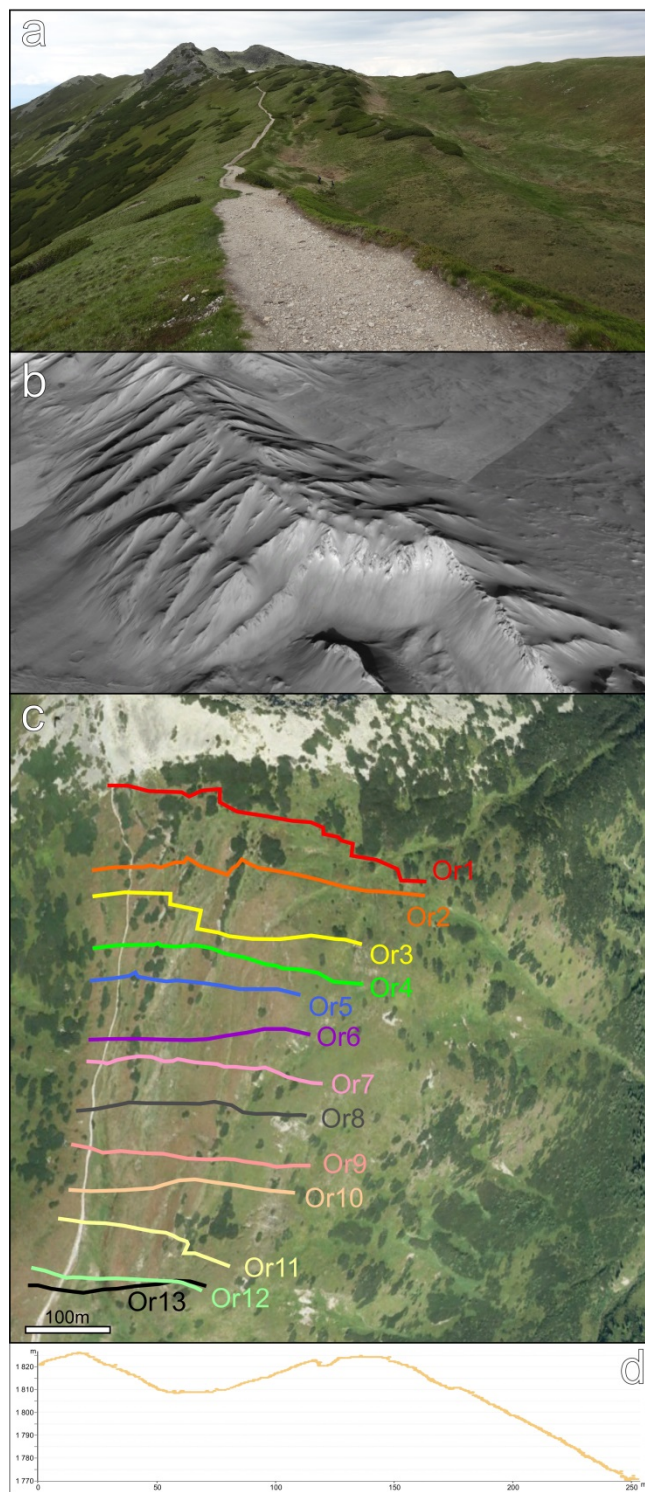


**Figure 1. a:** DSGS features on the intrinal ridge in Coprates Chasma; **b:** DSGS features on Ornak; **c:** localization of GPS profiles on Ornak; **d:** example of Ornak profiles - Or13.

**Introduction:** The Pułtusk meteorite is a breccia composed of H4 and H5 chondritic clasts, embedded in zones of cataclasis and crushing. In spite of moderate shock index of Pułtusk – S3 in classification scheme of [1], the chondrite registers sequence of impact processes, which acted on the parent body. Based on  $\mu$ -CT scanning and microscopic observation, as well as EPMA analyses, following products of impacts are identified: poikilitic, metallic veins, igneous-textured enclaves [*sensu* 2], impact melt clasts and darkened, cataclastic zones rich in xenolithic material. On the base of the spatial relationship of these textural elements, at least three impact events on the H chondrite parent asteroid are proposed

**First, synaccretional event:** Very common in many specimens of the Pułtusk are large, irregular, metallic veins. They are composed of ameoboid kamacite grains, which are usually connected with each other by protrusions. Chondritic rock around the veins is rich in large merrillite (up to 800  $\mu$ m) and plagioclase (150  $\mu$ m) crystals, which are broadly accepted to be phases of late accretional metamorphism [3]. The mineralogy and texture of the veins suggest that FeNi-metal was unmixed from impact melt and incorporated into the partly equilibrated chondritic rock. Slowly cooling metal supplied phosphorous to the chondritic rock and merrillite crystals formed. Formation of impact melt, its unmixing into silicate and metallic portion, and postimpact increase in temperature explain very well the coarse grained textures of igneous enclaves occurring in Pułtusk. They may be products of fractionation and crystallization of silicate melt in crater basement.

Probably, all the products were formed during one impact event, which must have acted synaccretionally. Similar textures were identified in Kernouvé [4], and Portales Valley [5] chondrites, which were deformed  $\sim$ 4.5 Ga, suggesting the impact could have affected large part of the parent body.

Two chemically and mineralogically different types of apatite occur in Pułtusk. Typical for the host rock are small, well equilibrated pure chlorapatite grains with the content of Cl up to  $5.1 \pm 0.8$  wt%. In the vicinity of the poikilitic veins, overgrowths of apatite on large merrillite crystals are very abundant. Apatites of this type reveal strong negative correlation of Cl and F content (1.5 – 6.5 wt% of Cl and 0 – 3.3 wt% of F), that can be observed even in single grains. As apatite crystals are more porous than merrillite and contain tiny veins into the chondritic rock, they were, likely, formed from merrillite. The presence of the two generations of apatite suggests two episodes of fluidisation, and one of them has to be related to postimpact fluid activity.

**Second, postaccretional impact:** Incorporated into the Pułtusk breccia, as its minor part, impact melt clasts occur. The melt is composed of olivine and pyroxene microcrystals embedded into plagioclase glass and unmixed FeNi and troilite eutectic intergrowths. All the minerals have strong affinity to the equilibrated H chondritic material. Measurements of the distances between kamacite globules in the eutectic structures show that the melt cooled rapidly, with rate of  $\sim$ 15  $^{\circ}$ C/s. Thus, it must have been quenched near the surface of the parent body [6], after formation of large impact crater. As many impact melt rock and impact melt breccias (IMBs) were formed

on the H chondrite parent body during severe  $\sim$ 3.7 Ga event [7,8,9], and because of strong compositional similarity of Pułtusk clasts to those IMBs, it is suggested here that the Pułtusk clasts were formed in severe impact event but, contrary to the IMBs with H chondrite affinity, the clasts were thrown away from I<sub>2</sub> crater and incorporated into the rock forming the cratered filling of I<sub>1</sub> impact.

**The youngest collision:** The most prominent in Pułtusk are cataclastic zones rich in pseudotachylyte-like bands. Spatially strictly related to the zones, but occurring in the host rock, microfaults also occur [10]. Structures of shearing and cataclasis cut all the products of former impact events, suggesting young collision in the rock evolution. As Pułtusk is only weakly shocked (S3), observed severe high strain-rate shear deformation is difficult to be explained, however, some evidence exist that the petrofabric could have been inherited after oblique collision [11,10].

In cataclastic zones of Pułtusk, CM2.6 xenoliths occur. They are hydrated, weakly shocked, but ductily sheared along with the host. As CM-type xenoliths are abundant in H chondritic breccias [12], they might have been incorporated during I<sub>3</sub>, oblique collision of H and CM-like bodies.

**Conclusion:** The Pułtusk breccia is product of impact processes on the surface of H chondrite asteroid. Research on different textural parts of the chondrite shows plausible sequence of three impact events in the history of the parent body. It shows that the evolution of the H chondrite parent asteroid was related to much more significant dynamical processes than it was supposed earlier having only taken into account chondritic gas retention ages [8,9,13].

**References:** [1] Stöffler D. et al. (1991), Shock metamorphism of ordinary chondrites. *GCA* 55, 3845–3867. [2] Jamsja N. and Ruzicka A. (2010), Shock and thermal history of Northwest Africa 4859, an annealed impact-breccia of LL chondrite parentage containing unusual igneous features and pentlandite. *M&PS* 45, 828–849. [3] Brearley A.J. and Jones R.H. (1998), Chondritic meteorites. Planetary materials. Papike J.J. (ed), *Reviews in Mineralogy*, vol. 36: 3–398. [4] Friedrich J. M. et al. (2013), Metal veins in the Kernouvé (H6 S1) chondrite: Evidence for pre- or syn- metamorphic shear deformation. *GCA* 116, 71–83. [5] Ruzicka A. et al. (2005), Portales Valley: Petrology of a metallic-melt meteorite breccia. *M&PS* 40, 261–295. [6] Scott E.R.D. (1982), Origin of rapidly solidified metal-troilite grains in chondrites and iron meteorites. *GCA* 46, 813–823. [7] Ganapathy R. and Anders E. (1973), Noble gases in eleven H-chondrites. *GCA* 37, 359–362. [8] Wittmann A. et al. (2010), Impact cratering on the H chondrite parent asteroid. *JGR* 115, E07009–E07030. [9] Folco L. et al. (2004), Extensive impact melting on the H-chondrite parent asteroid during the cataclysmic bombardment of the early solar system: Evidence from the achondritic meteorite Dar al Gani 896. *GCA* 68, 2379–2397. [10] Krzesińska A. (2010), Oblique impact-induced (shock-related) shearing and frictional melting in Pułtusk (H5) chondrite. *41<sup>st</sup> LPSC #1140*. [11] van der Bogert C. H. et al. (2003), Impact-induced frictional melting in ordinary chondrites: A mechanism for deformation, darkening, and vein formation. *M&PS* 38, 1521–1531. [12] Rubin A. E. and Bottke W. F. (2009), On the origin of shocked and unshocked CM clasts in H-chondrite regolith breccias. *M&PS* 44, 701–724. [13] Swindle T.D. et al. (2009), <sup>40</sup>Ar-<sup>39</sup>Ar ages of H-chondrite impact melt breccias. *M&PS* 44, 747–762.

**Introduction:** The minerals absorb and reflect thermal infrared (TIR) light of the different wavelengths depending on their composition and structure. Thus, every rock absorbs and reflects different wavelengths in TIR and has its own spectral signature. The TIR images can be used in the thermal inertia (TI) mapping and more precisely, in its approximation called apparent thermal inertia (ATI), which can be calculated from surface albedo ( $A$ ) and diurnal temperature difference ( $\Delta T$ ) [1]. Hereby, the thermal images can provide an information complementary to visible and near-infrared (NIR) data (e.g. CTX, CRISM, OMEGA).

For interpreting the TIR spectra of the Martian surface obtained from orbiters, we can use the spectral libraries of terrestrial rocks and minerals [2].

**Thermal data:** Thermal data for Mars were obtained by two instruments: Thermal Emission Spectrometer (TES) on board Mars Global Surveyor, and Thermal Emission Imaging System (THEMIS) on board the Mars Odyssey spacecraft. THEMIS IR data was applied in our research due to the better spatial resolution (100 m/pixel). High-resolution mapping of apparent thermal inertia of the Valles Marineris region has not been performed so far.

**Thermal data processing:** THEMIS IR images were processed online using the Themis Processing Web Interface (THMPROC, <http://thmproc.mars.asu.edu>). THMPROC enables calculation of i.a. emissivity and brightness temperature values. The brightness (radiant) temperature ( $T_{rad}$ ) can be then converted to kinetic temperature ( $T_{kin}$ ) based on broadband emissivity values ( $e$ ), according to the following equation:

$$T_{kin} = \frac{T_{rad}}{e^{1/4}} \quad (1)$$

The broadband emissivity has been calculated based on nine THEMIS IR bands with relation to the Planck's curve. Each pixel of the calculated emissivity map had nine different emissivity values – one from each band/wavelength. Those values were calculated having assumed that the band with the highest temperature had an emissivity of  $\sim 1$ . This band was used to anchor the Planck curve of blackbody radiation and to calculate the emissivities from the other bands which had lower emissivity values. The assumption that the highest temperature has an emissivity of  $\sim 1$  is a simplification. Nevertheless, this is the best way to calculate emissivity, since the absolute emissivity of the surface materials underneath each pixel is unknown.

**Apparent thermal inertia map:** As real thermal inertia (TI) cannot be measured by the remote sensing methods (conductivity, density and thermal capacity can be measured only by the contact methods), its approximation called apparent thermal inertia (ATI) was applied. ATI is defined as:

$$ATI = \frac{1-A}{\Delta T} \quad (2)$$

where  $A$  is the albedo in the visible range and  $\Delta T$  is the difference of the maximum and the minimum temperature.  $\Delta T$  can be determined by subtracting the digitally recorded nighttime temperature from the daytime temperature.  $\Delta T$  is low for the materials with high thermal inertia and high for those with low thermal inertia. Albedo was used to compensate the various absorptivity values of the rocks. [3]. For the calculation of  $\Delta T$ , the THEMIS images of good quality were chosen: the minimum and maximum “summing” parameter was set to 1 (it gives the full-resolution images only), the minimum and maximum “image rating values” were set to 4 and 7 respectively (they give the good-quality images only). The maximum (day) and minimum (night) temperatures were defined based on MARSTHERM model (<https://marstherm.boulder.swri.edu/>). The local times of minimum and maximum temperatures for the Valles Marineris are 06:00 (night) and 13:00 (day).

The albedo values were estimated based on the CTX/MRO images. They have been acquired using the PILOT website (<http://pilot.wr.usgs.gov/>), and processed online following the ISIS procedures: *spiceinit* (update camera pointing information), *ctxcal* (apply radiometric calibration), *ctxevenodd* (remove even odd detector striping from CTX) and *cam2map* (project from camera space to map space). After the PILOT processing, CTX images represent the ratio of reflected energy to incoming energy (irradiance/solar flux, often simply called I/F). In order to convert I/F factor into Lambert albedo, the I/F values were divided by the cosine of the solar incidence angle. In the calculations, one average value of incident angle was adopted for the whole CTX image. The preliminary calculation of ATI for a selected part of Valles Marineris (275.2°E, -7.4°N) was made. The obtained values are within the ranges cited in the literature [4].

**Perspectives:** The high-resolution apparent thermal inertia map will be calculated for selected landforms in the Valles Marineris region. The methodology will be verified and compared to the existing thermal inertia maps [5, 6]. The transparency of the atmosphere and the relief will be also included in the calculation.

**References:** [1] Xue Y. and Cracknell A. P. (1996), Thermal inertia determination from space – a tutorial review, *Int. J. Remote Sensing*, 17, 431-461. [2] Christensen, P.R., et al. (2003), Morphology and composition of the surface of Mars: Mars Odyssey THEMIS results, *Science*, 300, 2056-2061. [3] Sabins F.F. (2007), Remote Sensing: Principles and Interpretation (Third Edition), Waveland Press, Incorporated. [4] Kahle A., B. (1981), Geologic application of thermal inertia using HCMM data, Pasadena, Calif.: National Aeronautics and Space Administration, Jet Propulsion Laboratory. [5] Christensen et al. (2001), The Mars Global Surveyor Thermal Emission Spectrometer experiment: Investigation description and surface science results, *J. Geophys. Res.*, 106, 23,823-23,871. [6] Putzig, N. E., Mellon M. T., Kretke K. A. and Arvidson R. E. (2005), Global thermal inertia and surface properties of Mars from the MGS mapping mission, *Icarus*, 173, 325-341.

**Introduction:** Measurement of variable chlorophyll fluorescence is common approach to assess actual physiological status in plant physiology [1-4], since it is fast and non-destructive. This approach is being applied now even in extreme environments to characterize photosynthetic performance of extremophilic cyanobacteria and algae [5-7]. Variable fluorescence imaging may also serve as detection tool for photosynthetic microorganisms in the field as shown in Gómez et al. [8]. In this study, we tried to detect and characterize cryptoendolithic communities in sandstone and gypsum in Svalbard.

**Material and Methods:** The rock samples were collected in Petuniabukta (N 78°42' E 16°25'), Central Svalbard, on August 11-26, 2012. The elevation ranged 63 to 106 m a.s.l. into sterile zip-bags. The site and the sample were photographed by a digital camera (Fig. 1).



Fig. 1. Gypsum outcrops in Petuniabukta, Svalbard.

**Community structure.** The microbial community structure and species composition were observed using Olympus BX-53 microscope (Olympus C&S, Japan) equipped by Olympus DP71 digital camera (Olympus C&S, Japan). The pictures were processed by QuickPhoto Camera 2.3 software (Promicra, Czech Republic). The cyanobacterial morphospecies were identified according to Komárek and Anagnostidis [9].

**Fluorescence measurement.** The fluorescence measurements were performed using FluorCam MF800 fluorescence imaging camera (Photon Systems Instruments, Czech Republic) and processed by FluorCam 7 software (Photon Systems Instruments, Czech Republic). Protocol for maximum quantum yield was applied.

**Results:** In this initial study, total of 4 samples were proceeded.



**Community structure.** The microbial community consisted of coccal cyanobacteria only. Filamentous cyanobacteria or eukaryotic algae were not observed (Fig 2).

Fig. 2. Cf. *Gloeocapsa* sp.

**Fluorescence measurement.** The photosynthetically active area was detected in all samples (Fig. 3).

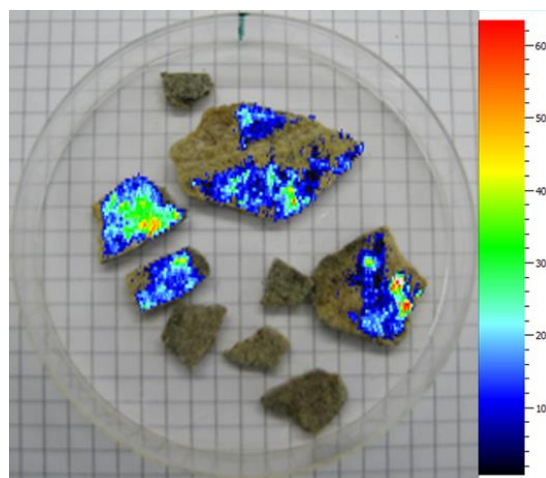


Fig. 3. The example of detection of photosynthetically active areas. The scale indicates fluorescence intensity in false colors; it may serve as chlorophyll content proxy.

The values of maximum quantum yields ranged 0.07 to 0.23, indicating thus stress conditions.

**Conclusions:** Variable chlorophyll fluorescence imaging revealed presence of photosynthetic microorganisms in endolithic communities and proved their photosynthetic activity. However, this method is restricted to chlorophyll containing microorganisms.

**Acknowledgements:** The lecture was supported in frame of projects LM2010009, CZ.1.07/2.2.00/28.0190 and RVO 67985939.

**References:** [1] Bohlar-Nordenkamp H.R. et al. (1989), Chlorophyll fluorescence as a probe of the photosynthetic competence of leaves in the field: a review of current instrumentation. *Funct. Ecol.*, 4, 497-514. [2] Campbell D. et al. (1998), Chlorophyll fluorescence analysis in cyanobacterial photosynthesis and acclimation. *Microbiol. Mol. Biol. Rev.*, 62, 667-683. [3] Maxwell K. and Johnson G.N. (2000), Chlorophyll fluorescence - a practical guide. *J. Exp. Bot.*, 51, 659-668. [4] Strasser B.J. et al. (2000), The fluorescence transient as a tool to characterize and screen photosynthetic samples. Yunus M. et al., *Probing photosynthesis: Mechanisms, Regulation and Adaptation*, 445-483. [5] Kvíderová J. (2010), Characterization of the community of snow algae and their photochemical performance in situ in the Giant Mountains, Czech Republic. *Arct. Antarct. Alp. Res.*, 42, 210-218. [6] Kvíderová J. et al. (2011), *In situ* response of *Nostoc commune* s.l. colonies to desiccation in Central Svalbard, Norwegian High Arctic. *Fottea*, 11, 87-97. [7] Marteinson V. et al. (2013), A laboratory of extremophiles: Iceland Coordination Action for Research Activities on Life in Extreme Environments (CAREX) Field Campaign. *Life*, 3, 211-233. [8] Gómez F. et al. (2011), Multidisciplinary integrated field campaign to an acidic Martian Earth analogue with astrobiological interest: Rio Tinto. *Int. J. Astrobiol.*, 10, 291-305. [9] Komárek J. and Anagnostidis K. (1999), Süßwasserflora von Mitteleuropa 19/1. Cyanopokaryota. 1.Teil: Chroococcales. Gustav Fischer Verlag.

# PLANETARY ROVER ROBOTICS EXPERIMENT IN EDUCATION: CARBONATE ROCK COLLECTING EXPERIMENT OF THE HUSAR-5 ROVER OF THE SZÉCHENYI ISTVÁN HIGH SCHOOL, SOPRON, HUNGARY.

Lang Á.<sup>1</sup>, Szalay K.<sup>1</sup>, Kocsis Á.<sup>1</sup>, Prajczner P.<sup>1</sup>, Bérczi Sz.<sup>2</sup>, <sup>1</sup>Széchenyi István Gimnázium High School, H-9400 Sopron, Templom u. 26. Hungary (mmecurie95@gmail.com) <sup>2</sup>Eötvös University, Institute of Physics, Dept. Materials Physics, H-1117, Budapest, Pázmány Péter s. 1/a. Hungary ([bercziszani@ludens.elte.hu](mailto:bercziszani@ludens.elte.hu)).

**Introduction:** The new experiment for the Husar-5 educational space probe rover consists of steps of the technology of procedure of finding carbonate specimens among the rocks on the field. 3 main steps were robotized: 1) identification of carbonate by acid test, 2) measuring the gases liberated by acid, and 3) magnetic test.

**Background:** The triggering sources for this experiment are the following. Spirit has found carbonates (by APXS measurements) at Comanche Spur rock comprised from magnesite, siderite, calcite, and rhodochrosite components. (Morris et al, 2010) [1] The discovery of the first carbonate meteorite (Bérczi et al. 2012) [2] which have fallen at Nagykovácsi, focused our attention to this type of rocks for identification by robotics methods on planetary surfaces.

**Experimental technology steps:** It is known that dropping acids produce rather quick reactions with carbonate rocks. This is the first robotic work to realize by electronics. The CO<sub>2</sub> gas produced will be observed by gas sensors. This is the second act to be robotized. Of the carbonates some are paramagnetic, especially siderite (iron-carbonate). This results in a third step: magnet contact and attraction of siderite by magnet.

**Construction of the experiment:** The basis of the robotic realization of the experiment is a rover which can move on the field. Onto this rover the mechanism of the experiments were built from Technics LEGO elements and we used LEGO-motors for making move these experiments. The operation was coordinated by an NXT-brick which was suitable

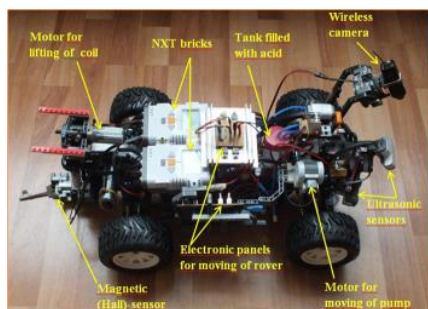


Fig. 1. The Husar-5 rover with the Carbonate experiment instruments.

to programming.

For the acetic-test the drops should be passed to the selected area. Passing a drop to a locality: From the small holder of the acid using densified gas we pump some drop onto the selected rock. We promote this process by pumping the atmospheric gas into another small gas-container, so we have another higher pressure gas there. This is pumped into the acid-holder.

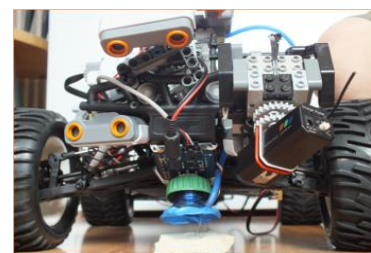


Fig. 2. The Husar-5 rover measuring (could not automatize it).

In the next step we can identify the the liberated gas by the gas sensor. This is not a typical LEGO-sensor, but it is a gas sensor measuring by the electric resistance change. LEGO compatibility was reached by soldering it into the box of the LEGO--sensor. This way we could attach it to one of the sensor-ports of the NXT. Using our gas sensor we can confirm the liberation of the CO<sub>2</sub> gas without outer observer.

The third step is the controll of the paramagnetic properties. Paramagnetic magnetism means that the body exhibits magnetic features by the effect of an outer magnetic field. In measuring this feature a Hall-sensor is our instrumentation. If we carry a permanent magnet, however, then our sensor will measure the magnetic field of that, not the magnetic field of the magnetized siderite. That is why we use a electric current generated magnet. The magnetic test has the following operations in the measuring procedure: first we measure with the Hall-sensor and this value is stored in the memory. Then we close the circuit of the coil by a relay. The



Fig. 3. The Husar-5 rover when coil of the magnetic experiment is in lowered position, under it the siderite-candidat

program read the Hall-sensor simultaneously with the circuit opening and compares the 2 magnetic field strengths and decides that the sample has paramagnetic property, or not.

During the measurements both the coil and the gas-

sensor should be positioned to be near to the surface. This means, that a lowering and an uplifting machinery should be constructed.

**Summary:** The sequence of the measurement is the following. 1) the camera – after giving panorama images – turns toward the soil surface, 2) the dropping onto the rock surface 3) at the same time the gas-sensor starts to move down above the rock 4) evaluation of the gas-sensor data 5) if CO<sub>2</sub> is present the magnet-test begins, therefore the rovers moves forward into a good position for the coil lowering 6) after magnetization measuring with Hall-sensor 7) summary of the 3 tests.

**References:** [1] Morris, R.V. et al. (2010): Identification of Carbonate-Rich Outcrops on Mars by the Spirit Rover. *Science*, **329**, No. 5990, pp. 421-424. DOI: 10.1126/science.1189667; [2] Bérczi Sz.. et al. (2012): Discovery of the First Iron-Carbonate Meteorite, Observed Fall of a Sedimentary Rock with Regmaglypts, Hot State and No Radioactive Carbon 14 Inside, At Nagykovácsi, Hungary.

**POTENTIAL OF MAGNETIC MEASUREMENTS FOR DETECTION OF HORIZONTAL MOVEMENTS OF THE MARTIAN CRUSTAL BLOCKS.** Lewandowski, M.<sup>(1,2)</sup>, Józwiak, W.<sup>(2)</sup>, and Mizerski, K.<sup>(2)</sup>.<sup>(1)</sup> Institute of Geological Sciences, P.A.S., Twarda St 51/55, 00-818 Warsaw, Poland e-mail: [lemar@twarda.pan.pl](mailto:lemar@twarda.pan.pl) <sup>(2)</sup> Institute of Geophysics, P.A.S., Ks. Janusza 64 St 01-452 Warsaw, Poland. e-mail: [jozwiak@igf.edu.pl](mailto:jozwiak@igf.edu.pl) e-mail: [kamiz@igf.edu.pl](mailto:kamiz@igf.edu.pl)

Geocentric axial dipole model is a crucial concept of paleo-magnetism. In this model, the magnetic field produced by a single magnetic dipole at the centre of the Earth and aligned with the rotation axis is considered. In a dipole magnetic field

$$\tan I = 2 \tan \lambda,$$

where  $I$  is an inclination of an ambient magnetic field vector and  $\lambda$  is a latitude ranging between -90 to +90 from the South pole through the equator, where  $\lambda=0$ , to the North pole. It is then expected that a vector of a natural remanent magnetization (NRM), acquired in rocks formed at the magnetic poles, will show vertical inclination. Any variation from this scheme may be interpreted in terms of horizontal displacement of the rocks under study. Alternatively, however, it could be also taken in favour of a central Martian axial dipole field (CMAD), once potentially existing on Mars.

Currently, Mars is featuring several magnetic poles. Their presence may be attributed to a second-rank magnetic non-dipole components that were frozen after the CMAD had vanished. In this presentation, I/we show a simple method to test, whether rocks sampled at a pole of the magnetic anomaly of Mars possess a vertical inclination of NRM, in line with the magnetic dipole hypothesis. A fundamental issue for the test is to measure the local magnetic anomaly at a one of magnetic poles of Mars, which may be considered an effect of a magnetic dipole, centred at depth of the planet. It then opens the possibility for speculations on possible tectonic mechanisms of development of the local crustal magnetic anomaly and modelling of such mechanisms.

**Introduction:** Recently, extensive gypsum deposits have been discovered in the Circumpolar Dune Field and on the Martian Northern Ice Cap (MNIC) [1, 2, 3,4,5]. One of the proposed mechanisms of their formation is by weathering within ice [6, 7, 8], however none of the previous studies have checked if this process is possible under current Martian conditions. Studies of Martian evaporitic minerals are crucial for constraining characteristics of the aqueous fluids, both past and present, on the surface of the Red Planet. This is especially important because areas of evaporitic mineral formation may be among the most hospitable environments on Mars [9, 10].

The aim of this paper is to numerically model if the weathering of dust grains within the MNIC is possible under current Martian conditions in order to explain the existence of extensive gypsum deposits at Meridiani Planum. To test this hypothesis, we check if radiant heating is sufficient to melt a thin layer of ice surrounding a single dust grain exposed within the south-facing side of the MNIC spiral trench.

**Analogue Studies:** The physical and geochemical conditions on the terrestrial Antarctic ice sheet are similar to those on the current MNIC [11, 12, 13, 14]. Despite temperatures well below 0°C, and thus without abundant liquid water present on the surface, ~5% of meteorites found in Antarctica include amounts of terrestrial evaporites that are detectable with the naked eye [15]. However, it is probable that a large portion of other Antarctic meteorites also include at least some amount of those minerals [16]. Those evaporites are formed by the interaction of rocks with water melted by stones heated by the solar irradiation. Similarly, tephra present within ice can be heated sufficiently to melt surrounding ice [17, 18]. Additionally, material within cryonite holes can have albedo as low as 0.1-0.4 [19], which leads to melting even if silicate material is covered by one meter thick layer of ice [20].

**Methods:** We model a single basaltic dust grain (2-200 μm in diameter) lying on glacial ice that is mixed with dust, exposed within a spiral trough of the MNIC and heated by solar irradiance during the warmest days of the summer. We assume that the surface of the grain is inclined so that solar rays are perpendicular to the surface of the grain at noon. To describe this process, we developed a 2D numerical model based on the equation of heat transfer (see [21] for more details):

$$\rho c_p \frac{\partial T(x,t)}{\partial t} = \frac{\partial}{\partial x} k(x) \frac{\partial T(x,t)}{\partial x} + Q(x,T,t)$$

The equation is solved for  $x=[0, D]$  with the following boundary conditions:

$$-k \frac{\partial T(x,t)}{\partial x} = AS - eCT^4 \quad \text{for } x = 0 \text{ (the surface)}$$

$$T = T_{low} \quad \text{for } x = D \text{ (the lower boundary).}$$

The calculations are made for different values of parameters within the range probable for the surface of Mars (e.g., initial surface temperature: 200-215 K, solar irradiation: 400-300 W/m<sup>2</sup>, albedo for visible radiation 0.13).

**Results:** The average temperature of the 2 μm grain can reach up to 1-2°C, which is sufficient to heat and melt ice surrounding it up to a depth of a few mm. A dust grain will have a temperature sufficient to melt adhering ice for up to a

few hours each day (Fig. 1) during the warmest weeks of the summer. The amount of melted ice depends mainly on: the solar constant (affected by latitude and the inclination of the slope where the dust grain is located), the thermal conductivity of ice-dust-air mixtures, and IR emissivity of the dust grain.

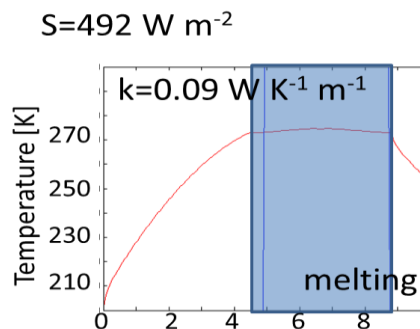


**Figure 1.** An example of temperature profile below a grain (200 μm) vs. time with assumed value of thermal conductivity of  $k=0.09 \text{ W/Km}$  and solar constant  $S=492 \text{ W/m}^2$ . Simulation covers 0.4 Martian day. The local noon is approximately at time = 5 h.

**Discussion:** Results of modeling the radiant heating of dust particles lying on the surface of the MNIC show that it is possible to produce liquid water on the surface of Mars under current conditions. Because average surface pressure in this location is ~660-760 Pa, which is above the triple point, liquid water ~0°C would not sublime. The evaporation can be further limited by the layer of ice developed on top of the grain, similarly to the ice-lead covered cryonite holes from Antarctica [20].

The interaction of the dust particles with small amounts of liquid water could lead to formation of evaporitic minerals, similar to evaporates formed on terrestrial, Antarctic meteorites [15]. Because MNIC may be a location on the surface of Mars where liquid water is the most abundant, it may be a place where chances of finding Martian microbes are the highest.

**References:** [1] Langevin et al. 2005, *Icarus* 144: 456-462. [2] Roach et al. 2007, *37th LPSC*, Abstract #1970. [3] Horgan et al. 2009, *J. Geoph. Res. Planets* 114: 1-27. [4] Masse et al. 2010, *Icarus* 209: 434-451. [5] Masse et al. 2012, *Earth Planet. Sci. Lett.* 317-318: 44-55. [6] Catling et al. 2006, *Icarus* 181: 26-51. [7] Zolotov and Mironenko 2007, *J. Geoph. Res. Planets* 112, doi:10.1029/2006JE002882. [8] Niles and Michalski 2009, *Nature Geoscience* 2: 215-220. [9] Horneck 2000, *Planet Space Sci. Lett.* 48:1053-1063. [10] Benison and LaClair 2003, *Astrobiology* 3: 609-618. [11] Harvey et al. 2006, *37th LPSC* Abstract #1044. [12] Socki et al. 2008, *Geomorph.* 121, 69-83. [13] Liu and Bish 2010, *41st LPSC* Abstract #1533. [14] Hallis 2013 *MAPS* 15: 1-15. [15] Losiak and Velbel 2011 *MAPS* 46:443-458. [16] Losiak 2009 *MS Thesis*, Michigan St. U.. [17] Harpel et al. 2008, *J. Volcanol. Geotherm. Res.* 177: 549-568. [18] Dadic et al. 2013, *J. Geoph. Res.: Earth Surface* 118: 1658-1676. [19] Hodson et al. 2008, *Ecol. Monogr.* 78: 41-67. [20] Paerl and Priscu 1998, *Microb. Ecol.* 36: 221-230. [21] Czechowski 2012, *Acta Geophys.* 60: 1192-1212.

# REMOTE SCIENCE SUPPORT TEAM DURING MARS2013: TESTING A MAP BASED SYSTEM OF DATA PROCESSING AND UTILIZATION FOR THE FUTURE LONG-DURATION PLANETARY MISSIONS.

Anna Losiak<sup>1,2</sup>, Izabela Gołębiewska<sup>3</sup>, Csilla Orgel<sup>2,4</sup>, Linda Moser<sup>2</sup>, Jane MacArthur<sup>2,5</sup>, Andrea Boyd<sup>2,6</sup>, Sebastian Hettrich<sup>2,7,8</sup>, Natalie Jones<sup>9</sup>, Gernot Groemer<sup>2</sup> (1) Institute of Geological Sciences, Polish Academy of Sciences, Wrocław (anna.losiak@twarda.pan.pl), (2) Austrian Space Forum, (3) University of Warsaw, (4) Eötvös Loránd University, (5) University College London, (6) Space Applications Services (7) German Federal Office for Radiation Protection, Oberschleissheim, (8) Meteorological Institute Munich, Ludwig Maximilian University of Munich, (9) The Royal Military College of Canada

**Mars Analog Missions:** Future manned Mars missions are likely to involve astronauts spending up to 17 months on the surface of the Red Planet [1] during which communication between Earth and the Mars Crew will be performed with a time delay ranging from 3 to 24 minutes [2]. Designing a mission architecture that will optimize the efficiency of the science operations under these conditions will have to differ significantly from the previous science exploration missions. Extravehicular activity during Apollo missions lasted up to 22 hours [3] and communication with Earth was in real-time. Because of that, the most efficient strategy involved limiting geological tasks performed by astronauts on the surface to describing surroundings and outcrops, geological sampling, and setting up geological experiments (e.g., seismometers) [4], while most of the hypothesis building and testing was performed by scientists on Earth before, during and after the mission. Robotic missions to Mars: Mars Exploration Rover [5], Phoenix mission [6] and Curiosity mission [7] operate in conditions of time-delayed communication, however in comparison with future manned missions to Mars they deliver few magnitudes less data. Because of that future manned Mars missions will be very complex operations what means that all possible interactions of mission components cannot be predicted theoretically, and extensive analog testing under terrestrial conditions before an actual mission is necessary to detect all the problems before they occur on Mars [8].

MARS2013 was an integrated Mars analog field simulation performed in February 2013 by the Austrian Space Forum. It consisted of a ~100 people team working at the Mission Support Center in Austria and ~10 people Field Crew in Morocco. Communication between “Mars” and “Earth” was performed with ten minutes delay. This was one of very few high fidelity analog studies that included a remote science support (RSS) team [8, 9, 10, 11].

**Remote Science Support team:** RSS team was responsible for [12]: 1) supporting activities of the Flightplan team, especially during the planning of the traverses, 2) supporting Field Crew, 3) assisting with experiments undertaken during the mission. The team consisted of ~15 people, mostly entry level students. Most of people was present in the Mission Support Center during only a fraction of the mission.

The RSS workflow was centered around a single-file, easily usable, spatially referenced database that included all the basic information about the conditions at the site of study, as well as all previous and planned activities [13]. This database was prepared in Google Earth software before the mission, and was updated based on data obtained in the field (Fig. 1).

**Results:** The lessons learned from MARS2013 RSS team operations include: 1) using a spatially referenced database is an efficient way of data processing and data utilization in a long-term analog mission with large amount of data to be handled, 2) mission planning based on iterations can be efficiently supported by preparing suitability maps (depicting

the suitability of the landing area for performing a specific experiment), 3) the process of designing cartographical products should start early in the planning stages of a mission, and involve representatives of all teams, 4) all team members should be trained in usage of cartographical products, 5) technical problems (e.g., usage of geological map while wearing a spacesuit) should be taken into account when planning a workflow for geological exploration, 6) a system that helps the astronauts to efficiently orient themselves in the field should be designed as part of future analog studies and be included in astronaut training.



**Figure 1.** The screen-shot of the Google Earth folder shows an example of the update map (for 24.02.2013) prepared for the MARS2013 mission for the Northern camp location. It includes the locations of all experiments performed in the field on February 24th 2013. Three experiment points (no. 17, 19 and 20) of the MAGMA rover were performed next to the camp (in the central part of the studied area). The SREC and ANTIPODES experiments were conducted simultaneously in the north-western part of the study area. The L.I.F.E. experiment took place in the north-eastern corner of the area. The inset on the left-bottom corner of the figure shows information describing 26\_LIFE\_2 point (e.g., start at 10:22 of February 26th 2013 by Luca Foresta, collection of two pictures and one sample). Every point visible on this figure is described in a similar way.

**References:** [1] Drake B.G. (2009) NASA-SP-2009-566. [2] Hettrich S. (2012) (M.S. thesis). U. of Innsbruck. [3] Apollo Program Summary Report (1975) NASA, JSC-09423. [4] Schaber, G.G. (2005) No. 2005-1190. [5] Bass D.S., et al. (2005) IEEE Aerospace Conference, doi:10.1109/AERO.2005.1559722. [6] Bass D.S. and Talley K.P. (2008) Journal of Geophysical Research 113 E00A06. [7] Grotzinger J.P. et al. (2012) Space Science Reviews 170: 5-56. [8] Eppler D. et al. (2013) Acta Astronautica 90: 224–241. [9] Leveille R. 2010. Planetary and Space Science 58: 631–638. [10] Osinski G.R. et al. (2010) Planetary and Space Science 58: 646-657. [11] Kereszturi A. (2011) Acta Astronautica 68: 1686–1701. [12] Groemer G. (2013) report# P10\_011B: oewf.org/cms/mars2013.phtml. [13] Losiak A. et al. (2014 *in press*). Astrobiology 14(5).

**MARTIAN BEACHES SANDS – THE CHARACTERISTICS OF OLIVINE WEATHERING IN A BEACH ENVIRONMENT.** Anna Losiak<sup>1</sup>, Barbara Woronko<sup>2</sup>, Robert A. Craddock<sup>3</sup>. <sup>1</sup>Institute of Geological Sciences, Polish Academy of Sciences, Wrocław (anna.losiak@twarda.pan.pl), <sup>2</sup>Wydział Geografii i Studiów Regionalnych, Warsaw University (bworonko@uw.edu.pl), <sup>3</sup>Center for Earth and Planetary Studies, National Air and Space Museum, Smithsonian Institution (craddockb@si.edu).

**Introduction:** It is probable that an ocean once existed on the surface of Mars [1]. Paleo-shorelines have been recognized in Viking Orbiter images [2], and these features were later confirmed by Mars Orbiter Laser Altimeter data [3] as well as by more recent and detailed analyses [4]. In terrestrial coastal zones repeated multiple grain-to-grain collisions from wave action produce a set of characteristic microstructures, such as V-shaped percussion cracks and dulled surfaces [5, 6]. Such characteristics are diagnostic of grains that have been weathered in a fluvial environment, and allow beach sediments to be distinguished from those eroded by aeolian, periglacial or other processes [7]. Additionally, the number of V-shaped percussion marks has been used as a way to classify aquatic environments and their energy [8]. For example, low-energy beach environments have few marks while those in high-energy beach environments have many. However, these characteristics have been found on quartz sand, while on Mars the sediments (including beach sands) are derived from basaltic rocks, which are largely composed of glass, pyroxene, plagioclase and significant amounts of olivine [9]. Only a few beaches on Earth are made of sand similar to what we would expect to find on Mars. One of them is Papakaloe on the Big Island of Hawaii. This famous green sand beach was formed by coastal erosion of the ~50 ka Pu'u Mahana Cinder Cone, which is leaving behind sand highly enriched in olivine [10].

The purpose of our study is to determine the microstructures present on the surface of basalt-derived sand weathered in a coastal (and/or more broadly fluvial) environment. The results can be used during the future surface missions to estimate the extent and duration of fluvial processes on the surface of Mars.

**Samples and Methods:** 40 transparent grains (volcanic glass and olivine) randomly selected from the ~300 g sample of sand from the Green Sand Beach (18.936379°N 155.646315°W) were analyzed under a scanning electron microscope JSM-6380LA equipped with energy-dispersive X-ray spectroscopy. All grains were analyzed using a protocol developed for quartz grains.

**Results and Discussion:** All analyzed grains show some degree of modification by the aqueous environment. However, V-shaped percussion cracks, which are characteristic of quartz grains transported in fluvial or coastal environments [6], are nearly absent.

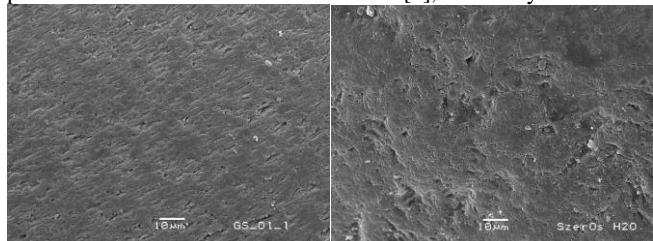


Figure 1. Comparison of microstructures present on a olivine surface with aligned elongated pits (left) and on a quartz grain with randomly distributed pits (right).

**Glass weathering.** Most surfaces of the glass grains or fragments of grains are smooth with no microstructures present, which is contrary to the findings of [11] who analyzed anthropogenic glass weathering in a coastal environment. The only mechanical microstructures visible, are rare conchoidal fractures and crescentic gouges resulting from the grain-to-grain impacts. The relative rarity (in comparison to quartz grains) of the mechanical microstructures is probably caused by the susceptibility of the volcanic glass to dissolution and thus quick removal of the signs of mechanical abrasion.

**Olivine weathering.** Olivine grains weathered in aqueous environment tend to develop a characteristic surface that at lower magnifications make the grain look polished because all the protruding elements are smoothed to the same level (Fig. 1). However, when examined at higher magnifications elongated and orientated pits become visible on the grains. Their development and elongation is related most probably to the crystal lattice of the olivine and recognized previously in thin section [12,13].

Elongated pits are ubiquitous and are absent only on the youngest grain surfaces that were probably produced by mechanical fracturing of the grain by high-energy collisions. Even though the mechanical microstructures seem to be absent on the surface of the analyzed olivine grains (including V-shaped percussion cracks), the abrasion we recognized appears to be an important part of grain erosion. Fresh olivine grains released from the tephra outcrops on the margin of the beach showed dulled surfaces on the crystal edges (Fig. 2). These dulled and abraded surfaces extend to the entire grain over time and exposure to the beach environment.

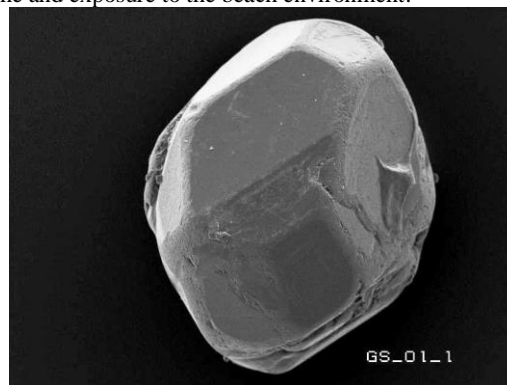


Figure 2. Relatively fresh olivine grains with visible signs of abrasion on the edges.

**Conclusions:** The olivine grains from Papakaloe Beach weathered in the coastal environment have been significantly modified. The duration of exposure to this fluvial environment can be recognized by increasing degrees of dulled surfaces.

**References:** [1] Clifford & Parker (2001) The Evolution of the Martian Hydrosphere: Implications for the Fate of a Primordial Ocean and the Current State of the Northern Plains, *Icarus*, 154, 40-79. [2] Parker et al. (1993) Coastal geomorphology of the martian northern plains, *J. Geophys. Res.*, 98, 11061-11078. [3] Head et al. (1999) Possible ancient oceans on Mars: Evidence from Mars Orbiter Laser Altimeter Data, *Science*, 286, 2134-2137. [4] Achille & Hynes (2010) Ancient ocean on Mars supported by global distribution of deltas and valleys, *Nature Geo.* doi: 19.1038/NGE0891. [5] Krinsley & Doornkamp (1973) Atlas of quartz sand surface textures. Cambridge Univ. Press. [6] Mahaney (2002) Atlas of Sand Grain Surface Textures and Applications: Oxford Univ. Press, 256p. [7] Woronko & Hoch (2011) The Development of Frost-weathering Microstructures on Sand-sized Quartz Grains: Examples from Poland and Mongolia, *Permafrost Periglacial Process.*, 22, 214-227. [8] Margolis & Kennett (1971) Cenozoic, paleoglacial history of Antarctica, recorded in subarctic deep-sea cores. *Am. Jour. Sc.* 271: 36pp. [9] Rogers & Aharonson (2008) Mineralogical composition of sands in Meridiani Planum determined from Mars Exploration Rover Data and comparison to orbital measurements. *J. Geophys. Res.*, 113 (E06S14). [10] Walker (1992) Puu Mahana Near South Point in Hawaii Is a Primary Surtseyan Ash Ring, Not a Sandhills-type Littoral Cone, *Pacific Sci.*, 46, 1-10. [11] Corcoran et al. (2010) First-cycle grain weathering processes: compositions and textures of sea glass from Port Allen, Kauai, Hawaii. *J. Sedim. Res.*, 80, 884-894. [12] Welch & Banfield (2002) Modification of olivine surface morphology and reactivity by microbial activity during chemical weathering. *Geochim. Cosmochim. Acta*, 66, 213-221. [13] Velbel (2009) Dissolution of olivine during natural weathering. *Geochim. Cosmochim. Acta*, 73, 6098-6113.

**Introduction:** Troilite is a iron sulfide (FeS), mineral common in meteorites and it constitutes about 5% of chondrites [1]. Troilite undergoes two phase transitions upon heating to temperatures below its melting point [2],  $\alpha/\beta$  transition occurs at  $411 \pm 3$  K, and  $\beta/\gamma$  transition at  $598 \pm 3$  K [3]. Due to this fact, troilite can be used as the cosmo-thermometer, as the shift of peak of  $\alpha/\beta$  transition peak exhibits the different relict temperature the sample experienced during its thermal history [4].

Specific heat capacities ( $C_p$ ) is the important thermophysical properties of extraterrestrial matter, used e.g. while modeling of the cooling rate of parent body of meteorite [5].

**Experimental:** The experiments were performed using a Differential Scanning Calorimeter (DSC) Q200 of TA Instruments. The measurement was done in the temperature range of 100 – 200°C for  $\alpha/\beta$  transition and -80 – 550°C for specific heat capacities determination at heating rate 20°C/min, under the constant nitrogen flow 50 ml/min. Samples of 5–6 mg, and ca. 20 mg was used, respectively for troilite and  $C_p$  evaluation. Standards of indium and sapphire were used for calibration of temperature and heat capacity.

**Results:** Obtained results of specific heat capacity are combined in Tab. 1. The  $C_p$  values of solid matters are temperature-dependend. Generally, the upward trend is observed, but the interior has higher  $C_p$  value than the crust.

Temperature of  $\alpha/\beta$  phase transition in troilite exhibits the temperature gradient in meteorite (between the crust and interior), while moving from the crust (124°C) inward (trough the edge, 1–2 mm part behind the crust (144°C), to the interior (147°C).

**Discussion and conclusion:** The  $T_{\alpha/\beta}$  is inversely proportional to the temperature experienced during the thermal history of sample [4], so data collected by authors are in accord with the temperature gradient evolved during atmospheric passage of the meteoroid.

The specific heat capacity should be measured at various temperature as they are temperature-dependend, not just simply extrapolated as it was commonly done so far, e.g. [6].

**References:** [1] Hutchison (2006), Meteorites a petrologic, chemical and isotopic synthesis. Cambridge University Press, New York. [2] Allton et al. (1993), Calorimetric thermometry of meteoritic troilite: feasibility study, LPSC XXIV, 21-22. [3] Chase M.W. Jr., et al. (1985), JANAF Thermochemical Tables, 3rd ed., J. Phys. Chem. Ref. Data, Vol 14., Suppl.1, P.1194. [4] Allton et al. (1994), Calorimetric thermometry troilite: preliminary thermometer relationship, LPSC XXV, 25-26. [5] Ghosh A., McSween H.Y., 1999 – Temperature dependence of specific heat capacity and its effect on asteroid thermal models, MAPS, 34, 121–127. [6] Henke et al. (2011), Thermal evolution and sintering of chondritic planetesimals, Astronomy and Astrophysics, 10.

Tab. 1. Specific heat capacity  $C_p$  of crust and interior [J/(kg·K)] of NWA 6255 meteorite samples at various temperatures.

T [K]	T [°C]	A crust	B interior
223	-50	476	532
263	-10	546	607
283	10	577	641
300	27	602	668
323	50	634	705
373	100	701	784
398	125	740	840
448	175	759	862
473	200	774	880
523	250	805	929
573	300	830	965
623	350	842	986
673	400	855	997
723	450	868	1007
773	500	876	1008
823	550	932	1017

# CLAST CLASSIFICATION IN MARTIAN METEORITE NWA7034/NWA8114. J. L. MacArthur<sup>1</sup> and J. C. Bridges<sup>2</sup>

<sup>1</sup>University College London, Centre for Planetary Science at UCL/Birkbeck, Dept. of Physics and Astronomy, Gower Street, London WC1E 6BT, UK, j.macarthur.12@ucl.ac.uk, <sup>2</sup>Space Research Centre, Dept. of Physics and Astronomy, University of Leicester, LE1 7RH, UK, j.bridges@le.ac.uk.

**Introduction:** NWA7034 and its six pairs (including NWA8114, NWA7533) represent a new unique Martian basaltic breccia class. They contain ~2.1 Ga (Rb-Sr) clasts [1] but also ~4.4Ga (U-Pb) zircons [2], and could have originated from a volcanic or an impact event. They contain many lithologic clasts and a variety of textures.

Agee et al. [1] reported a wide range of feldspar and pyroxene compositions, but noted many clasts appear to have been affected by secondary processes. Santos et al. [3] found two alkaline feldspar clasts, trachyandesitic and mugearitic, suggesting greater diversity. The abundances of nickel and iridium in NWA7533 suggest that 4-5% of the matrix may have come from C1 chondritic material, which supports the idea of it being formed in an impact and thus the meteorite has been interpreted as a polymict regolith breccia [4]. Further analysis comparing major element abundances of melt rock particles to the bulk breccia also indicate a formation via impact [5].

This study of NWA8114 investigates five types of clasts: feldspar, pyroxene, phosphate, iron-oxide and gabbroic.

**Methods:** A polished thin section and two polished thick sections from NWA8114 was examined using a XL30 ESEM, Hitachi S-3600N Environmental SEM and a Sirion 200 FEGSEM at the University of Leicester to classify different clast types.

High resolution backscatter electron images were obtained (Fig. 1,2) and composition was investigated using energy-dispersive X-ray spectroscopy (EDX).

Textures and zonation were observed and composition measurements were taken for the individual phases in each clast as well as measuring the bulk clast composition. Follow up work using an electron microprobe is planned.

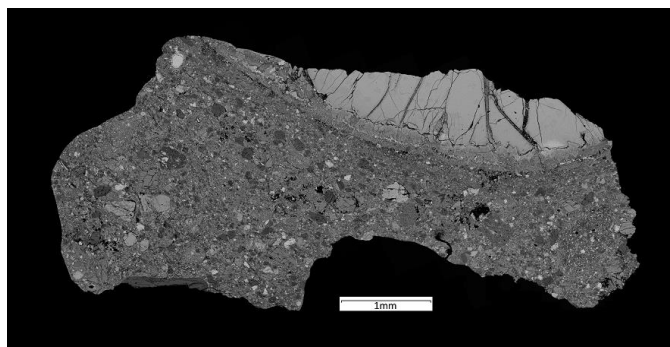


**Figure 1:** Backscatter electron image mosaic of a thick section of NWA8114 showing the variety of difference sizes and shapes of clasts, together with a pyroxene area, mainly iron-rich pigeonite ( $\text{En}_{30}\text{Fs}_{57}\text{Wo}_{13}$ ), containing veins.

**Results:** Most of the feldspar clasts are plagioclase in the range  $\text{An}_{28-55}$ , though two were of alkaline composition with cryptoperthite intergrowth of two feldspars (Fig. 2A). These clasts are likely to have cooled relatively slowly, as K-rich and Na-rich feldspar domains have separated from one another, showing either over 70% albite or over 70% sanidine compositions.

An iron-rich pyroxene clast, mainly pigeonite ( $\text{En}_{36-44}\text{Fs}_{46-53}\text{Wo}_{9-11}$ ), Fig. 2B, shows a regular Ca-rich and Ca-poor exsolution intergrowth. A further five exsolution pyroxene clasts have been identified.

Several phosphate clasts showed predominantly homogeneous Cl-apatite. Two clasts are predominantly ilmenite with separated iron oxide and titanium oxide towards the edges.

The gabbroic clasts show a range of pyroxene (augite  $\text{En}_{40-51}\text{Fs}_{16-24}\text{Wo}_{25-44}$  and low-Ca pyroxene  $\text{En}_{55-70}$ ) and plagioclase feldspar compositions in the  $\text{An}_{20-55}$  range.

A heavily brecciated gabbroic clast contains sub-clasts (Fig. 2C), giving rise to a wide compositional range, low-Ca pyroxene  $\text{En}_{55-70}$ ,  $\text{An}_{20-45}$ , alkali-feldspar and Cl-apatite.

Another gabbroic clast (Fig. 2D) is a mix of Cl-apatite, augite ( $\text{En}_{39-54}\text{Fs}_{16-27}\text{Wo}_{20-44}$ ) and iron-oxide, intergrown with a feldspar clast of composition  $\text{An}_{40-45}$ .

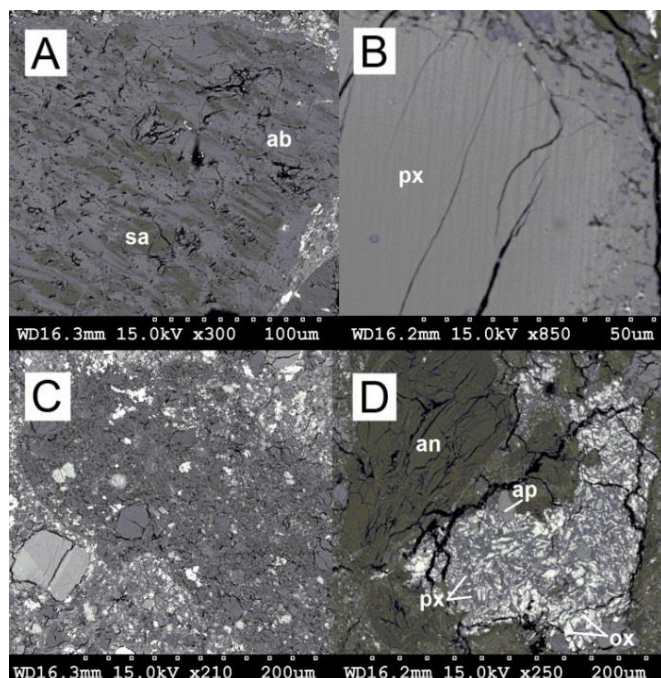


**Figure 2:** Backscatter electron images of: (A) Feldspar clast (B) Pyroxene clast (C) Gabbroic clast (D) Gabbroic clast sa=sanidine ab=albite px=pyroxene an=andesine ap=apatite

**References:** [1] Agee C. B. et al., (2013), Unique Meteorite from Early Amazonian Mars: Water-Rich Basaltic Breccia Northwest Africa 7034, *Science* 339, 780-785. [2] Humayun M. et al., (2013), Origin and age of the earliest Martian crust from meteorite NWA 7533, *Nature* 503, 513-517. [3] Santos A. R. et al, (2013), Martian Breccia NWA7034: Basalt, Mugearite, and Trachyandesite Clasts, *Meteoritics & Planetary Science*, 48, pp.A306-A306. [4] Humayun M. et al. (2013), Composition of Northwest Africa 7533: Implications for the origin of martian soils and crust, *44th Lunar & Planetary Science Conference Abstract* #1429. [5] Hewins R. H. et al., (2013), Petrology of NWA 7533: Formation by Impact on Ancient Martian Crust, *Meteoritics & Planetary Science*, 48, pp.A160-A160.

**Introduction:** Deep-seated gravitational spreading (DSGS) involves collapse of large blocks along structural features and faults, leading to formation of ridge-top splitting by crestal graben formation, uphill-facing scarps and downslope bulging [1,2]. DSGS occurs on high wallslopes, with small rate of displacement but height comparable to the whole slope height. Occurrences of DSGS are usually connected with formerly glaciated mountain ridges on Earth and on Mars [3]. Vertical offset does usually not exceed ~10 metres on Earth, whereas on Mars (Fig. 1) it is at least one order of magnitude higher, consistent with vertical scaling between slope height and vertical fault offset [4].

**Modelling:** Modelling was performed using the finite element code ADELI, initially developed for studies of mechanical behaviour of the lithosphere and the crust at geologic time scale [5]. Three possible slope destabilization factors are considered that may contribute to gravitational spreading: 1. Glacier loading then unloading, 2. Activation of pre-existing faults, joints, pore water pressure. 3. Slope anisotropy (layers).

**Results:** The models presented here (Fig.2) examine the influence of asymmetric profiles on strain distribution within topographic ridges. They were conducted for strongly fractured and jointed basaltic rock, after removal of glacier buttress. Slope angles were taken between 20° and 35°, which are common values in studied Valles Marineris DSGS cases. The results show that instabilities develop differently depending on symmetry of the slope and the slope angle values. In case of symmetric slopes (Fig. 2a, c, e) accumulation of plastic strain focuses in the middle of the ridge. Two curved failure planes generate vertical displacement parallel to the mountain slopes, resulting bulging at the toe of the slope. The vertical thickness of the sliding units scales with height of the mountain. In case of asymmetric slopes (Fig. 2b, d, f), a single curved failure plane develops, producing bulging at the toe of on one side of the mountain. The vertical thickness of the sliding unit scales with the slope height too. All the models presented here, shows plastic strain accumulation in the upper part of the slope, leading to ridge-top splitting.

**Conclusion:** Modeling showed that slope stability in a study case depended on stage of wallslope erosion. Fractures, cracks and joints influenced on cohesion of the rocks. Also important factor was removal of downslope buttresses and slope angle.

**References:** [1] Agliardi et al. (2001). Structural constraints on deep-seated slope deformation kinematics. *Engineering Geology* 59, 82-102. [2] Drecki I. and Żyszkowska J., (2008). Case study of double ridges in the Polish part of Tatra Mountains. *6<sup>th</sup> ICA Mountain Cartography Workshop, Mountain Mapping and Visualisation*, Switzerland. [3] Mège D. and Bourgeois O.(2011) Equatorial glaciations on Mars revealed by gravitational collapse of Valles Marineris wallslopes:. *Earth Planet. Sci. Lett.*, 310, 182-191. [4] Kromuszczynska O. et al. (2012). Giant sackung scarps in Valles Marineris. *43<sup>rd</sup> LPSC, 1161.pdf*. [5] Chéry J. and Hassani R. (2005). A 2D/3D Finite Element Software for thermomechanical modeling of geological deformation. Guide book.

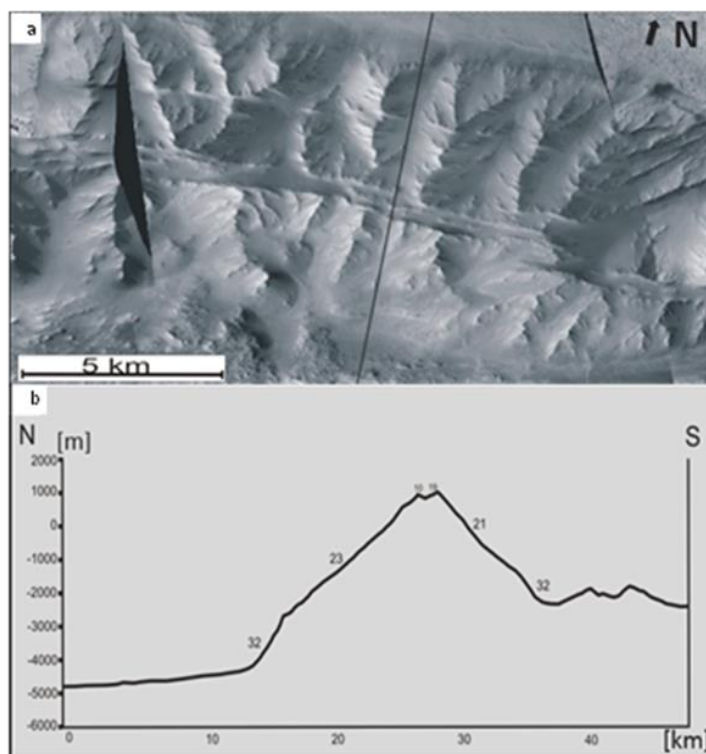


Fig. 1a: Topographic profile across a ridge located within Coprates Chasma (b located in a), eastern Valles Marineris; b: cross-section of internal ridge in Coprates Chasma.

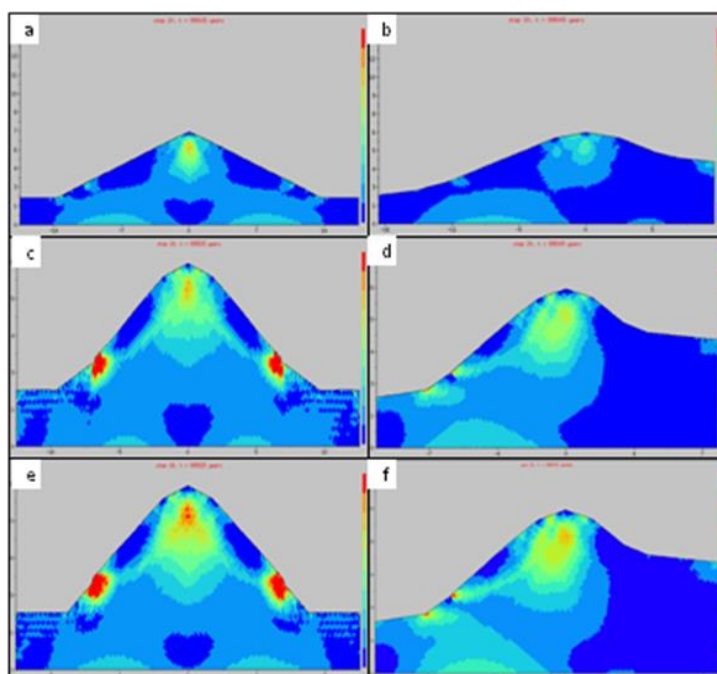
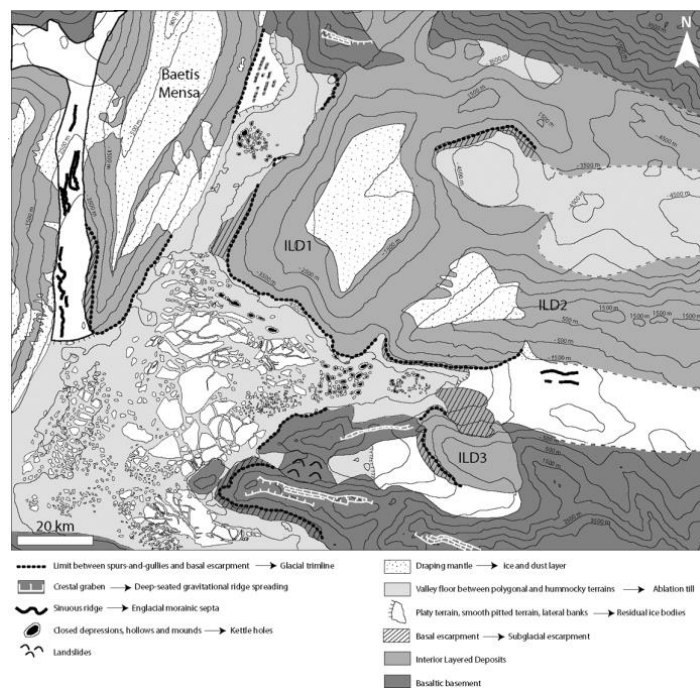


Fig. 2 Accumulation of plastic strain in the model, a symmetric slopes,  $\alpha=20^\circ$ . b asymmetric slopes,  $\alpha=20^\circ$ . c symmetric slopes,  $\alpha=30^\circ$ . d asymmetric slopes,  $\alpha=30^\circ$ . e symmetric slopes,  $\alpha=35^\circ$ . f asymmetric slopes,  $\alpha=35^\circ$ .

**ORIGIN OF THE OBSERVED DEFORMATION IN VALLES MARINERIS: AN EQUATORIAL FOSSILISED GLACIER SYSTEM AND NO REGIONAL TECTONICS.** Daniel Mège<sup>1,2</sup>, Olivier Bourgeois<sup>2</sup>, Marine Gourronc<sup>2</sup>, Frédéric Gueydan<sup>3</sup>, Olga Kromuszczyńska<sup>1</sup>, Magdalena Makowska<sup>1</sup>, Stéphane Pochat<sup>2</sup>, Krzysztof Dębniak<sup>1</sup>, Joanna Gurgurewicz<sup>1,4</sup>, <sup>1</sup>Institute of Geological Sciences PAS, Wrocław, Poland (daniel.mege@twarda.pan.pl), Laboratoire de Planétologie et Géodynamique, UMR CNRS 6112, Université de Nantes, France, <sup>3</sup>Géosciences Montpellier, UMR CNRS 5243, Montpellier, France, <sup>4</sup>Space Research Centre PAS, Warsaw, Poland.

**Introduction:** The distribution of surface ice deposits on Mars has varied through time, depending on orbital and atmospheric conditions. For instance, recurrent Mid to Late Amazonian glaciations have been documented in the Martian tropics, on the western flanks of the Tharsis volcanoes [1], as well as at higher latitudes [2]. In the equatorial region, the Marineris valleys display a huge range of glacial and postglacial landforms that testify to an ice sheet in the Late Noachian – Early Hesperian [3,4], coincidental with other evidence of a cold climate [5]. It is shown that the Valles Marineris 'rift' border fault scarps interpreted in earlier works are better explained by glacial trimlines, whereas other scarps, observed along the chasma walls, are attributed to postglacial slope relaxation.

**Valles Marineris tectonics:** Due to the parallelism of the boundaries of some of its troughs (chasmata), Valles Marineris has been compared to a terrestrial rift since the Viking era [6] and the idea that it is a rift, in the meaning of a crustal extensional failure feature, has become popular [7], supported by variations of the inferred stretching factor [8,9], structural segmentation [11], and detailed fault mapping [10,11].



**Figure 1.** Interpretation of landforms in central Valles Marineris [4].

Increased resolution of post-Viking image datasets made clearer the flaws of the interpretation of rift border faults scarps: the scarps do not show structural segmentation nor do they taper at the putative fault ends. They are also much higher than the scarplets that are observed at the base of terrestrial active normal faults, to which they have been compared [11], which makes necessary a very high, and problematic, crustal strength for such a deformation to be generated if they are monophased.

Every topographic ridge within the chasmata displays brittle deformation by uphill-facing, ridge-parallel fault scarps and/or development of crestal grabens. These features form in postglacial environments on Earth [3], where they form in response to valley deglaciation and resulting topographic debuttressing. These terrestrial fault scarps are much smaller than in Valles Marineris, but scaled to the dimensions of the topographic ridges involved, they are of similar size [12]. A postglacial environment in Valles Marineris is supported by a range of glacial and periglacial mountain landforms (Figure 1) [4,13]. The scarps that were formerly interpreted as rift border faults match the geomorphology of exhumed subglacial scarps separated from the overlying mountain periglacial landforms by trimlines.

**Implications:** The only brittle tectonics observed in Valles Marineris appears to be postglacial and results from body forces [14]. The widespread glacial and postglacial landforms indicate that glaciers were covering a huge portion of the chasmata [3,4]. It remains likely that Valles Marineris has been an extensional province too, but evidence is not provided by structural analysis of fault scarps. The extensional history, erased by subsequent surface processes, is to be found at depth (Figure 2) [9,11] and in dilation by dykes [15] currently exposed at the surface [16-17].

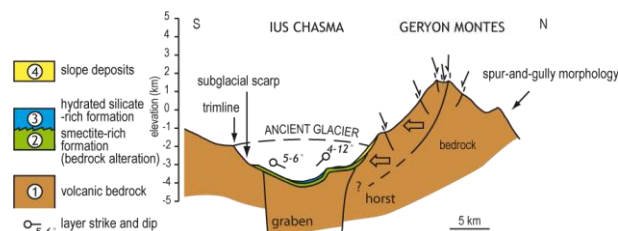


**Figure 2.** Model of Valles Marineris graben inversion and masking of rift structures by postglacial gravitational deformation of chasma wallslope and surface processes [3].

**References:** [1] Kadish et al. (2014), *PSS*, 91, 52–59. [2] Fastook J. L. and Head J. W. (2014), *PSS*, 91, 60–76. [3] Mège D. and Bourgeois (2011) *EPSL*, 310, 182–191. [4] Gourronc et al. (2014) *Geomorphology*, 204, 235–255. [5] Woodsworth et al. (2014) *Icarus*, 222, 1–19. [6] Masson P. (1977) *Icarus*, 30, 49–62. [7] Lucchitta et al. (1992), *Mars*, Univ. Arizona Press, 453–492. [8] Schultz R. A. (1995), *PSS*, 43, 1561–1566. [9] Mège D. and Masson P. (1996) *PSS*, 44, 749–782. [10] Peulvast and Masson (1993), *Earth, Moon Planets* 61, 191–217. [11] Peulvast et al. (2001) *Geomorphology*, 37, 329–352. [12] Kromuszczyńska et al. (2014) *MPSE 2014* abstract. [13] Dębniak et al. (2014) *MPSE 2014* abstract. [14] Makowska et al. (2014) *MPSE 2014* abstract. [15] Mège D. and Masson P. (1996) *PSS*, 44, 1499–1546. [16] Flahaut et al. (2011) *GRL*, 38, L15202, doi:10.1029/2011GL048109. [17] Huang et al. (2012) *GRL*, 39, L17201, doi:10.1029/2012GL052523.

**Summary:** Field geoscientists need to collect three-dimensional data in order to characterise the lithologic succession and structure of terrains, reconstruct their evolution, and eventually reveal the history of a portion of the planet. This is achieved by walking up and down mountains and valleys, conducting and interpreting geological and geophysical traverses, and reading measures made at station located at key sites on mountain peaks or rocky promontories. These activities have been denied to conventional planetary exploration rovers because engineering constraints for landing and surface displacement are strong, especially in terms of allowed terrain roughness and slopes. For the smallest bodies, rovers are ineffective because gravity is not enough for friction to occur between wheels and the ground. Galago, the Highland Terrain Hopper, a new, light and robust locomotion system currently in development (equiv. ESA TRL stages 2-4), addresses the challenge of accessing most areas on low-gravity planetary bodies for performing scientific observations and measurements, alone or as part of a commando. An illustration is given in Valles Marineris and on Phobos.



Figure 1. Galago is jumping in a Valles Marineris-type landscape.

**Galago, the Highland Terrain Hopper:** ASTRONIKA Sp. z o.o. and the Polish Space Research Centre are designing Galago, the Highland Terrain Hopper (Figure 1), a small ( $\varnothing \sim 25\text{-}50$  cm), light (2-10 kg), and low-cost jumping robot that may survey any type of landscape.

In order to save space and weight, the main system and payload will be highly miniaturized and designed simultaneously in order to share as much components as possible [1]; no moving parts will be allowed.

**Displacement capabilities and scientific strategy:** Galago is symmetric and can jump accurately to a height of 4.5 m on Mars (9 m on the Moon, and much more on Phobos and other small bodies). For one Galago, a nominal horizontal travel distance of 5 km (1000 jumps) is currently planned with the considered energy source, a battery reloaded by solar panels. A Galago may assist other types of robots, or humans, in accessing difficult terrain, or even replace them for specific measurements or campaigning. Its three independent legs make possible several types of motions: accurate jumping (to any place identified in advance), turning over, and tilting. Many risky displacements are made possible by robot

symmetry and leg configuration. In case of failed jump, one leg at least is in contact with the ground and can be used for a new jump and a new attempt. Due to low weight and cost, several galagos may be sent to study the geology and geophysics along profiles 10s of km long or grids covering up to hundreds of km<sup>2</sup>, with either duplicate or complementary payloads.

**Application to *in situ* Valles Marineris exploration:** The full stratigraphy of Mars, from the pre-Noachian [2] to some of the most recent deposits, may be obtained using a small swarm of galagos dropped along a traverse going through one of the main Valles Marineris chasmata equipped with a payload including a visible-NIR multispectral camera and an inclinometer. At the same time, data regarding rock fracturing, hydrogeologic and paleohydrologic conditions, paleogeography, paleoenvironments, soils and paleosoils, would be collected.

Such measurements would provide helpful information as to early volatile delivery [3] and the very early climate, as well as assessment of past habitability. Galagos carrying a ground resistivity meter could probe the subsurface and look for buried ice; with geophones the present geologic activity and surface dynamics (slope processes such as recurrent slope lineae [4], ice movement in rock- or dust-covered glaciers [5] etc.) could be monitored and identified [6]; a magnetometer would provide the first *in situ* measurements of Martian rock magnetization induced by the early dynamo [7].

**Phobos:** The whole surface can be visited with a very low energy consumption. The grooves and pit crater chains could be investigated in detail, contributing to the debate as to their formation [8]. The red and blue surface spectral units could also be examined and perhaps interpreted.

**References:** [1] <http://www.astc.uu.se>. [2] Flahaut, J. et al. (2012) *Icarus*, 221, 420–435. [3] Albarède F. (2009) *Nature*, 461, 1227–1232. [4] McEwen A. S., et al. (2014) *Nature Geosci.*, 7, 53–58. [5] Gourronc M. et al. (2014) *Geomorphology*, 204, 235–255. [6] Hibert, C., et al. (2011) *JGR*, 116, F04032. [7] Langlais, B., et al. (2004) *JGR*, 109, E02008. [8] Murray J. B., Heggie D. C., *Planet. Space Sci.*, in press.

**Introduction:**

Terrestrial planets and the Moon are example of Solar System bodies which underwent advanced surface modification including thermal metamorphism, impact melting, a number of geological processes, volcanism or advanced interaction with atmosphere in addition to space weathering. It is difficult to recognize the original chemical mixture of such bodies and large mineralogical changes, element fractionation as well as some isotope fractionation effects can be used to recover these processes. The physical and chemical composition of surface of space bodies are thought to be modified since the time of their formation. It is not easy to determine actual composition of these bodies by the current space instrumentation. Depth profiling measurements of chemical composition have to be applied.

A number of currently planned missions take into account various methods which would allow obtaining the subsurface material for further studies of its physical and chemical properties. Either simple dust removing devices, drills or removal of the upper surface material were applied so far (dust removing device (RAT) on Mars Exploration Rovers, drill on current Curiosity rover). In the next generation of space instrumentation the drilling devices will be used to obtain depth profiles. A deep surface profiling is planned for instance on Russian Luna missions. Also NASA will place a single geophysical lander on Mars to study its deep interior during planned for 2016 InSight Mission.

Using the combined device – i.e. mass spectrometer (MS) dedicated to measurements of elemental composition, and penetrator as a transport device, we can obtain sufficient data about surface and subsurface of the planets (Moon, Mars) and asteroids to answer a lot of questions about planetology and mile stones for the future exploration.

In recent years several miniature laser ablation/ionisation mass analysers (LIMS) became available for space research and the first space instrument, LAZMA flown on Phobos Sample Return spacecraft (Nov. 2011) [1]. LIMS is well-known analytical method for both applications such as the investigation of the elemental composition of solid materials and for the analysis of molecular compounds deposited in the surface of a solid sample [2]. The necessary of LIMS miniaturisation for the application in space research was achieved by combining a miniature laser ablation source with a various type of miniature mass analyser.

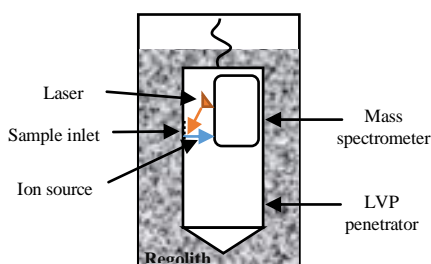


Fig. 1. Schetch illustrating the mass spectrometer onboard the Low Velocity Penetrator.

In order to measure subsurface parameters of the regolith spectrometer needs to be moved into subsurface region, for example by mole type Low Velocity Penetrator (LVP) [3] (fig.1).

To check the applicability of the spectrometer on the device with limited dimensions (20-30 mm in diameter) for under surface operations, a model of the quadrupole mass analyzer was developed. The model solves Maxwell equations using FEM approximations (COMSOL Multiphysics software) and takes advantage of the results obtained by Gibson (2000) [4]. The ions trajectories shown on fig. 2 were obtained by solving ODE for each particle moving under the Lorenz force.

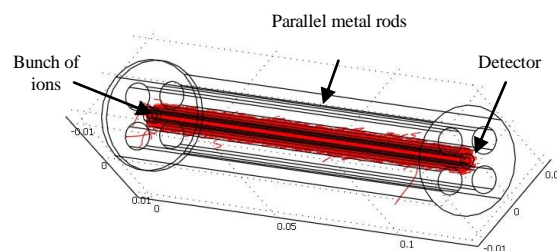


Fig. 2. Quadrupole mass analyser model.

The model has an interface to Matlab software which allows to automatically analyse the influence of the errors associated with inlet velocities and inaccuracies of electric field. These and other effects allow estimating the performance of mass analyzer to detect ions with different mass (see fig. 3).

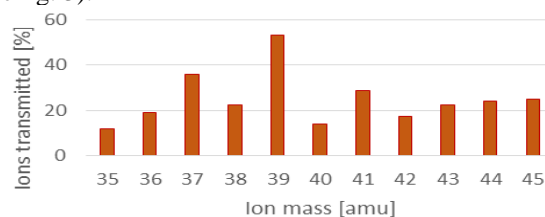


Fig. 3. Results for peak height, given as percentage of ions transmitted (4 MHz - frequency AC voltage).

The model enables the optimization of the mass analyser in terms of its dimensions and resolution. The influence of the volume minimization of mass analyser on their performance was checked.

Using the miniaturized mass spectrometer under the surface is important in context of the space bodies characterization as a key step in early phase of exploration. Apart from exploration, this kind of instrument is also important for scientific purposes, especially for better understanding of the evolution of planetary bodies.

**References:**

[1] Managadze GG., Wurz P., Sagdeev RZ., Chumikov AE., Tuley M., Yakovleva M., Managadze NG., Bondarenko AL. (2010), Study of the main geochemical characteristics of Phobos' regolith using laser time-of-flight mass spectrometry. *Solar Syst Res+*, 44, 376-384. [2] Vertes A., Gijbels R., Adams F. (1993), *Laser ionisation mass analysis*, Wiley: New York. [3] Seweryn, K., Grygorczuk, J., Wawrzaszek, R., Banaszkiwicz, M., Rybus, T., Wiśniewski, Ł. (2014), Low velocity penetrators (LVP) driven by hammering action – definition of the principle of operation based on numerical models and experimental tests, *Acta Astronautica*, 99, 303 – 317. [4] Gibson, JR., Taylor, S., Leck, HJ. (2000), Detailed simulation of mass spectra for quadrupole mass spectrometer systems, *J. Vac. Sci. Technol. A*, 18, no. 1.

Within “Morfortectonics” subject (30 h, 2 ECTS) at the 2<sup>nd</sup> grade (MSc) studies at the Faculty of Geology of the University of Warsaw only tectonic structures from Earth were interpreted as yet. In 2013 an idea occurred to realize this subject in the academic year 2014/2015 partially (10 h) at the basis of data from Mars. Good visibility of Martian landforms, directly connected with the bedrock geology (caused by lack of vegetation, and relatively slow weathering rate), and easy availability on the Internet were main advantages of this solution.

Data from HiRISE (High Resolution Imaging Science Experiment) telescope onboard NASA Mars Reconnaissance Orbiter (MRO) were used. At the basis of very high resolution imagery (0,25 – 0,5 m per pixel) at the University of Arizona Digital Terrain Models (DTM) of excellent resolution were generated (horizontal spacing 1 – 2 m, vertically - tenths of cm). 175 of this DTMs (with full set of initial data, mainly HiRISE images) are now available at the University of Arizona page (<http://www.uahirise.org/dtm/>).

From this 175 DTMs a dozen or so should be chosen – with visible tectonic structures (or at least parts of this structures) with clear connections with morphology, and relatively easy to interpret. It was not easy: only ca 20 DTMs presented layered rocks, and from this number only 12 presented tectonic structures (usually tilted strata, faults, rarely folds). However, among this 12 DTMs some are quite interesting – one of them (Layered rock outcrops in southwest Candor Chasma, DTEEC\_001918\_1735\_001984\_1735\_U01) – beautiful fold – will be analyzed as an example. (Fig. 1).

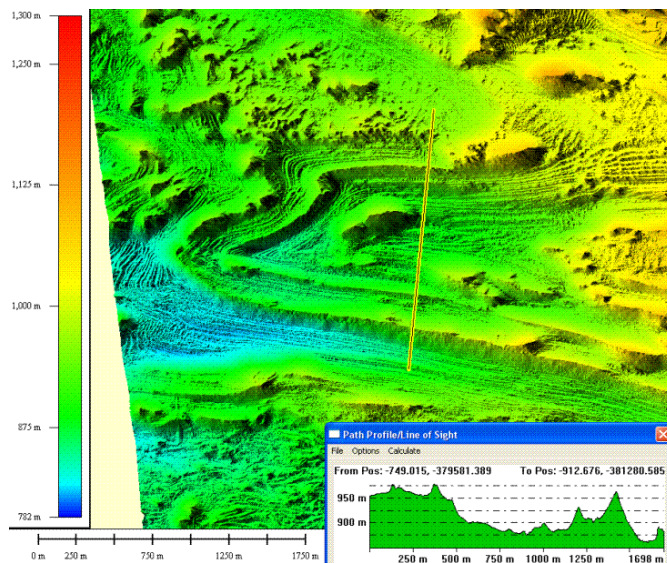


**Fig. 1.** Part of the DTM Layered rock outcrops in SW Candor Chasma (<http://www.uahirise.org/dtm/>) – hipsometry with morphological cross-section.

**A NEW MODEL OF PHYSICAL DECAY OF JUPITER FAMILY COMETS.** Hans Rickman<sup>1,2</sup>, Sławomira Szutowicz<sup>1</sup> and Kamil Wójcikowski<sup>3</sup>, <sup>1</sup>Space Research Centre Polish Academy of Sciences, Bartycka 18A, 00-716 Warszawa, Poland, [slawka@cbk.waw.pl](mailto:slawka@cbk.waw.pl), <sup>2</sup>Dept. of Physics and Astronomy, Uppsala University, Box 516, SE-75120 Uppsala, Sweden, [hans.rickman@physics.uu.se](mailto:hans.rickman@physics.uu.se), <sup>3</sup> PhD student - Space Research Centre Polish Academy of Sciences, Bartycka 18A, 00-716 Warszawa, Poland.

**Introduction:** Some asteroidal objects can be extinct or dormant comets. However, the fraction of dormant comets within the asteroid population or real asteroids in cometary orbits is still poor known. We aim to find the physical lifetimes of Jupiter Family comets. For this purpose, we try to model several processes that govern dynamical and physical evolution of comets. We pay special attention to physical evolution that lead from active cometary nucleus to dormant or desintegrated comets; attempts at such modelling have been made before, but we propose a more accurate model, which will include more physical effects. The model is tested in a sample of fictitious comets based on real Jupiter Family comets with some orbital elements changed to a state before the capture by Jupiter. We model four different physical effects: erosion due to sublimation, splitting, dust mantling and rejuvenation - mantle blow-off. While for sublimation and splitting there already are some models, and we only wish to make them more accurate, dust mantling and rejuvenation have not been included in previous, statistical physical evolution models. Each of these effects depends on one or more tunable parameters, which we establish by choosing the model that best fits the observed comet sample in a way similar to [1]. In contrast to di Sisto et. al., our comparison also involves the observed active fractions vs nuclear radii, the total absolute magnitude distribution, and the number of asteroids in cometary orbits interpreted as dormant comets.

**Acknowledgements:** This work was partially supported by Grant No. 2011/01/B/ST9/05442 of the Polish National Science Center

**References:**

[1] Di Sisto, R.P.; Fernández, J.A.; Brunini, A., (2009), On the population, physical decay and orbital distribution of Jupiter family comets: Numerical simulations, *Icarus* 203, 140-154

**Introduction:** We compare three different methods of statistical impact probability calculations: our Hill sphere method that uses a super-sizing of the planet's collisional cross-section, the numerical averaging of Wetherill's formula [1], and the novel MOID method developed by us. The first and third are Monte Carlo simulations methods. In the first we count the number of Hill sphere passages for a large, random sample of orbits. In the third we search for orbits with MOID less than the collisional radius in a similar sample, calculating the MOID by the method of Wiśniowski and Rickman [2], after which we compute the encounter timing range leading to collision for each selected object and compare with the target's orbital period.

Our extensive comparisons use a constant semi-major axis of 3.5 AU for the projectiles, and we focus on the parametric plane of perihelion distance and inclination. They show an excellent agreement among all the methods under practically all circumstances. However, in the vicinity of the singularities appearing in the Wetherill formulae (zero relative inclination, and equal perihelion distances) we find that only the MOID method yields accurate results. Due to the approximations inherent in the other methods, the super-sizing method underestimates the impact probability, and the Wetherill averaging overestimates it.

This work was supported by the Polish National Science Center under Grant No. 2011/01/B/ST9/05442.

**References:** [1] G. W. Wetherill, 1967, Collisions in the Asteroid Belt, *JGR*, 72, 2429-2444, [2] T. Wiśniowski, H. Rickman, 2013, Fast Geometric Method for Calculating Accurate Minimum Orbit Intersection Distances (MOIDs), *Acta Astronomica*, 63, 293-307.

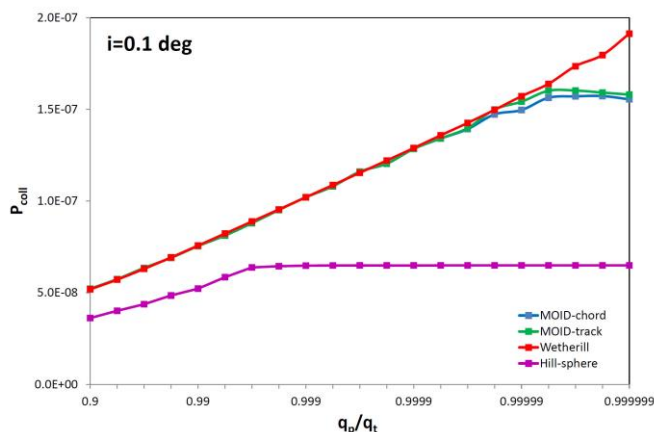


**Figure:** Collision probability with Mars (using its current orbital and physical properties) per orbital revolution as a function of the projectile perihelion distance ( $q_p$ ) divided by Mars' perihelion distance ( $q_t$ ) according to different methods. The variations are shown for the immediate vicinity of  $q_p = q_t$ , using an abscissa proportional to  $\log(1 - q_p/q_t)$ .

**Introduction:** The aim of this project was to develop the best method for detection of microorganisms, their building compounds or metabolites in the soil. Invented method for measuring quality of soil samples will be used in the laboratory module designed for mobile scientific platform SCORPIO 4, which will start in the European Rover Challenge 2014 and future editions of URC. In my poster, there are presented some interesting results and plans for the future. All biochemical experiments have been performed at Institute of Biochemistry and Biophysics, Polish Academy of Sciences.

All of the processes described can be automatically performed in the Autonomic Laboratory Module, called Life Obtaining Ground Analyzer (LOGAn) (Fig. 1). It is designed to be mounted on SCORPIO 4 rover and can autonomously perform detection of proteins and send back the results.

There are several advantages of LOGAn:

- it can investigate three individual soil samples at the time and analyze them simultaneously;
- it will be equipped with three separate ground probes, which can uptake soil from different locations;
- the results are detectable in visual spectrum, in blue color, between  $\lambda=600$  and  $700$  nm (maximum at  $700$  nm), therefore the module is cheap and easy to build;
- samples can be measured both qualitatively and quantitatively using comparison to a known concentration of bacterial culture (prepared at the same time with the same method) and comparison between samples from each location.

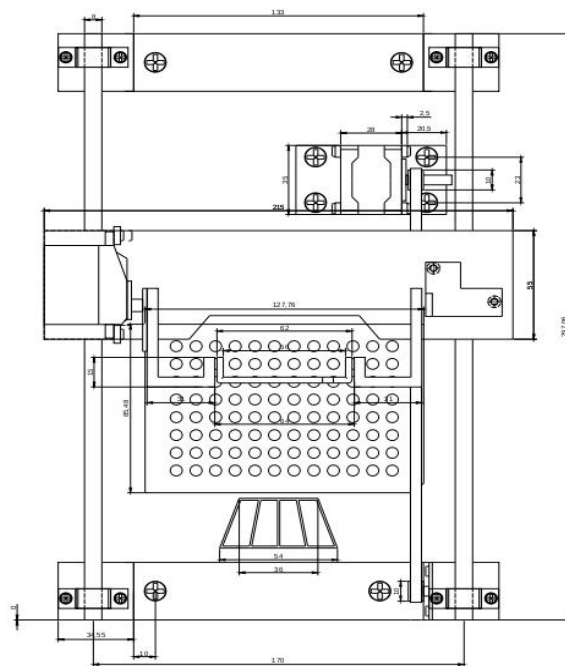


Fig. 1. Schematic of the main part of the module.

**Introduction** In recent years the interests of characterization of the planetary bodies are moving from surface to subsurface regions [5]. This process is accompanied by the growing interest in utilization of the planetary bodies, e.g., mining of the specific resources. There is a number of techniques developed recently that are supporting such operations: from Low velocity penetrometers [4] also called percussive/ pneumatic penetrometers[6] to drilling systems e.g. [2].

The drilling technique is a well known process that is very often used in terrestrial conditions for deep underground oil and gas production. There is a principal difference between research activities connected with drilling in terrestrial and in space conditions. In the first area the effort is focused on production optimization for maximum economic recovery. This can usually be done by increasing the rate of penetration and power of the system. In space conditions the time of drilling is not an important factor, while minimization of mass and power consumptions has the highest priority. Therefore, the designs are focused on minimization of power which needs to be delivered to regolith or rock to allow the system to work in volume drilling regime. The important element is also connected with automatic operations and mobility of the space drills which is usually not required for terrestrial applications. Despite many differences the following elements are common for the terrestrial and space conditions: necessity of hole bottom and bit cleaning by efficient transport of drilling cuttings and securing the bore hole.

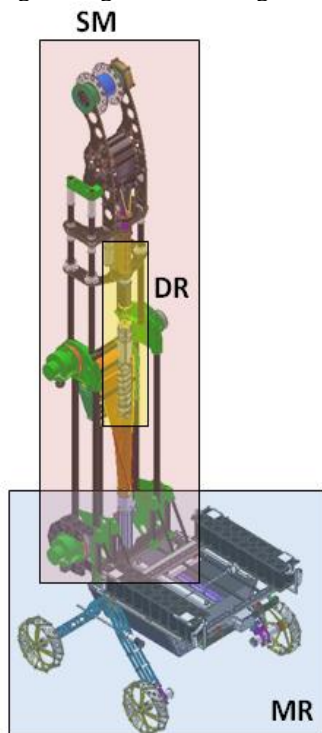


Fig. 1 Subsystems of Mobile Drilling System: MR – Mobile Robot. SM – Support Module, DR – Drilling subsystem

### Operational scenario

In the early phase of the project it was defined that the testing approach should take advantage of the UAV helicopter (Aquila) as mobile drilling carrier. The scenario covers the autonomous delivery to the desired place, mobile robot operations, drilling and collecting the samples, disconnecting from drills (SM and DR are left at borehole place) and finally return trip of the MR with samples to helicopter. The details about operational scenario of the ultralight mobile drilling system will be provided during presentation.

### Measurements in the borehole

The operation of the drilling system gives a unique possibility to have an access to:

- the core of the regolith each time delivered to separate container,
- hole bottom each time when the DR subsystem is removed from borehole.

These chances can be used to do following measurements:

- heat flow measurements at each depth to characterize under surface heat flux,
- chemical composition measurements using e.g. TOF mass spectrometer,
- density measurements using radioactive methods.

In addition measurements of the drilling process effectiveness can bring information about geotechnical properties of the regolith which can be useful for exploration and future resources utilization.

### References:

- [1] Cannon, et al., 2007, *Journal of Field Robotics*, vol. 24/10 pp. 877–905.
- [2] Coste, et al., 2010, *In Proc. of the 12th Int. Conf. on Eng., Sci., Const., Honolulu, Hawaii*.
- [3] Mitchell, et al., (1974), *Geochimica et Cosmochimica Acta* Vol. 3, pp. 3235-3253. The M.I.T. Press.
- [4] Seweryn, et al., (2014), *Acta Astronautica*, vol 99, pp. 303-317.
- [5] *The Global Exploration Roadmap, International Space Exploration Coordination Group, 2011*.
- [6] Zacny, et al., (2013), *Earth Moon Planets*, vol 111, pp. 47-77.

## ALTERATION FEATURES IN BASALTS IDENTIFIED BY ATOMIC FORCE MICROSCOPY AND IMPLICATIONS FOR MARS.

Marta Skiścim<sup>1</sup>, Joanna Gurgurewicz<sup>1,2</sup>, Daniel Mège<sup>1,3</sup>, <sup>1</sup>Institute of Geological Sciences, Polish Academy of Sciences, Research Centre in Wrocław, Podwale St. 75, PL-50449 Wrocław (marta.skiscim@twarda.pan.pl), <sup>2</sup>Space Research Centre PAS, Bartycka St. 18A, PL-00716 Warsaw, Poland, <sup>3</sup>Laboratoire de Planétologie et Géodynamique, UMR CNRS 6112, Université de Nantes, 2 rue de la Houssinière, 44322 Nantes, France.

**Introduction:** Studies of Martian meteorites, as well as the analysis of data obtained during space missions, indicate the presence of basalts on the Martian surface [1-5]. Analysis of their alteration features may provide insights into the climate evolution and its local variations. However, no adequate method that would help retrieve such information from orbit or *in situ* has been found so far [6].

Atomic force microscopy (AFM) has already been used in space missions and its advantages include, among others, low instrument weight and high resolution capability [7]. AFM allows to observe objects in the nanoscale and analyze their topography and roughness. We investigate whether AFM can be used as a tool to identify diagnostic alteration features on a basaltic surface. The objective of this work is to determine to what extent the AFM method complements the results obtained with SEM, in the context of climate evolution, and whether it can be used for this purpose independently.

**Experiment:** Basalt samples from arid cold (Udokan, Siberia) and arid hot (Ogaden, Ethiopia) environments, two of the possible Martian end-member paleoenvironments [8], have been studied. Scanning electron microscope (SEM) has been used in complement to AFM to identify the minerals (Fig. 1). Interesting places in the samples were marked with a diamond stylus for easy identification with AFM and SEM. In Fig. 1, images of a selected area of the internal part of basalt sample from the Udokan volcanic field are shown as an example. An L-shape cavity on the plagioclase crystal indicated on the BSE image, not only can be seen in a better resolution, but also the details of its topography can be recognized. Both the granular internal part of the cavity and crystal structure of its edges are imaged (Fig. 1b).

**Results:** Mineralogical analysis based on backscattered electron spectra (BSE) was carried out in selected areas of the samples. Structures examined by AFM were assigned to specific mineral phases. The images obtained in BSE and using AFM differ considerably in resolution (Fig. 1). Using AFM, it is possible to perceive details of structures that may result from weathering. Even very subtle alteration features may be observed.

**Conclusions:** With the used experimental approach, the same area in a given sample can be studied both by SEM and AFM. The structure of minerals identified in the spectrum of backscattered electrons can be located and observed at higher resolution on AFM images, leading to interpretations at a scale that was not attainable before. Such interpretations may reveal differences in nanostructure reflecting temperature-dependent alteration processes. In the future, this may allow the microscopic examination of the surface of Martian rocks, using AFM mounted on space assets.

**References:** [1] Nyquist L. E. et al. (2001) *Space Sci. Rev.*, 96, 105–164. [2] Christensen P. R. et al. (2000) *JGR*, 105, 9609–9621. [3] McSween H. Y. et al. (2004) *Science*, 305, 842–845. [4] Mustard J. F. et al. (2005) *Science*, 307, 1594–1597. [5] Salvatore M. R. et al. (2010) *JGR*, 115, E07005. [6] Gurgurewicz et al. *IEEE Trans. Geosci. Remote Sensing* (in revision). [7] Gautsch et al. (2002), *Surface and Interface Analysis*, 33, 163–167. [8] Carr M. H. and Head J. W. (2010) *EPSL*, 294, 185–203.

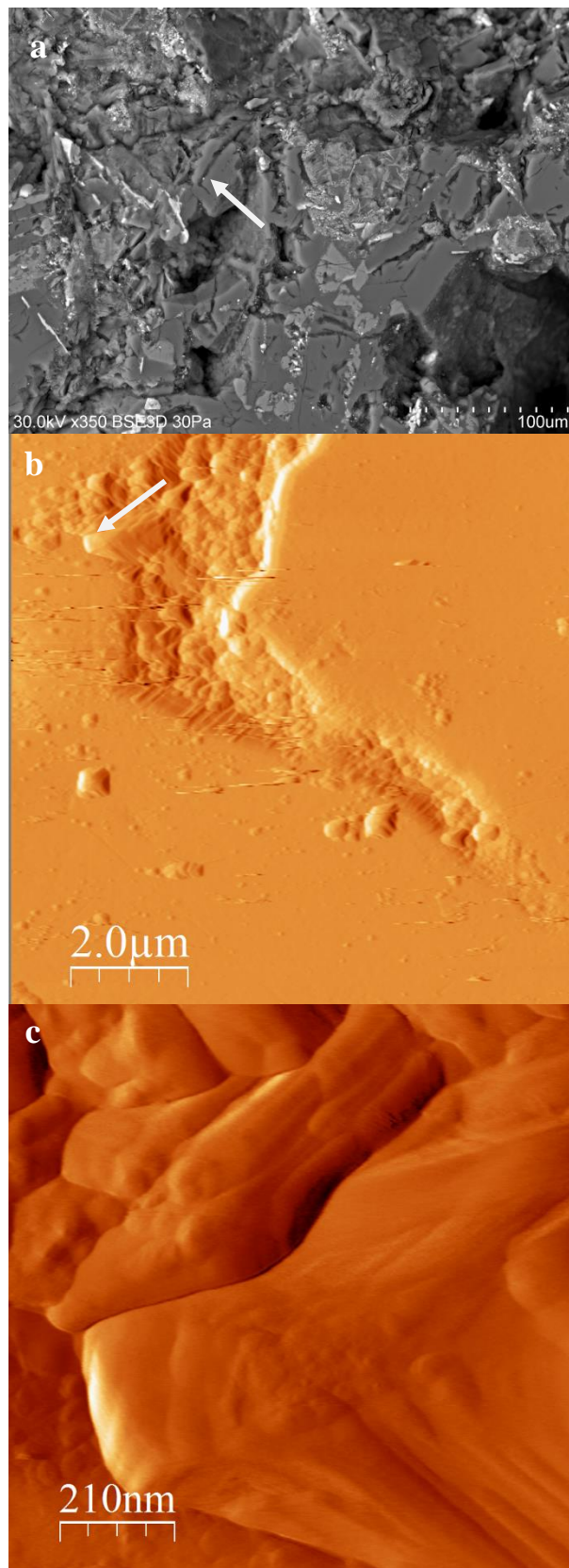


**Figure 1.** Closeups to the internal part of the Udokan basalt. (a) BSE image, an arrow indicates a cavity formed in a plagioclase crystal; (b) topography image obtained using AFM in the so-called deflection mode; an arrow indicates the edge of the cavity; (c) closeup to the edge of the cavity.

**Introduction:** We present a global orthomosaic and an atlas of the Martian satellite Phobos. The products are based on image data obtained by the High Resolution Stereo Camera (HRSC) [1], the pushbroom scanner on Mars Express (MEX). The new atlas is an update of the previously released version [2], which was derived from images of the Super Resolution Channel (SRC) [3], the CCD frame camera of the HRSC.

**Method:** We selected 18 HRSC scenes, obtained during MEX Phobos flybys from 2004 to 2011. A photogrammetric adjustment for the selected scenes (5 images each) was carried out [4], which yields improved orientation data for all 90 images having resolutions between 3.7 m/ pixel and 98.5 m/ pixel. 10 images were selected guaranteeing the Phobos coverage for the production of a global mosaic. We used the newly updated Digital Terrain Model (DTM) [4] for orthorectification. The 10 images were resampled to a uniform resolution of 16 pixels/ degree or 12.11 m/ pixel, and subsequently superimposed. A gap on the trailing hemisphere, which could not be covered by HRSC due to lack of illumination, was closed by three Viking orthoimages (see Figure 1).

**Result:** The produced atlas consists of 6 topographic image maps, which were created at a scale of 1: 50,000 [5]. The mosaics in the equator region are in Mercator projection. Sub-mosaics using 3 images in each case were generated for the North and South poles in Stereographic projection. The atlas

shows two different types of contour lines: sheet 1 (map 1 to 3) displays dynamic height contours obtained from gravity field modeling [6], useful to identify down-slope direction and mobility of surface materials. On sheet 2 (map 1 to 3), contour lines represent geometrical heights above the sphere (Rmean = 11.1 km) derived from the global DTM [4]. For simplicity, the same sphere was chosen as horizontal reference. Finally, 17 craters with approved names by the International Astronomical Union (IAU) are marked in the map, for which the coordinates and dimensions were re-determined.

**References:**

- [1] Jaumann, R. et al. (2007), The High Resolution Stereo Camera (HRSC) experiment on Mars Express: Instrument aspects and experiment conduct from interplanetary cruise through the nominal mission, *Planet. Space Sci.*, 55, 928–952.
- [2] Wählisch, M., et al. (2010), A new topographic image atlas of Phobos. *Earth and Planetary Science Letters*, 294 (3-4), 547-553.
- [3] Oberst, J. et al. (2008), The imaging performance of the SRC on Mars Express, *Planet. Space Sci.*, 56, 473–491.
- [4] Willner, K., et al. (2013), Phobos’ Shape and Topography Models, <http://dx.doi.org/10.1016/j.pss.2013.12.006>.
- [5] Wählisch, M., et al. (2013), Phobos and Deimos Cartography, <http://dx.doi.org/10.1016/j.pss.2013.05.012>.
- [6] Shi, X. et al. (2012), Working models for the gravitational field of Phobos, *Science in China G: Physics and Astronomy*, 358-364.

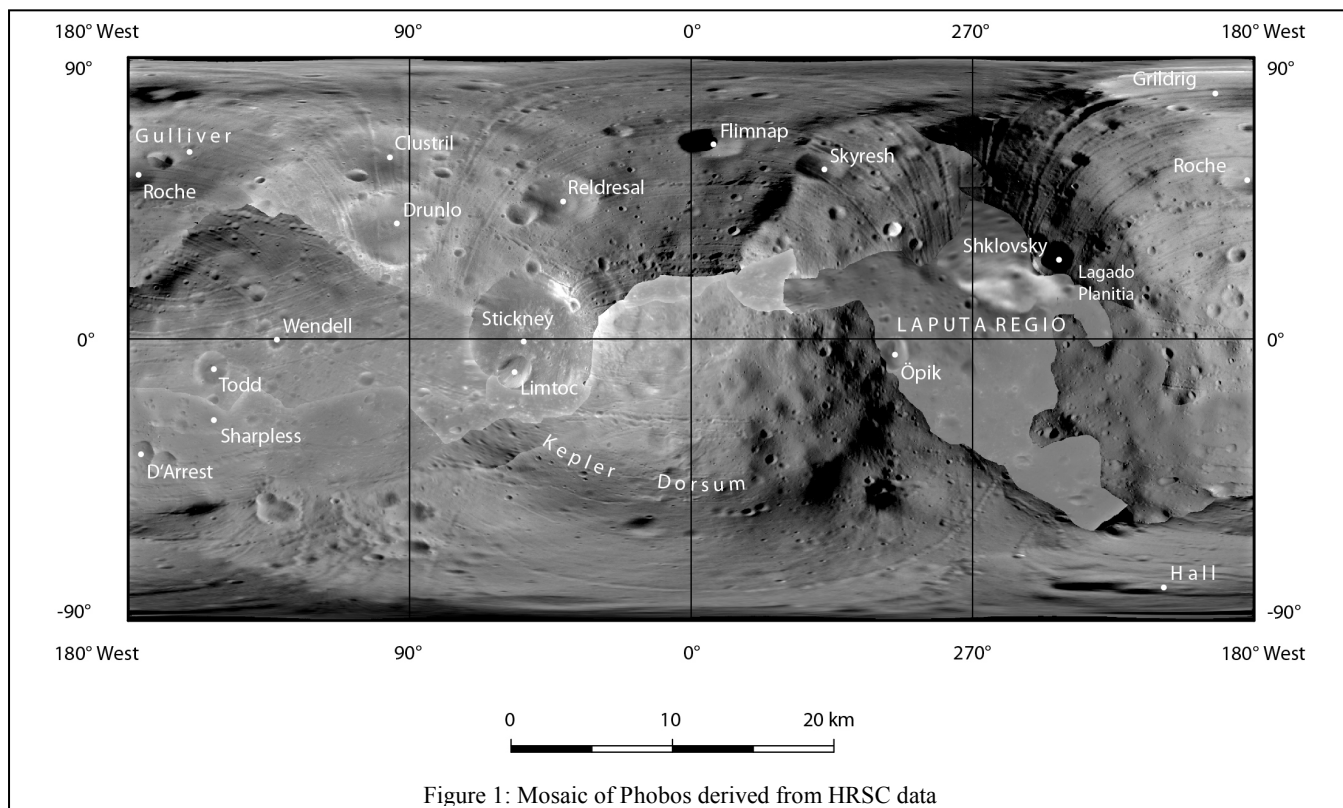


Figure 1: Mosaic of Phobos derived from HRSC data

## OPTICAL SENSORS DESIGNED IN FRAME OF THE AEROFAST PROJECT IN SPACE RESEARCH CENTRE PAS.

Piotr Wawer<sup>1</sup>, Mirosław Rataj<sup>1</sup>, Paweł Grudziński<sup>1</sup>, Łukasz Platos<sup>1</sup>, Maciej Kalarus<sup>1</sup>, Space Research Centre of the Polish Academy of Sciences, Bartycka 18A Str, 00-716 Warsaw, [wawer@cbk.waw.pl](mailto:wawer@cbk.waw.pl), [rataj@cbk.waw.pl](mailto:rataj@cbk.waw.pl)

**Introduction:** The main goals of the AEROFAST (AEROcapture for Future spAce transportation) project are, to design an AEROCAPTURE vehicle and to improve the AEROCAPTURE technology. AEROCAPTURE is a insertion of a spacecraft from the hyperbolic flyby orbit into a planetocentric orbit, through the atmosphere.

An important step, is to develop advanced transportation systems to move humans and cargo during lunar and Martian mission with large amount mass saving. This technology is well adapted for large weight missions (sample return missions and manned missions).

In Space Research Centre two instruments were designed in frame of this project and there will be presented and described.

First one is a pyroelectric sensors for analysis of the chemical reaction and temperature measurement at the spacecraft shield during aerocapture phase. This sensor allows to give additional information about the interaction between the atmosphere and thermal protection system and consists of pyroelectric detector with additional optical system.

Second instrument is a Imaging Multispectral Sensor (IMS) dedicated for imaging and spectral analysis of the planet's surface during orbiting phase (after AEROCAPTURE). This sensor consists of panchromatic and multispectral pushbroom scanners.

**Pyroelectric sensor:** Five pyroelectric sensors are planned to be placed in the aerocapture shield. Sensor's concept and model is presented below.

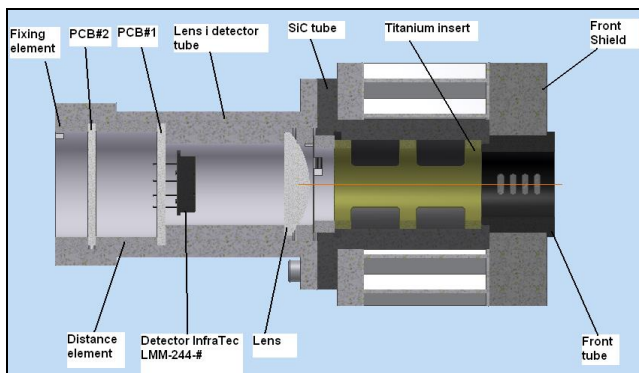


Fig. 1 Pyroelectric sensor

Pyroelectric sensor entrance window is situated in front of the TPS (Thermal Protection Structure). The SiC tube and optical element base is mounted to the cold structure without connection with the TPS – hot structure. SiC tube and optical and electronical elements base (aluminum element: Lens & detector tube) are connected to the Al structure. To make the system more stiff inside the SiC tube, the titanium insert is implemented.

One of the method to reduce the possibility of the pollution during burning of the ablative thermal protection shield is to use the front SiC or ceramics tube which protect the optical system from the particles of the cork. This tube is fixed to the front of the sensor structure.

Tube do not disturb the pyro-sensor measurements because the optical system detects the radiation from the gas “cloud” in front of the TPS - “visible” through the main hole of the sensor.

The basic elements used in optical system are: the lens and the pyro-electric detector with a spectral filters.

Plano – convex lens (focal length: 25.4 mm, diameter 25.4 mm) focuses the ray beam on the detector. Possible lens material with wide transmission range is sapphire (transmission range: 0,15 – 5  $\mu\text{m}$ ) or Zinc Selenide (transmission range 0.6 – 16  $\mu\text{m}$ ).

Detector is a pyro detector InfraTec LMM-244-#. with four channel (four sensitive areas).

By using the narrow band pass filters on every channel possible is to identification the different species as NO, CO, CO<sub>2</sub> which could appear during the aerocapture phase. Moreover, this kind of measurements give an information about the species changes in concentration during aerocapture phase. In every sensor one channel (with wide spectral transmission) could be use for the temperature measurement.

**Imaging Multispectral Sensor:** Payload dedicated for spatial-spectral analysis of the planet in four channels covering spectrum of visible and near- infrared bands. It consists of two modules. First one panchromatic and multispectral pushbroom scanner (based on the Three Mirror Anastigmat telescope) with the Focal Plane Assembly and readout electronics (figure below).

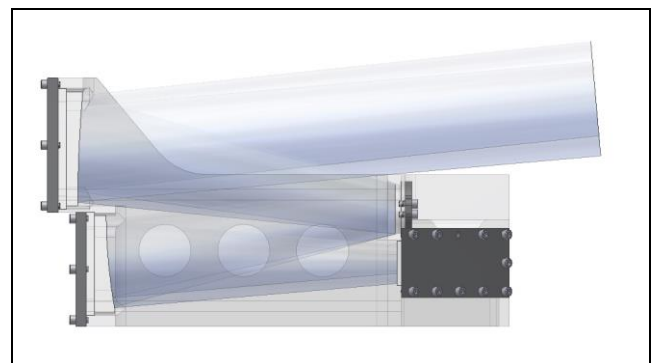


Fig. 2 Imaging Multispectral Sensor

Second module-block of electronic to perform quantisation, filtering, data compression and communication with the spacecraft.

The IMS is expected to work in different modes apart from nominal measurements (i.e. image acquisition). Additional modes are needed to perform tasks on request according to the user defined parameters. Thus, the proposed operational modes can be as follows:

1. Self test procedure (at power-up, on request).
2. Calibration of the instrument (periodic calibrations on request) (on-cruise, in-orbit).
3. Nominal measurements: basic software filtering and data corrections, compression, storage.
4. Data management.

**References:** [1] Robert Fisher, Biljana Tadic-Galeb, Paul Yoder, “Optical System Design”, McGraw-Hill, 2008. [2] Tinku Acharya, Ajoy K. Ray, „Image Processing: Principles and Application”, John Wileyand Sons, 2005.

**Introduction:** Safe and effective traversability on the Martian surface is an important issue for recent robotic missions. As it was presented by MER Spirit, the safe movement on the planetary surface covered by various material and sediments can be tricky. The FASTER project is focused on on-board traversability assessment system designed as a potential support for ExoMars mission. Few aspects of development of FASTER project Data Fusion (DF) module is discussed here.

**Soil sensors – case of FASTER project:** In case of FASTER project [2], four different sensors, mounted on small, reconnaissance Scout rover and on base Bridget rover (mock-up of final ExoMars mission rover) were developed and common DF subsystem was prepared. The list of the sensors includes:

*Wheel-Leg-Soil Interaction Observation system (WLSIO)* – simple sensor mounted on two front wheels of Scout rover, using visual and IMU data for estimation of sinkage and slippage of wheels to predict the terrain ‘softness’ and final traversability properties as for base rover. The wheel-legs offer both high terrain crossing capabilities, as well as the direct, semi-static wheel-leg and soil interaction analysis. Each wheel-leg is equipped with foot realising the same contact pressure as for base rover.

*Dynamic Plate (DP)* – scout sensor uses the principle of measurement of reaction for hammer hit applied to the circular plate located on the soil. The sensor is deployed on request, when the WLSIO sensors give MAYBE answer. This sensor is estimated to give the higher reliability of data.

*Wheel Bevameter (WB)* is mounted directly on base rover. It is using well known technique for terrain parameters estimation (called Bekker’s parameters) widely applied in military devices for traversability assessment [1].

Additional data source for terrain traversability assessment, *Remote Sensing (RS)* subsystem, returns localization and estimated size of rocks across camera Field Of View (FOV).

**Existing data for planetary soil assessment:** Among various datasets acquired from last Martian mission, there are not many directly useful for terrain traversability assessment. There are no direct geotechnical measurements related to terrain traversability. Engineering data from motors and actuators, are not easy achievable. However, visual data give the possibility to characterize the variability of Martian surface and describe typical sediments and geomorphic features present on the surface. Additional analysis of spectroscopic data, e.g. Mini-TES etc., can give the additional information related to surface material variability and activity of geomorphic forms (e.g. dunes, ripples) [3]. Common analysis of such data can give the general base for assumptions of terrain traversability.

**Data fusion concept:** The aim of Data Fusion module is to integrate data from all sensors and put them on one grid map. The output map will be used by path planner for safe path estimation. Sources from all sensors are unified in the each sensor driver to trafficability percentage scale, where everything below 30% is not-traversable, between 30-65% is uncertain and above 65% should be traversable for Primary rover. The task for Data Fusion module is to return trafficability map built based on trafficability percent estimation from different sources, relative positions of these measurements and confidence parameters estimated for each sensor during a test trail.

Before fusion the measurements are inflated to specific radii of influence. This pre-processing step is necessary because sensors yield point measurements but output map should produce path useful for Primary rover, which is 2-3 times wider than Scout. Moreover, the measurement uncertainty, with the sensor confidence value in the measurement point, is increased with distance from measurement point. That approach allows to leave the same measurement value over whole circle with changing uncertainty, which take part during fusion process.

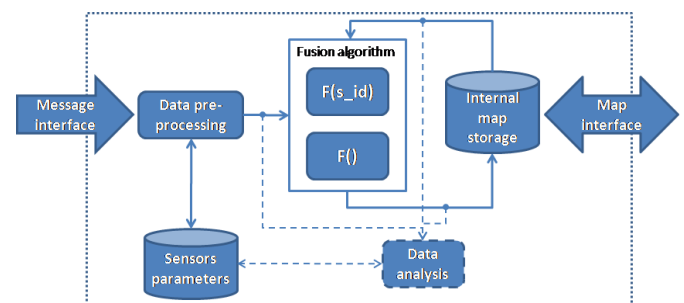


Fig.1 General structure of DF algorithm

Fusion problem was divided to two steps: information fusion over each sensor separately, where Bayes rule is applied, and merging of that information to the output map. General idea for algorithm is presented in Fig.1. Following Thrun et.al. [4] this information should not be fused by Bayes rule in one step because each sensor estimates trafficability based on different physical phenomena. In other words, there is no certainty, that two sensors returning the same trafficability estimation, producing results based on different methods, are detecting the same aspects of soil character. The Bayes fusion in first step takes under consideration current measurement, previous measurements intersected with recent one and confidence parameters in each point over measurement inflation radius. This step produces map for each sensor, which is merged to one output map in the second step. Merging step uses function that put on output map only the most certain and worst case value from all sensors’ maps. That approach ensures safe and useful map generation.

**Summary:** Data Fusion subsystem for traversability measurements data should deliver exact and reliable data for various planetary soils to support mission planning and enhance overall safety and effectiveness of the mission. Presented solution of FASTER project covers at least few of the elements giving the opportunity to make a rover planetary operations more effective than recently.

**References:**

[1] Bekker M.G. (1956), Theory of Land Locomotion. The University of Michigan Press. Ann Arbor, MI. [2] Nevatia Y. H. et.al. (2013). Improved Traversal for Planetary Rovers through Forward Acquisition of Terrain Trafficability, IEEE ICRA, Planetary Rovers Workshop, Karlsruhe. [3] Sullivan R., et al. (2008), Wind-driven particle mobility on Mars: Insights from Mars Exploration Rover observations at “El Dorado” and surroundings at Gusev Crater, J. Geophys., 113, E6, DOI:10.1029/2008JE003101. [4] Thrun S. Burgard W. and Fox D. (2005), Probabilistic Robotics, The MIT Press.

**Summary:** The paper reports on a conceptual study of a hopper robot dedicated to exploration of highland terrains of extraterrestrial bodies. It is a light (up to 8 kg) robot that possesses three elastic actuating legs distributed symmetrically on the robot's structure, allowing for omnidirectional jumps above vertical obstacles up to 4 m high on Mars. The proposed design is completely dust-free, with actuators hidden in spring-bellows, which are also a storage of the energy. It will be able to carry a few scientific instruments, and complements conventional rovers that are not able to explore complex and uneven terrains.

**Surface locomotion:** The difficulty in exploring uneven terrains of extraterrestrial bodies is that it requires new types of robots possessing special features especially concerning its motion performance. Ideally systems with high dexterity, autonomy and terrain adaptability are applicable. Examples are underactuated systems that take advantage of dynamical stabilization similar to the one observed in animals and humans [7]. Nevertheless, such systems are high power demanding and for the moment not reachable. Reliable yet simplified solutions have to be proposed.

Among many forms of locomotion, hopping on the surface of celestial bodies is potentially the most effective way for traversing even vertical obstacles that are much higher than the robot itself. In this paper, we propose the development of a hopping robot (Figure 1), a light and robust jumping locomotion system designed to be dropped anywhere on the surface of low gravity planetary bodies. Having quickly analysed the surroundings, it will hop, leap, or crawl to wherever investigators want it to work, within a maximum single jump distance of several meters vertically and horizontally. It will be reversible and fully symmetric. No matter how it lands, three spring-loaded legs will always assure stability and accurate directional control in any difficult ground configuration, and it will be able to perform scientific tasks.

**Technological constraints:** The hopper robot is a system containing three identical actuating spring legs symmetrically distributed (every 120°) along the circumference of the hopper robot disc structure. As it can be noticed in Figure 1, the driving springs will protect the overall structure of the robot as well as provide its dumping during landing, with a high probability of safety regardless the angle of landing. The system is also maintained in the upside-down symmetry, making unnecessary the return to the initial (pre-jumping) position, as is the case in most of the known hopper solutions. This will limit the use of drives to only three, ensuring the reliability of the system. By controlling the tension of the spring in each actuating leg separately, the hopper robot will be able to select the direction of motion and resulting energy of each jump. A principle of the design is that the joints and mechanical parts have to be shielded from dust. For this reason, not only will the actuating legs consist of elliptically-shaped spring sheets partly accumulating energy, but also, will energy be stored in the spring bellows, inside of which drive for tensioning the system will be hidden from the dust. Such solution is leading-edge in the domain of space mechanisms and for the best of our knowledge has not been proposed in any previous hopping system, of which only rare solutions are known, e.g. [1], [2], [4], [5], [6].

The hopper is designed to perform jumps up to 1.5 m on Earth, corresponding to 4 m on Mars and 9 m on Moon. As a result, its dimensions and mass have to be limited. The assumed overall mass of the system is less than 8kg, allowing for about 0.8kg for a few scientific instruments, like a mass spectrometer, a camera, a magnetometer, temperature and humidity sensors etc.

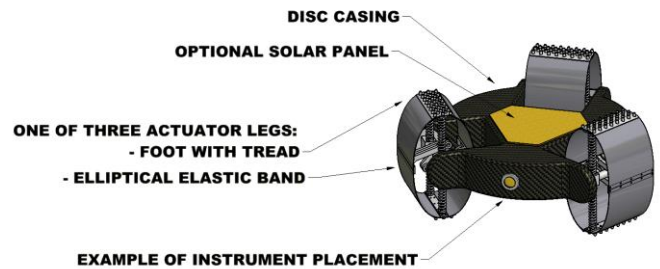


Figure 1: View of the hopper robot.

**Potential application:** Since the dimensions and mass of the proposed hopper robot are relatively small (max. 8kg and envelope of Ø500x250mm), it can assist a big rover in the identification of priority targets and provide guidance in difficult terrain areas. The hopper lightness also makes it suitable for deployment in small groups or larger swarms. This possibility will be extremely helpful if, for instance, dropped in Valles Marineris, a swarm of hoppers could investigate the upper 10 kilometres of the Martian crust along a 100 km long profile [3].

Besides Mars, the considered destinations are lower gravity bodies such as the Moon and smaller celestial bodies, like Phobos or asteroids. For those, rovers are not able to operate due to presence of micro-gravity conditions and, as a result, lack of weight which generates the friction between the wheels and the surface. The hopping system developed within this project will be easily adaptable by radical decrease of stored energy in the actuating legs to allow for gentle operation.

**References:** [1] Fiorini, P., Marchesi M. (2004), Robustness concepts for hopping robots, in Proc. 8<sup>th</sup> ASTRA, Netherlands. [2] Fiorini, P., Munteanu, M. Gh. (2008), Solving the landing problem of hopping robots: the elastic cage design, in Proc. 10<sup>th</sup> ASTRA, The Netherlands. [3] Mège, D. et al. (2013), Highland Terrain Hopper: Scientific applications on low-gravity planetary objects, European Planetary Science Congress, United Kingdom. [4] Montminy, S., Dupuis E., Champlaud H. (2008), Mechanical design of hopper robot for planetary exploration using SMA as a unique source of power, Acta Astronautica, Vol. 62, pp. 438-452. [5] Ulamec S. et al. (2011), Hopper concepts for small body landers, Advances in Space Research, Vol. 47, pp. 428-439. [6] Yoshimitsu T. et al. (2012), Advanced robotic system of hopping rovers for small solar system bodies, in Proc. i-SAIRAS, Italy. [7] Wiśniewski Ł., Zielińska T., Grygorczuk J. (2013) An introductory study on underactuated mobile robot with dynamical stabilization – a test-bed for next generations of planetary explorers, in Proc. 2<sup>nd</sup> Conference on Aerospace Robotics, Poland.

**Abstract:** Thanks to improving resolution of images and data concerning topography of Mars, a number of ancient alluvial deltas have been identified. Most of them exist in impact craters and some are also located on what is thought to be shoreline of hypothetical ocean [1]. We investigate the processes of sediment transport and deposition using numerical model based on hydrodynamic equations. We compare the results for Mars with simulations of fluvial deposition on Earth and Titan, the largest moon of Saturn [2].

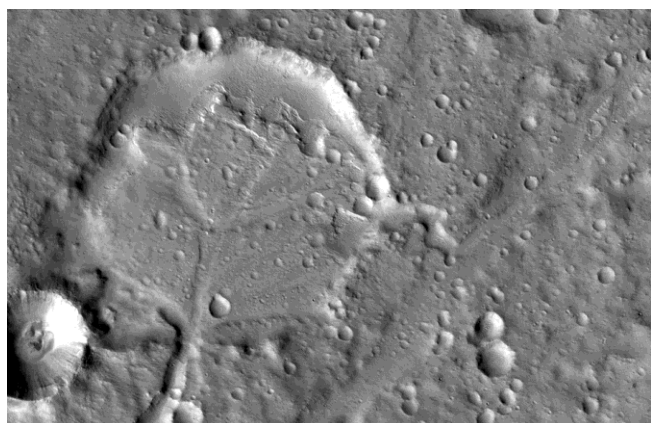


**Figure 1:** An example of Martian delta in Xanthe Terra at the terminus of the Nanedi valley, in an impact crater located approximately on 8.65 N, 48.0 W. The crater has diameter of 5 km. The deposits fill almost entire crater, several distributary channels are visible. Credit: NASA/JPL-Caltech/MSSS.

**Methods and results:** We use two-dimensional depth-averaged numerical model based on the Navier-Stokes equations and the continuity equation. Additional equations describe sediment transport. We explore the flow properties and the deposition of material as a function of several parameters in simplified geometry of the flow.

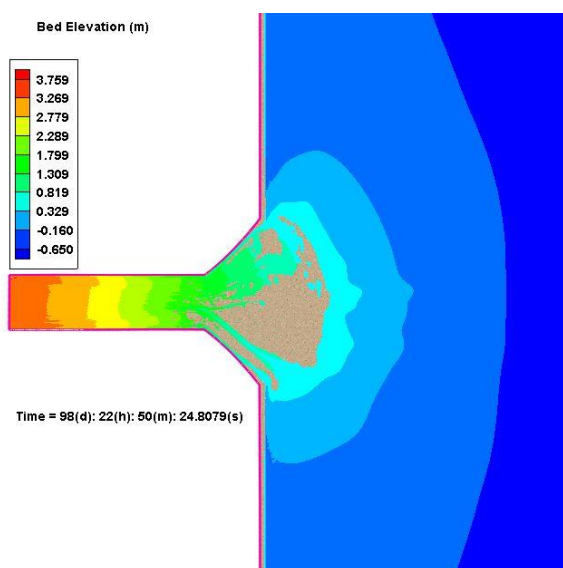


**Figure 2:** Result of sediment transport simulations for a channel leading to large reservoir on Earth: bed elevation above the reference level after ~99 simulated days. The discharge at the inflow is assumed to be  $10 \text{ m}^3/\text{s}$ .

We model sedimentation at the mouth of the river creating river delta in conditions corresponding to surfaces of Mars, Titan and Earth. The differences of models include gravity, density of sediments, density and viscosity of the liquid. In Martian models we assume the liquid can be either the fresh water or the brine, and the sediments have basaltic composition. In terrestrial conditions we investigate transport of quartz grains by the fresh water, and on Titan the sediments are composed of water ice and the medium is liquid methane-nitrogen mixture. We compare the results obtained for conditions on surfaces of Mars, Earth and Titan.

We intend to extend our research on laboratory experiments on sedimentation and compare the results with those obtained by the numerical simulations.

The research is performed in the frame of the Extraterrestrial Rivers Modeling Group.

[1] Di Achille, G., & Hynek, B. M. (2010). Ancient ocean on Mars supported by global distribution of deltas and valleys. *Nature Geoscience*, 3(7), 459-463.

[2] Witek, P. and Czechowski, L. (2013). Fluvial deposition processes on Titan – origin and evolution of landforms. Abstract EPSC2013-365, presented on the European Planetary Science Congress 2013.

**Introduction:** We present temperature profiles retrieved from measurements by the VIRTIS (Visual Infrared Thermal Imaging Spectrometer) instrument aboard Venus Express mission. VIRTIS-M spectrometer measures a radiation emerging from the atmosphere and provides spectra from the spectral range from 1000 nm to 5100 nm with the sampling step 11 nm. Only a couple of channels at 1.01, 1.10 and 1.18 micron can monitor the surface of Venus. Instantaneous field of view for VIRTIS-M is 0.25x0.25mrad what corresponds to a horizontal resolution for individual pixels 16.5x16.5 km [1], [2].

The retrieval of venusian atmospheric temperature is based on the absorption band by CO<sub>2</sub> at 4.3 micron. In order to model the measured spectra by VIRTIS, the multiple scattering in the atmosphere is taken into account because of cloudy atmosphere and its optical properties. Clouds on Venus are mainly composed of H<sub>2</sub>SO<sub>4</sub>, which have significant scattering properties (ssa > 0.5). In our study clouds contain of liquid droplets of a mixture composed of 75% of H<sub>2</sub>SO<sub>4</sub> and 25% H<sub>2</sub>O with complex refractive indices given by [3]. They can occur between 50 km and 65 km and affect greatly to the retrieval of temperature profiles in these altitudes.

Temperature profiles are obtained from VIRTIS measurements using two retrieval methods. Both approaches are the iterative process. In order to retrieve thermal structures we define vector state  $x$  which is in our case the vertical temperature profile. The problem of retrieval relies on finding the state vector  $x$  ( $x_1, x_2, x_3, \dots, x_n$ ) knowing measurements  $y$  ( $y_1, y_2, y_3, \dots, y_m$ ). The measurement vector  $y$  is equal to the sum of the forward model  $F(x)$  calculated for atmospheric parameters described by the state vector  $x$  and an error of a measurement  $y$ .

One of the methods involves the relaxation equation to derive the temperature profile for the next iteration [4]. This method was successful applied for measurements from the Venera spacecraft [5], Galileo-NIMS spectra [6], VIRTIS measurements by [7]. Second method is based on the Bayesian approach described by [8]. The theorem applies the probability density functions to define a function of the state vector and the measurement vector. However, the problem of retrieval on Venus is non-linear strongly, thus it is necessary to use the Gauss-Newton iteration. Furthermore, in order to have some information about atmospheric temperatures the Levenberg – Marquardt method was applied.

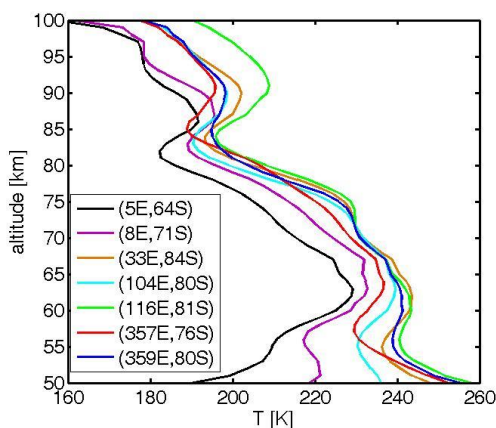


Fig.1. Vertical temperature profiles obtained from measurements over the south polar vortex using the relaxation method.

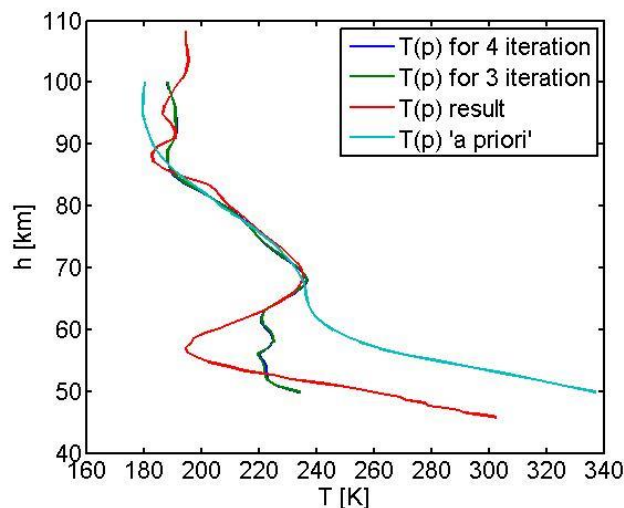


Fig.2. Temperature profiles retrieved for spectrum 309 from orbit 38.

By using the relaxation method, we calculated some temperature profiles around the south polar vortex (Fig.1) and from orbit 38 using the Bayesian approach (Fig.2). As we can see temperature profiles below 65 km are different due to clouds.

**References:**

[1] Piccioni G. et al. (2007), VIRTIS: The Visible and Infrared Thermal Imaging Spectrometer, *Eur. Space Agency Spec. Publ.*

[2] Grassi D. et al. (2008), Retrieval of air temperature profiles in the Venusian mesosphere from VIRTIS-M data: Description and validation of algorithms, *Journal of Geophys. Res. - Planets*, vol.113, E00B09, doi:10.1029/2008JE003075.

[3] Palmer K. and D.Williams (1975), Optical constants of sulfuric acid: Application to the clouds of Venus?, *Appl. Opt.*, 14(1), 208 – 219.

[4] Chahine, M. T. (1970), Inverse problems in radiative transfer: Determination of atmospheric parameters, *J. Atmos. Sci.*, 27, 960 - 967

[5] Zasova, L. V. et al. (1999), Structure of the Venus middle atmosphere: Venera 15 Fourier spectrometry data revisited, *Adv. Space Res.*, 23(9), 1559 – 1568.

[6] Roos-Serote M. et al. (1995), The thermal structure and dynamics of the atmosphere of Venus between 70 and 90 km from the Galileo-NIMS spectra, *Icarus*, 114(2), 300 – 309.

[7] Grassi D. et al (2010), Thermal structure of Venusian nighttime mesosphere as observed by VIRTIS-Venus Express, *Journal of Geophys. Res. - Planets*, vol. 115, E09007, doi:10.1029/2009JE003553.

[8] Rodgers, C., D. (2000), *Inverse Methods for Atmospheric Sounding: Theory and Practice*, World Sci., Singapore.

# MARS CLIMATE SOUNDER OBSERVATIONS OF WAVE STRUCTURE IN THE NORTH POLAR MIDDLE ATMOSPHERE OF MARS DURING THE SUMMER SEASON.

Paulina Wolkenberg<sup>1</sup> and R. J. Wilson<sup>2</sup>, <sup>1</sup>Centrum Badań Kosmicznych Polska Akademia Nauk, [paulina@cbk.waw.pl](mailto:paulina@cbk.waw.pl), <sup>2</sup>NOAA Geophysical Fluid Dynamics Laboratory, Princeton, New Jersey, USA

**Introduction:** Our study is based on observations from the Mars Climate Sounder (MCS) [1] on the Mars Reconnaissance Orbiter (MRO) mission [2]. The temperature field was retrieved from the observations with possible errors of 0.5 – 2 K for all altitudes [3]. The vertical range of the temperature profiles is from 5–10 km above the surface up to 80-90 km. We examine the temperature field at over a full range of heights during the northern summers of Mars Years 28-31 over the northern polar region of Mars from 50°N to 90°N. We observe three temperature maxima, forming a well-defined wave-3 structure in the middle atmosphere, during each of our 3 Mars years at the same season at around 0.1 Pa (~70 km). Fourier analysis is employed to find the amplitudes and phases of the various wave components as a function of latitude, altitude, and time. Amplitudes of the wave-3 component are greater than 7 K in all three years. The T-average and T-difference fields are considered to study a possibility of appearance for non-migrating and stationary waves during MY 29, 30 and 31. We use the MY31 MCS multi-track data to show that these waves are not stationary, but have diurnal and semi-diurnal components. With only 2x/sol data, it was not previously possible to identify the semi-diurnal tide. We also present MGCM results to support our interpretation.

The wave-2 and -3 components appear to be non-migrating waves that arise due to interaction between the thermal tides and topography derived from the calculation of phase velocities based on observations and multi-track measurements.

We also make use of MCS observations employing cross-track viewing in addition to the usual along-track viewing, as described in [4]. These measurements began in September 2010 (MY30, Ls=144) and have been carried out in 30 sols on, 30-sols off sequences since then. The period of most relevance for this study is Ls= 101-114 in MY31. During this analysis, we form zonal averages using a bin size of 5° in latitude from 65°N to 90°N. Subsequent analyses involved the full range of available MCS pressure levels and a wider range of latitudes.

During Ls = 0–135° season we have found a weak temperature inter-annual variability, thus we have averaged the data in blocks in 5 of latitude degrees from 85S to 85N, in the 10 of longitude degrees and in the 5 of Ls degrees for three Martian years from MY 29 to 31 together. After Ls = 135 there was early-season dust lifting in MY 29. However, the T avg and T diff fields are not enough to resolve amplitudes of particular tides. The multi-track data, which provide observations of 6-7 times per sol, allow us to find semidiurnal tides [4].

We will explore the strength and persistence of the wave-1, wave-2, and wave-3 structure as a function of latitude, altitude, and season. We make a selection of temperature field for daytime and nighttime data around LT = 15 and LT = 3, respectively. Then we have calculated the difference temperature field from  $0.5 \cdot (T(LT=15) - T(LT=3))$  and the averaged temperature field from  $0.5 \cdot (T(LT=15) + T(LT=3))$  from 85S to 85N in binned 5 deg. in latitude, zonally and in time averaged at each 10 of Ls. These fields are applied to find Fourier components and identify the presence of non-migrating, migrating and stationary waves. In order to resolve particular

tides we use multi-track observations by fitting diurnal and semi-diurnal temporal harmonics.

**Results:** Thank to multi-scan data, this means that temperatures are available at different local times, thus we are able to distinguish the contributions of particular waves. After detail analysis of Ls = 101 – 114 at 0.1 Pa we found that the main contribution to the temperature field is diurnal westward propagating tide with  $s = 1$  (DW1) with amplitudes from around 8 to 10 K. Then the significant impact is due to the semidiurnal westward propagating tide with  $s = 2$  (SW2) although this decreases northward. It is evident that diurnal tides dominate at 0.1 Pa over the semidiurnal one. Amplitudes of the diurnal eastward nonmigrating tide with  $s = 1$  (DE1) increase up to 4.1 K northward which constitute the component of T-difference for  $m = 2$ . Contrary to the DE1, the semidiurnal eastward propagating tides with  $s = 1$  (SE1) decreases northward achieving around the 2 K amplitude. The tide contributes to the T-average field for  $m = 3$ . The diurnal eastward tide (DE2) exhibits the same behavior with latitude, which comprises the T-difference field for  $m = 3$ . It is worth to indicate the semidiurnal zonally symmetric tides with amplitude around 4.3 K which is also important in the T-average field for  $m = 2$ . However, the wave 2 component of T-average dominates that of T-difference, as it is appropriate for a semi-diurnal tide. Thus, the  $m = 2$  wave structure is due to A(0,2) and A(-1,1) while the  $m = 3$  structure is due to A(-2,1) and A(-1,2) that had been speculated by previous modeling and observational studies [5], [6], [7]. Together, they sum to a significant temperature variation that appears to be present.

## References:

- [1] McCleese, D. J., et al. (2007), Mars Climate Sounder: An investigation of thermal and water vapor structure, dust and condensate distributions in the atmosphere, and energy balance of the polar regions, *J. Geophys. Res.*, 112, E05S06, doi:10.1029/2006JE002790.
- [2] Zurek, R. W., and S. E. Smrekar (2007), An overview of the Mars Reconnaissance Orbiter (MRO) science mission, *J. Geophys. Res.*, 112, E05S01, doi:10.1029/2006JE002701,
- [3] Kleinböhl, A., et al. (2009), Mars Climate Sounder limb profile retrieval of atmospheric temperature, pressure, dust, and water ice opacity, *J. Geophys. Res.*, 114, E10006, doi: 10.1029/2009JE003358.
- [4] Kleinböhl, A., et al. (2013), The semidiurnal tide in the middle atmosphere of Mars, *Geophys. Res. Lett.*, 40, doi:10.1002/grl.50497
- [5] Wilson, R. J. (2002), Evidence for nonmigrating thermal tides in the Mars upper atmosphere from the Mars Global Surveyor accelerometer experiment, *Geophys. Res. Lett.*, 29 (7), 10.1029/2001GL013975.
- [6] Angelats i Coll, M., et al. (2004), Upper atmosphere of Mars up to 120 km: Mars Global Surveyor accelerometer data analysis with the LMD general circulation model, *J. Geophys. Res.*, 109, E01011, doi:10.1029/2003JE002163.
- [7] Bougher, S. W., et al. (2001), Mars Global Surveyor radio science electron density profiles: neutral atmosphere implications, *Geophys. Res. Lett.*, 28, 3091 – 3094.

**EVIDENCE OF WATER FROM LHB ON THE LARGEST MARTIAN CRATER HELLAS IN COMPARISON TO OTHER CRATERS FROM OF THE SAME PERIOD.** Natalia Zalewska<sup>1,2</sup> <sup>1</sup>Space Research Center PAS, Bartycka 18A, 00-716 Warsaw, [natalia@cbk.waw.pl](mailto:natalia@cbk.waw.pl) <sup>2</sup>Institute of Aviation, al. Krakowska 110/114 02-256 Warsaw [natalia.zalewska@ilot.edu.pl](mailto:natalia.zalewska@ilot.edu.pl)

**Introduction:** The age of the largest craters on Mars suggests that they have been formed during the LHB period [1]. The formation of craters Hellas, Isidis and Argyre happened during that period. Age of Hellas is determined on  $3.99 \pm 0.01$  billion years, Isidis to  $3.96 \pm 0.01$  and Argyre  $3.85 \pm 0.01$  which is already at the end of the Great bombardment. The layer of clay minerals in each of the craters originates from Noachian age, but in Hellas crater those layers are converted by the glacier and may appear in subsequent ages. Clay minerals are unshakable proof of the existence of water. One can draw conclusions, that large amounts of water appeared at an early Noachian. In subsequent ages, there is no large amounts of these minerals. Formations of Hellas and in comparison of Isidis crater are associated with the ingress of water on these terrains, in contrast Argyre formed after water left because the impact revealed layers of clay minerals. The question arises, what are the evidence to prove the age and the origin of this crater contained within the traces left by water.

**Evidence of water:** A good indicator of the presence of water is the occurrence of clay minerals and other hydrated minerals [2]. Geomorphology of craters also indicates a degree of erosion. Hellas has a lot more features of erosion than Argyre [3]. Channels which are on the east side of Hellas could have been water flows at some point in the history of Mars [4]. Such a significant erosion of the inside of Hellas crater could have been caused by the huge flows of water, where accumulation of clay minerals and hydrated silica in the interior of the crater and on the north side is observed [5]. Glaciation that probably occurred in the Amazonian era clearly exaggerated the erosion of the crater.

Recent research indicate the occurrence of hydrated silica in the north-western part of Hellas. It doesn't suggest the presence of large amounts of sulfates and clay minerals and carbonates. Hydrated amorphous silica (opal) has been identified on the basis of measurement of devices such as TES, THEMIS and CRISM [2]. Inside the Tereby crater located on the north shore of Hellas hydrated silica, such as opal were identified too [6].

Hydrated silicates on the surface of Hellas has been converted by the glacier and can be identified in all Martian eras from Noachian to Amazonian. However minerals arose, in the era of Noachian. According to Banfield, before glaciation Hellas crater was filled with water for a long period of time as long as weather conditions allowed [2].

This hypothesis of lake in the Noachian is confirmed by the survey spectra from CRISM and OMEGA from western shore of Hellas basin, where large clusters of clay minerals were identified [6]. On the rim of Hellas multiple channels and deltas are noticeable which were probably water flows in the direction of the crater in the Noachian era.

Clay minerals can be identified on the basis of spectra from OMEGA in the middle of the crater and in surrounding channels Dao Vallis [7]. Minerals are present on the surface of the Amazonian and Hesperian era. They were probably reworked by the ice sheet, which stack up in Amazonian [2]. We also believe that the age of the crater area shown on the maps are too generalized and shows the diversity of geology at low resolution. Clay minerals in the central part may actu-

ally be in the Noachian period, as in Isidis, whose occurrence was not taken under consideration on the maps or not noticed.

The origin of the Hellas' channels Harmakhis, Dao and Niger Vallis and their age is being explained differently. Features of lake accumulation and runoff channels from Dao, Harmakhis and Niger Vallis (DHN) is estimated at Late Hesperian and Early Amazonian. It is possible that the channels were carved by water flowing from under the ground, which formed a frozen layer and was melted by late volcanic activity in the area. These flows are defined as a catastrophic. Water layer had already been formed during the Noachian era. Channels show features like sinkholes, or the sudden collapse of the land. On these surfaces of the channel large accumulation of clay minerals is not observed, rather embedded volcanic material. Theory of outflows of aquifers has many inaccuracies yet and it is served as one of the examples. Another more likely phenomenon is melting ice cap on the surface so that these channels exhibit characteristics of melting forms, due to the melting of residual ice on the surface under the influence of the late episodes of volcanism [4]. These examples demonstrate the appearance of water not only during Noachian.

In conclusion based on these studies, it is estimated that the clay minerals in the area were formed mainly in the Noachian era when Hellas could have been filled with water forming a kind of sea or lake. The appearance of clay minerals in areas from Hesperian and Amazonian suggests rework of the material by the glacier. Runoff water appeared not only in the Noachian era but also in the late Hesperian and early Amazonian, from the melting of subsurface ice layer and / or lingering ice caps due to episodes of late volcanism. It is when great DHN Vallis channels were formed.

So it looks like the main existence of liquid water on Mars was attributed to the early and middle period of LHB and later impact such as Argyre from the end of LHB only bared layers of hydrated minerals being the evidence of earlier liquid water activities. We can also assume that the layers exposed by impact originate from before LHB thus pre-Noachian. It is probable that the activity of water could have still lasted for a long period of time in some of the more favorable places on smaller latitudes of Mars up to a total change in density of Martian atmosphere.

**References:** [1] Werner S.C. (2008), The early martian evolution—Constraints from basin formation ages, *Icarus* 195, 45–60, [2] Bandfield J.L. et al. (2013), Extensive hydrated silica materials in western Hellas Basin, Mars, *Icarus* 226, 1489–1498, [3] Siili T. et al. (1999), Modelling of the combined late winter ice cap edge and slope winds in Mars' Hellas and Argyre regions, *Planetary and Space Science* 47, 951–970, [4] Kostama V-P. et al. (2010) Evidence for multiple ice deposits on the northeastern rim of Hellas basin, Mars, *Earth and Planetary Science Letters* 294 (2010) 321–331, [5] Crown D.A., et al., 2009) Geologic mapping of the NW rim of Hellas Basin, Mars, 40th *Lunar and Planetary Science Conference*, 1705, [6] Carter J. et al. (2011) Mineralogical evidence for major aqueous activity in the northern Hellas province, Mars, *EPSC Abstracts*, Vol. 6, EPSC-DPS2011-1044, [7] Zalewska (Andrzejewska) N. (2013) Hellas Planitia as a potential site of sedimentary minerals, *Planetary and Space Science* 78, 25–32.

**THE NEW TOPOGRAPHY OF OUTER SATELLITES – IO, GANYMEDE AND ENCELADUS, – DERIVED FROM VOYAGER, GALILEO AND CASSINI IMAGES.** A. Zubarev<sup>1</sup>, I. Nadezhkina<sup>1</sup>, E. Lazarev<sup>1,2,3</sup>, V. Patraty<sup>1</sup>, I. Karachevtseva<sup>1</sup>, A. Kokhanov<sup>1</sup>, N. Kozlova<sup>1</sup> and J. Oberst<sup>1,4</sup>, <sup>1</sup>Moscow State University of Geodesy and Cartography (MIIGAiK), MIIGAiK Extraterrestrial Laboratory (MExLab), Gorokhovskiy pereulok 4, 105064 Moscow, Russia I\_karachevtseva@miigaik.ru, <sup>2</sup>Sternberg Astronomical Institute (SAI) (MSU), 119992, Universitetskii pr., 13, Moscow, Russia, <sup>3</sup>Lomonosov Moscow State University, Geographical Department, Chair on Cartography and geoinformatics, 119991, GSP-1, Leninskiye Gory, 1, Moscow, Russia. <sup>4</sup>German Aerospace Center (DLR), Institute of Planetary Research, Rutherfordstrasse 2, 12489 Berlin, Germany.

**Introduction:** While Galilean satellites have been observed by different spacecrafts, including Pioneer, Voyager-1 and -2, Galileo, New Horizons, and Enceladus by Cassini and Voyager-2, only data from Galileo, Cassini and the two Voyagers are useful for precise mapping [1, 2]. For purposes of future missions to the system of outer planets we have re-computed the control point network of the Io, Ganymede and Enceladus to support spacecraft navigation and coordinate knowledge. Based on the control networks, we have produced global image mosaics and maps.

**Geodesy approach:** We developed a new techniques of processing of frame space images and generation of control point networks. For future mission Laplace-P we mainly focused on Ganymede which coverage is nearly complete except for polar areas (which includes multispectral data). However, large differences exist in data resolutions (minimum global resolution: 30 km/pixel). Only few areas enjoy coverage by highest resolution images, so we suggest to obtain regional Digital Elevation Models (DEMs) from stereo images for selected areas. Also using our special software, we provide calculation of illumination conditions of Ganymede surface in various representations [3].

Finally, we propose a careful evaluation of all available data from the previous Voyager and Galileo missions to re-determine geodetic control and rotation model for other Galilean satellites – Callisto and Europe.

**Mapping:** Based on re-calculated control point networks and global mosaics we have prepared new maps for Io and Enceladus [4] and preliminary geodetic dataset for Ganymede for future modeling and mapping. To date due to the difference in resolution between the images, which were also taken from different angles relative to the surface, we have been able to prepare only regional high resolution shape models, so for demonstrating of topography and mapping of the satellites we used orthographic projection with different parameters. Our maps, which include roughness calculations based on our GIS technologies [5], will also be an important tool for studies of surface morphology.

**Conclusions:** Updated data collection, including new calculation of elements of external orientation, provides new image processing of previous missions to outer planetary system. The developed techniques of control point measurements and global network analysis for planetary bodies using the PHOTOMOD [6] software are fast and efficient. Based on improved orbit data for Galileo we have used larger numbers of images than were available before, resulting in a more rigid network for Ganymede. The obtained results will be used for further processing and improvement of the body shape parameters and shape modeling, libration, as well as for studying of the surface interesting geomorphological phenomena [7].

For the Enceladus we prepared DTM and new topographic map of 23% surface of Enceladus. This topography can be used for further morphometric investigations and comparative planetologic analysis of the satellite relief. The

upcoming Cassini flybys of Enceladus will help to fill gaps with new data.

**Acknowledgments:** The study of was partly supported by ROSKOSMOS and Space Research Institute under agreement № 36/13 “Preliminary assessment of the required coordinate and navigation support for selection of landing sites for lander mission Laplace-P (Ganymede) and partly funding by grant from the Ministry of Education and Science of the Russian Federation Agreement № 11.G34.31.0021 (Io and Enceladus).

**References:** [1] Nadezhkina et al. Vol. 14, EGU2012-11210, 2012. [2] Zhukov et al. International Colloquium and Workshop "Ganymede Lander: scientific goals and experiments", Space Research Institute, Moscow, Russia, 4-8 March, 2013. [3] Zubarev et al. International Colloquium and Workshop "Ganymede Lander: scientific goals and experiments", Space Research Institute, Moscow, Russia, 4-8 March, 2013. [4] Lazarev et al. *Izvestia VUZov*. 2012, No 6, pp. 9-11 <http://miigaik.ru/journal.miigaik.ru/2012/20130129120215-2593.pdf> (in Russian). [5] Kokhanov et al. Current problems in remote sensing of the Earth from space. 2013. Vol. 10. No 4. pp. 136-153. [http://d33.infospace.ru/d33\\_conf/sb2013t4/136-153.pdf](http://d33.infospace.ru/d33_conf/sb2013t4/136-153.pdf) (in Russian). [6] PHOTOMOD: Racurs.ru: Products, 2012. <http://www.racurs.ru/?lng=en&page=634>. [7] Oberst et al., 2013 International Colloquium and Workshop "Ganymede Lander: scientific goals and experiments", Space Research Institute, Moscow, Russia, 4-8 March, 2013.

# AUTHOR INDEX

## Author Index

<b>Surname</b>	<b>First name</b>	<b>Abstracts</b>
Alberti	Giovanni	C5, C6
Alizade	Ali	C15
Appéré	Thomas	C18
Balme	Matt	C4
Banaszkiewicz	Marek	C1, C38, C51
Barciński	Tomasz	C49
Bérczi	Szannislo	C29
Białek	Agata	C1*
Błęcka	Maria	C2*
Borykov	Timur	C3*
Bourgeois	Olivier	C13, C37
Boyd	Andrea	C32
Bridges	John	C35
Brož	Petr	C4*
Carrère	Véronique	C14
Castaldo	Luigi	C5*, C6*
Chicarro	Agustin	R1*, R2*
Ciążela	Jakub	C27
Craddock	Robert	C33
Czechowski	Leszek	C7*, C8*, C31, C50
de Vera	Jean-Pierre	R3*
Dębniak	Krzysztof	C9*, C27, C37
Dinkelaker	Aline	C15
Dobrowolski	Marcin	C37
Dzwończyk	Szymon	C10*
Felix	Carmen	C15
Gabryszewski	Ryszard	C42
Gaudin	Anne	C14
Ghasemzadeh	Leila	C15
Gobi	Sándor	C19
Gołębiowska	Izabela	C32
Gourronc	Marine	C37
Groemer	Gernot	C11*, C32
Grudziński	Paweł	C47
Grygorczuk	Jerzy	C1, C12*, C38, C49
Gueydan	Frédéric	C36, C37
Guidat	Thomas	C13*
Gurgurewicz	Joanna	C5, C6, C14*, C27, C37, C38, C45, C49
Hauber	Ernst	R4*, R10, C4
Hettrich	Sebastian	C15*, C32
Hewins	Roger	R5*
Horvai	Ferenc	C16*
Jones	Natalie	C32

<b>Surname</b>	<b>First name</b>	<b>Abstracts</b>
Jorgensen	Uffe	R9
Józefowicz	Mateusz	C17*
Józwiak	Waldemar	C30
Kalarus	Maciej	C47
Karachevtseva	Irina	C20, C54
Kauerhoff	Tilo	C15
Kawamura	Taichi	R6
Kędziora	Bartosz	C12
Kereszturi	Akos	C18*, C19*
Kocsis	Ábel	C29
Kokhanov	Alexander	C20*, C54
Konopikhin	Anatoliy	C20
Kossacki	Konrad	C21*, C22*
Kostylew	Joanna	C14
Kozakiewicz	Joanna	C23*, C24*
Kozlova	Natalia	C20, C54
Krasowski	Jacek	C12
Kromuszczyńska	Olga	C25*, C37
Krzesińska	Agata	C26*
Kubiak	Marta	C27*
Kuciński	Tomasz	C38, C49
Kułak	Andrzej	C24
Kvíderová	Jana	C28*
Lang	Ágota	C29
Lazarev	Evgeniy	C54
Lewandowski	Marek	C30*
Lognonné	Philippe	R6
Łosiak	Anna	C11, C31*, C32*, C33*
Lucas	Antoine	C25
Lupu	Elena	C15
Łuszczek	Katarzyna	C34*
MacArthur	Jane L.	C32, C35*
Makowska	Magdalena	C36*, C37
Mangeny	Anne	C3
Markiewicz	Wojciech J.	C22
Massé	Marion	C9
Mège	Daniel	C3, C5, C6, C9, C14, C25, C27, C36, C37*, C38*, C45, C49
Meszyński	Sebastian	C17
Mikołajek-Zielińska	Beata	-
Misiura	Katarzyna	C8
Mitrokhina	Ljudmila	C20
Mizerski	Krzysztof	C30
Młynarczyk	Janusz	C24
Montmessin	Franck	R7*
Morizet	Yann	C14
Moser	Linda	C32
Nadezhdina	Irina	C20, C54

<b>Surname</b>	<b>First name</b>	<b>Abstracts</b>
Nicolau-Kuklińska	Agata	C39*, C49
Oberst	Jürgen	R8*, C20, C46, C54
Orgel	Csilla	C32
Orosei	Roberto	C5, C6
Ozimek	Wojciech	C40*
Palau	Marie-Catherine	-
Patraty	V.	C20, C54
Pfeil	Isabella	C15
Płatos	Łukasz	C47
Platz	Thomas	C4
Pochat	Stephane	C13, C37
Prajczer	Péter	C29
Rataj	Mirosław	C47
Richard	Patrick	C3
Rickman	Hans	R9*, C38, C41*, C42*, C49
Rossi	Angelo Pio	R10*
Rumińska	Agnieszka	C43*
Salteri	Efstratia	C15
Sejkora	Nina	C15
Seweryn	Karol	C1, C12, C39, C44*
Skiścim	Marta	C14, C45*
Skocki	Krzysztof	C38, C48
Souček	Ondřej	C13
Szalay	Kristóf	C29
Szutowicz	Sławomira	C41
Tokarz	Marta	C12
Valsecchi	Giovanni	C42
Wach	Radosław	C34
Wählisch	Marita	C46*
Wajer	Paweł	C42
Wawer	Piotr	C47*
Wawrzaszek	Roman	C1, C12
Węclewski	Piotr	C48*
Willner	Konrad	C46
Wilson	R. John	C52
Wiśniewski	Łukasz	C12, C38, C49*
Wiśniowski	Tomasz	C42
Witek	Piotr	C8, C50*
Wójcikowski	Kamil	C41
Wolkenberg	Paulina	C51*, C52*
Woronko	Barbara	C33
Zalewska	Natalia	C53*
Zubarev	Anatoliy	C20, C54*

\* First author

# Affiliations and e-mail addresses of registered participants

## Affiliations and e-mail addresses of registered participants

<b>Surname</b>	<b>First name</b>	<b>E-mail address</b>	<b>Affiliation</b>
Augustynek	Tomasz	tma14@leicester.ac.uk	University of Leicester
Bérczi	Szaniszo	bercziszani@ludens.elte.hu	Eötvös University
Białek	Agata	aprzeziorka@cbk.waw.pl	Space Research Centre, Polish Academy of Sciences
Błęcka	Maria	mib@cbk.waw.pl	Space Research Centre, Polish Academy of Sciences
Borykov	Timur	timur.borikov@twarda.pan.pl	Institute of Geological Sciences, Polish Academy of Sciences
Brož	Petr	petr.broz@ig.cas.cz	Institute of Geophysics, Academy of Sciences of the Czech Republic
Castaldo	Luigi	luigi.castaldo@twarda.pan.pl	Institute of Geological Sciences, Polish Academy of Sciences
Czechowski	Leszek	lczech@op.pl	University of Warsaw
Dębniak	Krzysztof	krzysztof.debniak@twarda.pan.pl	Institute of Geological Sciences, Polish Academy of Sciences
Dinkelaker	Aline	Aline.dinkelaker@gmail.com	Humboldt University of Berlin
Dzwończyk	Szymon	szymek@dzwonczyk.pl	Wrocław University of Technology
Frankowski	Juliusz	stregozzo@gmail.com	PsychoTech
Gabryszewski	Ryszard	r.gabryszewski@cbk.waw.pl	Space Research Centre, Polish Academy of Sciences
Groemer	Gernot	gernot.groemer@oewf.org	Austrian Space Forum
Grygorczuk	Jerzy	jurekgry@cbk.waw.pl	Space Research Centre, Polish Academy of Sciences
Guidat	Thomas	guidatt@td.ie	Trinity College Dublin
Gurgurewicz	Joanna	jgur@cbk.waw.pl	Institute of Geological Sciences and Space Research Centre, Polish Academy of Sciences
Hettrich	Sebastian	Sebastian.hettrich@web.de	German Federal Office for Radiation Protection
Horvai	Ferenc	horvai@nkalap.hu	Nagy Karoly Astronomical Foundation
Józefowicz	Mateusz	mateusz.jozefowicz@abrmSPACE.com	ABM Space Education
Kenyon	Andrew	adkenyon@gmail.com	Bellrock Technology Ltd
Kereszturi	Akos	kereszturiakos@gmail.com	Research Center for Astronomy and Earth Sciences
Kocsis	Ábel	s_kokhanov@mexlab.ru	Széchenyi István Gimnázium, Sopron
Kokhanov	Alexander	kjossac@igf.fuw.edu.pl	Moscow State University of Geodesy and Cartography
Kossacki	Konrad	joanna.kostylew@ing.uni.wroc.pl	University of Warsaw
Kostylew	Joanna	j.kozakiewicz@uj.edu.pl	University of Wrocław
Kozakiewicz	Joanna	okromuszczynska@twarda.pan.pl	Jagiellonian University
Kromuszczynska	Olga		Institute of Geological Sciences, Polish Academy of Sciences

<b>Surname</b>	<b>First name</b>	<b>E-mail address</b>	<b>Affiliation</b>
Krzesińska	Agata	agatakrz@twarda.pan.pl	Institute of Geological Sciences, Polish Academy of Sciences
Krzeszewski	Wiktor	w.krzeszewski@erisproject.com	ERIS Projekt
Kubiak	Marta	marta.kubiak@twarda.pan.pl	Institute of Geological Sciences, Polish Academy of Sciences
Kvídová	Jana	Jana.kvídová@ibot.cas.cz	Academy of Sciences, Czech Republic
Lang	Ágota	mmeurie95@gmail.com	Széchenyi István Gimnázium, Sopron
Leliwa-Kopystyński	Jacek	jkopyst@mimuw.edu.pl	University of Warsaw
Lewandowski	Marek	lemar@twarda.pan.pl	Institute of Geological Sciences, Polish Academy of Sciences
Łosiak	Anna	anna.łosiak@twarda.pan.pl	Institute of Geological Sciences, Polish Academy of Sciences
Łuszczek	Katarzyna	katarzyna.luszczek@pwr.edu.pl	Wrocław University of Technology
MacArthur	Jane	j.macarthur.12@ucl.ac.uk	University College London
Makowska	Magdalena	magdalena.makowska@twarda.pan.pl	Institute of Geological Sciences, Polish Academy of Sciences
Marek	Julia	farenka@gmail.com	Wrocław University of Technology
Mège	Daniel	daniel.mege@twarda.pan.pl	Institute of Geological Sciences, Polish Academy of Sciences and LPG, Nantes
Mikolajek-Zielińska	Beata	beata.mikolajek-zielinska@nauka.gov.pl	Ministry of Science and Higher Education
Nicolau-Kuklińska	Agata	ank@cbk.waw.pl	Space Research Centre, Polish Academy of Sciences
Ozimek	Wojciech	wojciech.ozimek@uw.edu.pl	University of Warsaw
Palau	Marie-Catherine	Marie-Catherine.PALAU@astripolska.pl	Astri Polska
Pankine	Alexey	apankine@spacescience.org	Space Science Institute, Boulder
Prajczer	Péter		Széchenyi István Gimnázium, Sopron
Rumińska	Agnieszka	a.m.ruminska@gmail.com	Wrocław University of Technology
Seweryn	Karol	kseweryn@cbk.waw.pl	Space Research Centre, Polish Academy of Sciences
Skiścim	Marta	skiscim@ifd.uni.wroc.pl	Institute of Geological Sciences, Polish Academy of Sciences
Skocki	Krzysztof	krzysztof.skocki@astripolska.pl	Astri Polska
Szalay	Kristóf		Széchenyi István Gimnázium, Sopron
Szutowicz	Stawomira	slawka@cbk.waw.pl	Space Research Centre, Polish Academy of Sciences
Wählisch	Marita	Marita.Waehlich@dlr.de	DLR Berlin
Wajer	Paweł	wajer@cbk.waw.pl	Space Research Centre, Polish Academy of Sciences
Wawer	Piotr	wawer@cbk.waw.pl	Space Research Centre, Polish Academy of Sciences
Węclewski	Piotr	piotr.weclewski@astripolska.pl	Astri Polska
Wisniewski	Łukasz	lwisniewski@cbk.waw.pl	Space Research Centre, Polish Academy of Sciences
Wiłek	Piotr	ppwit@igf.fuw.edu.pl	University of Warsaw

<b>Surname</b>	<b>First name</b>	<b>E-mail address</b>	<b>Affiliation</b>
Wolkenberg	Paulina	paulina@cbk.waw.pl	Space Research Centre, Polish Academy of Sciences University of Warsaw
Woronko	Barbara	bworonko@uw.edu.pl	Space Research Centre, Polish Academy of Sciences, Institute of Aviation Glazewski Robotics
Zalewska	Natalia	natalia@cbk.waw.pl	Przemysłowy Instytut Automatyki i Pomiarów
Glazewski	Wojciech	wojciechglazewski@op.pl	Przemysłowy Instytut Automatyki i Pomiarów
Wolski	Mateusz	mwolski@piap.pl	Przemysłowy Instytut Automatyki i Pomiarów
Zawieska	Karolina	kzawieska@piap.pl	Przemysłowy Instytut Automatyki i Pomiarów
Chicarro	Agustin	achicarr@rssd.esa.int	European Space Agency
de Vera	Jean-Pierre	jean-pierre.devera@dlr.de	DLR Berlin
Hauber	Ernst	Ernst.Hauber@dlr.de	DLR Berlin
Hewins	Roger	hewins@rci.rutgers.edu	Rutgers University and Museum d'histoire naturelle, Paris
Kawamura	Taichi	taichikawamura0408@gmail.com	Institut de Physique du Globe, Paris
Montmessin	Franck	franck.montmessin@latmos.ipsl.fr	LATMOS
Oberst	Jürgen	Juergen.Oberst@dlr.de	DLR Berlin
Rickman	Hans	Hans.Rickman@physics.uu.se	Space Research Centre, Polish Academy of Sciences and University of Uppsala
Rossi	Angelo Pio	an.rossi@jacobs-university.de	Jacobs University

*Notes*

*Notes*

*Notes*



